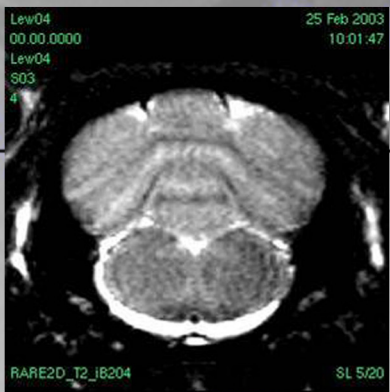
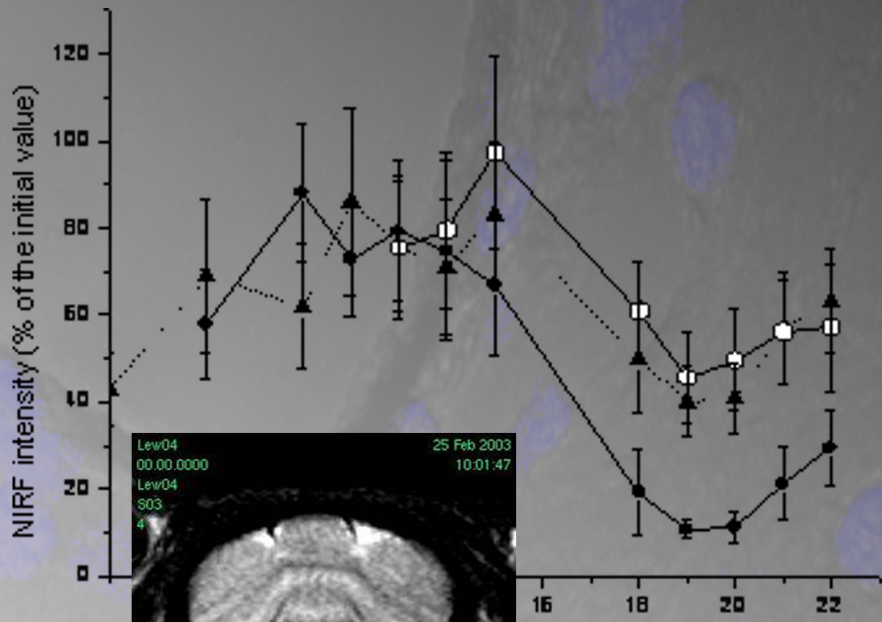
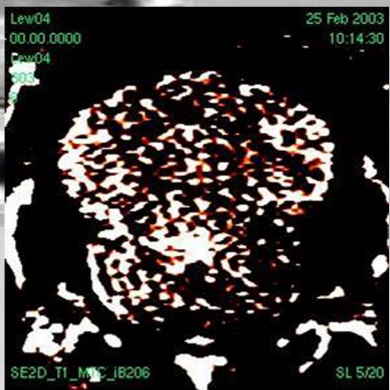
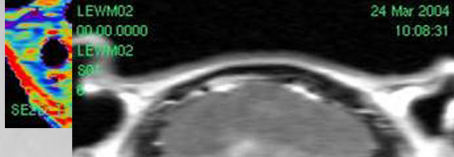
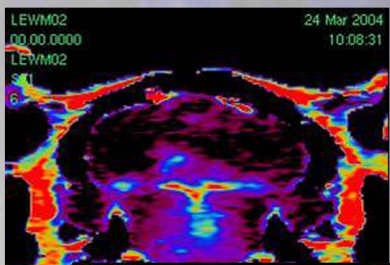
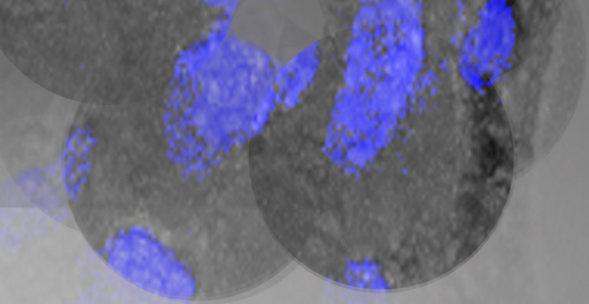
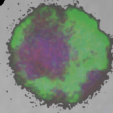


Labeling of immune cells for in vivo monitoring of cell migration using magnetic resonance imaging and near-infrared imaging



Cedric Berger
2003-2006



LABELING OF IMMUNE CELLS FOR IN VIVO
MONITORING OF CELL MIGRATION USING
MAGNETIC RESONANCE IMAGING AND
NEAR-INFRARED IMAGING

Inauguraldissertation

zur

Erlangung der Würde eines Doktors der Philosophie

vorgelegt der

Philosophisch-Naturwissenschaftlichen Fakultät

Der Universität Basel

von

Cedric Berger

aus Frankreich, Franche-Comté

Basel, 2006

Genehmigt von der Philosophisch-Naturwissenschaftlichen Fakultät

auf Antrag von

Prof. Dr. Joachim Seelig und Prof. Dr. Markus Rudin

Basel, den 17. März 2006

Prof. Dr. Hans-Jakob Wirz
Dekan

*to my father,
Roland Berger*

Acknowledgements

First of all, I really want to thank Prof. Dr. Markus Rudin for giving me the chance to carry out my PhD thesis in his group at Discovery Technologies of Novartis Pharma (Basel, Switzerland). Despite of his busy time schedule, he always generously supported me in a administrative or scientific way. His wise guidance was always constructive and helped me to consider the world of science with more concern.

I would like to address my special gratefulness to Prof. Dr. Joachim Seelig for his highly efficient academical assistance and his valuable scientific interest in my thesis. It was a real pleasure for me to appreciate his great experience and always feel supported. Working closely to his group at the Biozentrum allowed me to broaden my scientific knowledge.

I am grateful to all the people from the Analytical and Imaging Sciences (AIS) group for the time they dedicated to me and their valuable scientific pieces of advice.

I would like to thank especially Dr. Martin Rausch for his availability; Dr. Nicolau Beckmann for his experienced advices, great scientific explanations and his happy being; Dr. Catherine Cannet for her high-quality expertise in histology and her associates (Marinette Erard, Christelle Gérard and Jean-Marc Blum) for all they teach me and the great not-scientific moments I spent with them during AFH congresses.

A address special thanks to Dr. Hans-Ulrich Gremlich and his assistant Alexandra Suter for helpful discussions about NIRF imaging and the exciting life at Novartis.

A also express my special thanks the chemists: Dr. Rainer Kneuer for always keeping me informed of the last publications concerning my work; Dr. Philipp Schmidt and Sonia Kerrad, for their expert opinion on chemical aspects of my work and their patience to explain them to a biologist.

I would like to thanks all the people who allow me to perform specific works concerning my PhD thesis: Diana Kindler-Baumann for teaching me her expertise in practicing *in vivo* MR experiments; Dr. Anis Mir for providing me facilities and support for cell culture; Colette Kristofic for immune cell handling; Reto Haberthuer for always being available for *in vivo* stuffs; Ursula Sauder for electronic microscopy investigations; Brigitte Greiner for confocal microscopy support; Dominique Pralet and Cécile Cazaubon for FACS analysis and Dr. Hiestand and Sven Bolliger for their time and support concerning the EAE model.

Without their aid, this thesis would never have attained the present form.

I also have a thought to all the rats I sacrificed to obtain these results.

Special thanks go to all the people more friends than colleagues who shared my life at work or during my life-time in Basel and who will make my PhD time unforgettable: Stefan Zurbruegg for fun, for SchwitzerTutsch tips and his generosity; Rogério Panizzutti for bringing sun in my European life and accompanying me to do creasy things; Yann Sénéchal for psychological moments and philosophical discussions; Thomas Mueggler for his help to start my PhD life; Valentina Aureggi and Aurelien Bigot for delicious Italian diners and all things I discovered with them; Marcelin Sablone and Doris Weider for extra-lab evenings; Harry Karmouty-Quintana for correcting my English mistakes; François-Xavier Blé for caring the coffee machine but also Bruno Tigani, Annabelle Milard and Lucas Lecourtier, Gregory Gerebtzoff, André Ziegler, Alekos Tsamaloukas, Susanna Notz, André Schade, San Pun, meine Salsa Tanzpartnerinen Sandra und Linda, people from the Judo Club Kano especially Philippe Heinz for friendly randoris, people from the Gymnastic club Alsatia: the traveling circus family Sandrine, David and Emeline and particularly Jerome Wentzel for his happy being and his valuable computing skills.

Looking back to my PhD time and all the good time we spent together during my busy weekends, I have warm thoughts for Tahin, Sebastien and Laetitia, Master Greg and Virgine, Dalibor and his friends, Gillou, Sandrine and Sebastien Fluck, Sebastein Chevalier et Cindy, Christine and Gerhart, Oma und Opa Kopp, François and his gang of friends, Jerome and Line, Robert, my cousin Arnaud, Marion and Aurore, Pauline Stephanie and Caroline, Julien Tillier and his future wife, le vélo jaune pipi, Nicky, Sandrine Eric and Noëlle, as well as my aunt Denise, Evelyne and Marie-Louise.

Very warm thanks go to my family: to my parents who first gave me “the tools” to achieve this thesis and to my sister Jessy and my brother Hervé for helping me to focus my mind on really important things and always supporting me.

Finally and most of all, thanks to Claudine for making my every-day life so wonderful and always believing in me.

Contents

ABBREVIATIONS.....	10
SUMMARY.....	11
<i>INTRODUCTION.....</i>	<i>13</i>
1 NMR AND IMAGE CONTRAST.....	14
1.1 THE NMR EXPERIEMENT.....	15
1.2 RELAXATION.....	19
1.2.1 Description of T1, T2 and T2* Relaxation Times.....	19
1.2.2 Measurement of T1.....	21
1.2.3 Measurement of T2.....	22
1.3 PRINCIPLES OF IMAGING.....	23
1.3.1 Magnetic Field Gradient.....	23
1.3.2 Frequency Encoding.....	23
1.3.3 Pulse Sequences.....	24
1.4 CONTRAST MECHANISMS IN MRI.....	27
1.4.1 Spin Density - Water Proton Density.....	27
1.4.2 Magnetic Susceptibility.....	27
1.4.3 Diffusive Properties of Water.....	29
1.4.4 Proton/Spin Exchange.....	29
1.5 CONTRAST ENHANCEMENT USING CONTRAST AGENTS.....	30
1.5.1 General Requirement for Contrast Agent.....	30
1.5.2 Theoretic Consideration of Relaxivity Enhancement.....	31
1.5.3 Inner Sphere and Outer Sphere Relaxation.....	32
1.5.4 In Vivo Stability, Excretability and Toxicity.....	33
1.5.5 Contrast Agents In Vivo Distribution.....	33
1.6 T1 CONTRAST AGENTS.....	35
1.6.1 Gadolinium Compounds.....	35
1.6.2 Dendrimers.....	36
1.6.3 In Vivo Distribution.....	38
1.7 T2 CONTRAST AGENTS.....	39
1.7.1 Ferumoxides.....	39
1.7.2 In Vivo Distribution.....	41
2 NEAR INFRARED IMAGING.....	42
2.1 FLUORESCENCE.....	43
2.1.1 Excitation-Emission.....	43
2.1.2 Interactions of Light with Biological Tissues.....	44
2.2 <i>IN VIVO</i> NEAR INFRA-RED FLUORESCENCE IMAGING.....	46
2.2.1 Fluorescence Reflectance Imaging.....	46
2.2.2 Fluorescence Mediated Tomography.....	47
2.2.3 Elements for Fluorescence Detection.....	47
2.3 CONTRAST AGENTS.....	48
2.3.1 Theory.....	48
2.3.2 Cyanine Dyes.....	49

3 ORGANIZATION OF THE NERVOUS SYSTEM.....	50
3.1 CELLS OF THE CENTRAL NERVOUS SYSTEM.....	51
3.1.1 <i>Neurons</i>	51
3.1.2 <i>Myelin And Nerve Conduction</i>	51
3.1.3 <i>Glial Cells</i>	52
3.2 BLOOD VESSELS AND BLOOD BRAIN BARRIER.....	54
3.2.1 <i>Endothelium</i>	54
3.2.2 <i>Tight Junctions</i>	56
4 INFLAMMATION IMMUNE MECHANISMS.....	57
4.1 BASIS OF THE IMMUNE SYSTEM.....	58
4.1.1 <i>Cells of the Immune System</i>	58
4.1.2 <i>Cytokines, Messengers of the Immune System</i>	59
4.2 MECHANISMS OF INFLAMMATION.....	61
4.2.1 <i>Acute Inflammation Process</i>	61
4.2.2 <i>Chronic Inflammation</i>	61
4.3 CHEMICAL AND CELLULAR MEDIATORS.....	62
4.3.1 <i>Chemicals Mediators</i>	62
4.3.2 <i>Leukocytes Activation and Extravasation</i>	62
4.3.3 <i>Phagocytosis</i>	63
5 MULTIPLE SCLEROSIS AND EAE MODEL.....	65
5.1 MULTIPLE SCLEROSIS.....	66
5.1.1 <i>Definition</i>	66
5.1.2 <i>Pathology</i>	66
5.1.3 <i>Etiology</i>	67
5.2 THE EAE RODENT MODEL.....	70
5.2.1 <i>Description</i>	70
5.2.2 <i>Inoculation</i>	70
5.2.3 <i>EAE Animal Studies Inform about MS</i>	71
5.3 BRAIN INFLAMMATION IN MS AND EAE.....	72
5.3.1 <i>Immune Privilege of the Normal Brain</i>	72
5.3.2 <i>Induction of Initial Brain Inflammation</i>	73
5.3.3 <i>Amplification of the Inflammatory Response</i>	74
5.4.5 <i>Mechanisms of Immune-Mediated Tissue Damage</i>	74
5.4.6 <i>Physiopathology of MS Brain Lesions</i>	75
5.4.7 <i>Clearance of Inflammation</i>	76
6 IN VIVO MRI OF BRAIN IMPAIRMENT.....	77
6.1 MRI VISUALIZATION OF BRIAN INFLAMMATION.....	78
6.2 IMAGING OF STRUCTURAL CHANGES.....	79
6.2.1 <i>Assessment of BBB Leakage: Gd-Enhancing Lesions</i>	79
6.2.2 <i>T₂-Hyperintense Lesions and Multi-Component-T2-Mapping</i>	80
6.2.3 <i>Magnetization Transfer Contrast</i>	81
6.2.4 <i>T₁-Hypointense Lesions</i>	82
6.3 CELL LABELING.....	83
6.3.1 <i>Macrophage Tracking by MRI</i>	83
6.3.2 <i>Non-Phagocytic Cells Labeling</i>	85

7 OBJECTIVES AND OUTLINES OF THE THESIS.....	87
7.1 TRACKING TAGGED MACROPHAGES BY MRI.....	87
7.2 NEW METHODS TO LABEL T LYMPHOCYTES FOR MR AND NIRF IMAGING.....	87
7.3 OUTLINE OF THE THESIS.....	88
<i>EXPERIMENTAL SECTION</i>	89
8 MACROPHAGE LABELING FOR MRI.....	90
8.1 MACROPHAGES TRACKING DURING BRAIN INFLAMMATION.....	90
8.1.1 <i>Abstract</i>	90
8.1.2 <i>Introduction</i>	91
8.1.3 <i>Material and Method</i>	92
8.1.4 <i>Results</i>	95
8.1.5 <i>Discussion</i>	98
8.2 MONITORING MACROPHAGES: A TOOL TO EVALUATE DRUG EFFECTS.....	101
8.2.1 <i>Abstract</i>	101
8.2.2 <i>Introduction</i>	102
8.2.3 <i>Material and Method</i>	103
8.2.4 <i>Results</i>	106
8.2.5 <i>Discussion</i>	111
9 TAGGING T CELLS FOR BIOMEDICAL IMAGING.....	113
9.1 T CELLS LABELING FOR MR IMAGING: AN <i>IN VITRO</i> STUDY.....	113
9.1.1 <i>Abstract</i>	113
9.1.2 <i>Introduction</i>	114
9.1.3 <i>Material and Method</i>	116
9.1.4 <i>Results</i>	120
9.1.5 <i>Discussion</i>	129
9.2 T CELLS LABELING FOR NIR IMAGING.....	134
9.2.1 <i>Abstract</i>	134
9.2.2 <i>Introduction</i>	135
9.2.3 <i>Experimental Protocol</i>	137
9.2.4 <i>Results and Discussion</i>	143
10 OVERALL CONCLUSION.....	153
REFERENCES.....	156

Abbreviations

NMR	nuclear magnetic resonance
MRI	magnetic resonance imaging
NIRF	near infrared fluorescence
FRI	fluorescence reflectance imaging
PET	positron emission tomography
CT	computed tomography
CNS	central nervous system
BBB	blood brain barrier
MS	multiple sclerosis
EAE	experimental autoimmune encephalomyelitis
ROI	region of interest
MTR	magnetization transfer ratios
CA	contrast agent
Gd-enh	gadolinium enhancement
FeO	ferumoxides
SPIO	small particles of iron oxide
USPIO	ultra small particles of iron oxide
IHC	immuno-histochemistry
TAs	transfection agents
PLL	poly-L-lysine
PEI	poly-ethylene-imine
Tat	trans-activator peptide derived from the HIV virus
NIRF	Near-Infrared Fluorescence
Cy5.5	1H-Benz[e]indolium, 2-[5-[3-(5-carboxypentyl)-1,3-dihydro-1,1-dimethyl-6,8-disulfo-2H-benz[e]indol-2-ylidene]-1,3-pentadienyl]-3-ethyl-1,1-dimethyl-6,8-disulfo-, inner salt
dpi	Days post immunization
AT	Activated T cells coming from EAE animals
NT	Non-activated T cells coming from naïve animals

SUMMARY

MS was first described in 1868 by Charcot noting the accumulation of inflammatory cells in a perivascular distribution within the white matter of the brain and the spinal cord of patients. The autoimmune demyelination process causing the disease was first established by Thomas Rivers in 1933 with the repeated injection of rabbit and spinal cord fragment into primates to induce an EAE model. The main lesson from the use of the EAE model is that the minimal requirement for inducing inflammatory, autoimmune CNS demyelinating disease is the activation of myelin-reactive T cells in the peripheral immune system.

First applications of MR imaging to MS in the early 1980s, increased the reliability of the diagnosis and enhanced the understanding of lesion development. MR imaging with the help of contrast agents (CAs) provided new tools (e.g. T1 and T2 relaxation based methods, magnetization transfer) for detecting newly forming lesions, to differentiate them from other lesions not specific for MS, and even evaluate BBB breakdown and edema formation, as well as visualizing immune cells in the EAE model. Contrast agents such as Gd complexes or iron-based nanoparticles can be used to precisely localize zones of BBB impairment or macrophages infiltration in the brain parenchyma.

By focusing on the neuroinflammatory demyelinating processes in a rat model of EAE, the general purpose of this thesis was to develop new methods to label immune cells to identify immunological events characteristic of EAE. Macrophages and T lymphocytes are immune cells that play a major role in brain impairment. These cells have been tagged with new-generation contrast agents (CA) for monitoring their migration non-invasively using MRI and near infra-red fluorescence imaging (NIRF).

Our first goal was to label macrophages for MRI and determine their role in the three characteristic phases of the EAE model (i.e. acute, remitting and relapsing phases). As macrophages are typical phagocytotic cells, ultra small particles of iron oxide (USPIOs) have been injected intravenously in the tail vein of animals in order to be internalized by monocytes in blood circulation. Circulating monocytes loaded with iron migrated to inflammation areas in parenchymal brain tissues. MR measurement have been preformed on EAE animals and we determined iron-rich region as hypointense areas in T2-weighted images as region of interest (ROIs) for further investigations.

In addition to macrophage localization, the opening of the blood brain barrier (BBB) as well as demyelination processes have been measured by MRI mapping gadolinium (Gd) related signal enhancement and magnetic transfer (MT), respectively. By successively applying this protocol at different time points during the EAE model progression, we were able to analyse the interdependence of immuno-cellular processes leading to axonal damage as well as the longitudinal evolution of pathological hallmarks of EAE.

Furthermore, these techniques have been used to validate and quantify the anti-inflammatory effect of EDG-1 inhibitor FTY720 on EAE symptoms. Repeated USPIO administrations and MRI measurements combining the analysis of MT ratios and Gd-enhancement have been performed on vehicle and FTY720 treated animals. This study demonstrates that FTY720 can prevent inflammatory events in EAE rats by sequestering immune cells in lymphoid organs during acute inflammation episodes.

The third goal, was to translate the iron-labeling protocol from macrophages to T lymphocytes. As T cells are initiators of the immune cascade leading to the occurrence of symptoms in the EAE model, it would be highly relevant to visualize T lymphocytes prior to the onset of symptoms. Yet, as lymphocytes have no natural phagocytotic activity, *in vivo* tagging with CA was not feasible. We decided to label them *in vitro* with ferumoxides (FeO) and then, transfer iron-presenting cells adoptively to EAE animals intravenously. Different techniques have been used to evaluate the efficiency of lymphocytes labeling combining iron oxide particles with commonly available transfection agents (TAs) and the feasibility of labeling T lymphocytes *in vitro* has been demonstrated. However, the adoptive transfer of iron-tagged T cells to EAE rats did not lead to the detection of these cells by MRI.

As MR detection of iron-tagged cell *in vivo* was unsuccessful probably due to the inherent lack of sensitivity of the MRI technique for molecular changes and the dilution of labeled cells in the blood, we decided to switch to a more sensitive technique. Thus, the goal of the last part of the thesis was to label primary cultured T lymphocytes with a fluorescent dye: cyanine 5.5 (Cy5.5). The Tat peptide from the HIV virus chemically has been bound to the Cy5.5 to cargo the dye across T cells membrane. The ability of this probe to penetrate T cells and its potential toxicity has been evaluated *in vitro*. Subsequently, Cy5.5-Tat labeled lymphocytes were transferred to EAE rats in order to monitor their bio-distribution during EAE. Prominent signals have been obtained from rat brain and histological experimentation using confocal microscopy analysis have been performed to confirm the localization of Cy5.5 within the brain parenchyma.

INTRODUCTION

1 NMR AND IMAGE CONTRAST

The first section gives an overview of the physical principles governing the phenomenon of nuclear magnetic resonance (NMR). A short definition of the proton spin precedes the description of the NMR event: the interaction of an external magnetic field with nuclear spins (chapters **1.1**). Different modalities of spin relaxation (**1.2**) and principal pulse sequences used for MR imaging (MRI) (**1.3**) are presented before discussing contrast mechanisms that allow tissue discrimination by MRI (**1.4**). Specific methods for mapping animal brain by contrast enhancement (**1.5**) and commonly used contrast agents are described in the chapter **1.6**. A brief description of both T1 and T2 sensitive contrast agents is given in chapters **1.6** and **1.7**

1.1 Interaction of Magnetization with a Magnetic Field, the NMR Experiment

The intrinsic angular momentum (spin) is a fundamental property of elementary particles such as protons, neutrons and electrons. These particles called fermions possess a net spin of $1/2$. In atoms, pairs of neutrons and protons align to cancel out their spins. Nuclei with an odd number of protons and/or neutrons have a non-zero nuclear moment characterized by integer or half-integer nuclear spin quantum number I . Almost every element has an isotope with a non-zero nuclear spin (Table 1.1). NMR can only be performed on isotopes whose natural abundance is high enough to be detected. For biological applications, the most relevant nuclei are the ^1H , ^{13}C , ^{19}F and ^{31}P .

Nuclei	Unpaired Protons	Unpaired Neutrons	Net Spin
^1H	1	0	1/2
^2H	1	1	1
^{13}C	0	1	1/2
^{14}N	1	1	1
^{19}F	1	0	1/2
^{23}Na	1	2	3/2
^{31}P	1	0	1/2

List of the principal natural compound of biological tissues a non-zero net nuclear spin.

When placed in a magnetic field, nuclear magnets arrange themselves in the direction of the main magnetic field \mathbf{B}_0 . Nuclear magnets align themselves in a discrete (quantized) manner: $(2I+1)$ energy levels are observed for a nuclear spin I . Hence, for $I=1/2$ two orientations occur, either parallel or anti-parallel to the applied field B_0 (i.e. $m_I = \pm 1/2$). The energy of the two states depends on the type of nucleus characterized by the so-called gyromagnetic ratio γ and on the magnetic flux B_0 :

$$E(m_I) = -\gamma \cdot \hbar \cdot B_0 \cdot m_I \quad [1]$$

With \hbar being the Plank constant.

For nuclei with $\gamma > 0$ (e.g. proton) the state with the z-component of the spin aligned parallel to the magnetic field has a lower energy. The macroscopically observable magnetization is the vector sum of the individual nuclear magnets,

$$\vec{M}_0 = \sum_{i=1}^N \vec{I}_i \quad [2]$$

which is oriented along the static magnetic field B_0 which shall be oriented along the z-axis. The z-component of the magnetization is

$$M_{z,0} = \sum_{i=1}^N m_{I,i} \quad [3]$$

With $m_{I,i} = -I, -I+1, \dots, +I$ i.e. $2I+1$ values. For magnetic field strengths of the order of few Tesla, the energy difference between the two levels is small as compared to the thermal energy, i.e.

$$\Delta E = E(\frac{1}{2}) - E(-\frac{1}{2}) \ll kT \quad [4]$$

with k being the Boltzmann constant and T the absolute temperature in Kelvin.

As a consequence, for a field strength of 4-8 T, every 10^5 nuclei, there is about one extra aligned with the B_0 field as opposed to the field i.e. the excess population of the lower energy state is only approximately 10 ppm (part per million). This explains the inherently low sensitivity of nuclear magnetic resonance experiments.

Application of an oscillating electromagnetic field perpendicular to the main field axis (z) will deflect the magnetization from its equilibrium position, provided that its frequency corresponds to the resonance frequency, the so-called *Larmor* frequency, defined by

$$\omega_0 = \Delta E / \hbar = \{E(m_I + 1) - E(m_I)\} / \hbar = \gamma \cdot B_0 \quad [5]$$

For commonly used magnetic field strengths the resonance frequency is in the radiofrequency (RF) domain of the order of 100-500 MHz.

Application of an RF field induces

- a) transitions between the two energy states involved (in both directions) and
- b) coherences among the individual nuclear spins.

While in the absence of the of the RF field the individual spins have random phases, there transverse component aligns along the RF field leading to an observable transverse magnetization (Figure 1.1). This oscillating, hence time dependent transverse magnetization induces a voltage in a pick-up coil, the nuclear magnetic resonance (NMR) signal.

The oscillating field is commonly decomposed into two counter-rotating fields,

$$\begin{aligned} B_1(t) &= B_1 \cdot \cos \omega \cdot t = B_1 \cdot \frac{1}{2} \cdot \{(\cos \omega \cdot t + i \cdot \sin \omega \cdot t) + (\cos \omega \cdot t - i \cdot \sin \omega \cdot t)\} \\ &= B_1 \cdot \frac{1}{2} \cdot \{\exp(+i \cdot \omega \cdot t) + \exp(-i \cdot \omega \cdot t)\} \end{aligned} \quad [6]$$

It is well known that only the component that rotates in phase with the *Larmor* precession will lead to observable signals, while the anti-phase component can be neglected in a good approximation. This is the basis of the so-called *rotating frame* description of NMR experiments: the magnetic moments are randomly distributed on a surface of two cones with the axis parallel to the static magnetic field. During equilibrium for nuclei with $\gamma > 0$, the position parallel to the field requires less energy than the antiparallel one, there is an excess of dipoles in the less energetic state. The total sum of all longitudinal projections is positive and represents the equilibrium magnetization \vec{M}_0 (Figure 1.1A). There is, however, no transverse equilibrium magnetization.

This M_0 net magnetization is pointing in the direction of the main magnetic field B_0 . In a coordinate system rotating at the *Larmor* frequency around the main magnetic field axis, the RF field can be considered a static vector \mathbf{B}_1 e.g. along the y-axis of the rotating frame (Figure 1.1B). The interaction with the equilibrium magnetization causes the net magnetization \vec{M}_0 to spiral away from the B_0 field axis in the y-z plane. \vec{M}_0 rotates from a longitudinal position a distance proportional to the time length of the RF pulse. If the RF field is applied for a sufficiently long time, the component will be tilted by $\pi/2$ leading to a maximal transverse magnetization (\vec{M}_1 in Figure 1.1).

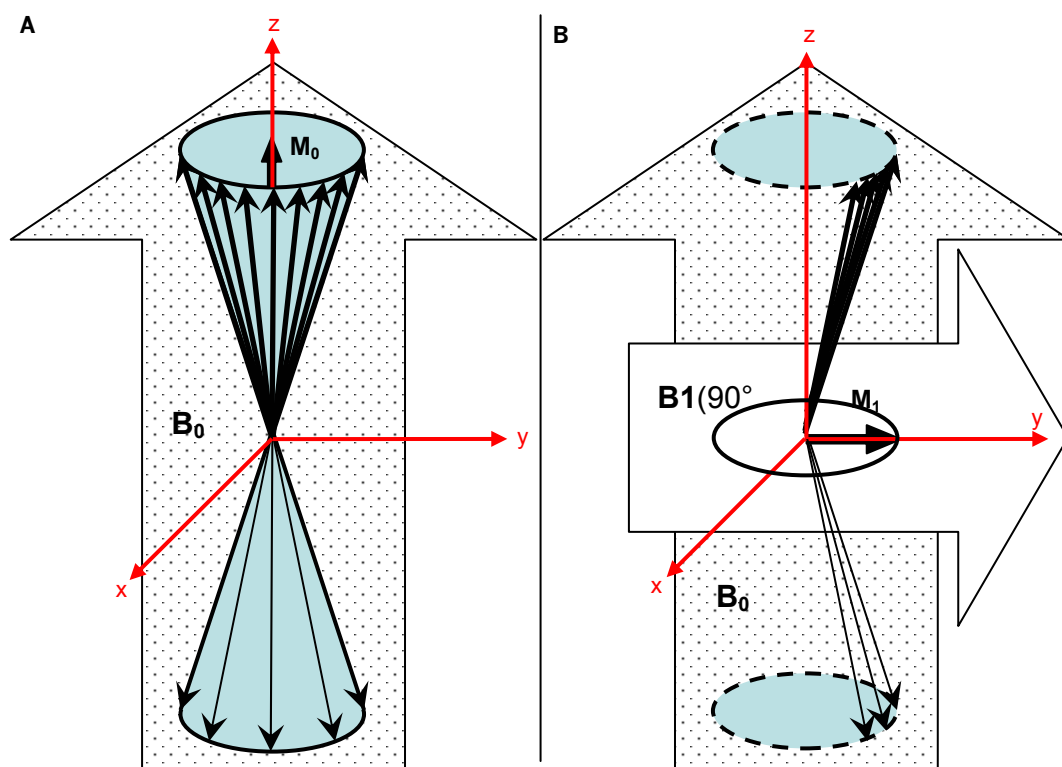
Hence, the duration t_p of the RF-pulse determines the flip angle β by which the magnetization vector(s) will be tilted,

$$\beta = \gamma \cdot \hbar \cdot B_1 \cdot t_p \quad [7]$$

Once the RF field is switched off the only interaction experienced by the magnetization is that with the static field B_0 , around which it would precess undamped in the absence of any further interactions.

Yet in a physical system, the magnetization is embedded in an environment (in a lattice), with which energy will be exchanged. This process will force the system back to equilibrium. It is phenomenologically described by introducing *relaxation times*.

Figure 1.1



At the equilibrium, the majority of proton process aligned in the direction of the main field B_0 . After applying a 90° pulse with the main B_1 field, the net magnetization M_1 process in the x-y plane at the Larmor frequency.

1.2 Relaxation

The nonequilibrium magnetization state, when left undisturbed, always returns to equilibrium after a sufficient period of time. This is named: **relaxation**.

1.2.1 Description of the T1, T2 and T2* relaxation times

T1 relaxation: time that characterizes the recovery of the longitudinal magnetization to its equilibrium value M_0 .

The return of excited nuclei (after applying B_1 field) from the high energy state to the low energy or ground state (a jump the lower cone to upper cone in the Figure 1) is associated with loss of energy to the environment i.e. surrounding nuclei or lattice. The longitudinal relaxation is also called a **spin-lattice relaxation**.

It is a tissue-specific time constant for protons, a measure of the time taken to realign with the external magnetic field. The T1 constant will indicate how quickly the spinning nuclei will emit their absorbed RF into the surrounding tissue.

T2 relaxation: time that characterizes the decay of the transverse magnetization M_1 is known as transverse relaxation time **T2**.

Microscopically, T2 relaxation or **spin-spin relaxation** occurs when spins in the high and low energy state exchange energy but does not loose energy to the surrounding environment. It happens when two spins jump at the same time: one jump upwards, the other one jump from the upper cone to the lower cone (see Figure 1.1). No energy is released to the lattice and no net change in the longitudinal magnetization occurs. Because this involves two spins, such a process is called a spin-spin relaxation. T2 is the decay of \vec{M}_1 magnetization in an ideal homogeneous field.

In a different way from T2, T2* is the spin-spin relaxation time constant that describes the decay of transverse magnetization taking into account inhomogeneities in static magnetic fields i.e. in magnetic susceptibility.

It is characterized macroscopically by loss of transverse magnetization at a rate greater than T2. The relation $T2^* \leq T2$ is always hold. Under *in vivo* imaging (and spectroscopy) conditions, the decay of transverse magnetization is governed by T2*.

Effects due to static susceptibility are deterministic. That means that the signal lost due to T_2^* relaxation can be recovered (see spin echo sequences section 1.4.3)

Relaxation times depend on the microphysical environment of the spins and, hence, are tissue-specific. They form a principal source of contrast in MR images (Table 2).

Table 1.2

Material	T1(msec)	T2(msec)
Pure water	2000-3000	2000-3000
CSF	800-20 000	110-2000
White matter	760-1080	61-100
Grey matter	1090-2150	61-109
Meninges	500-2200	50-165
Muscle	950-1820	20-67
Fat	200-750	53-94

The hydrogen T1 and T2 values at 1.5 T for common brain tissues are listed in the following table. In biological materials, the T2 time is considerably shorter than the T1 time.

For example, due to the slow molecular motion of lipid molecules, longitudinal relaxation occurs rather rapidly and longitudinal magnetization is regained quickly leading to a short T1 time for fat. Water relaxes not as efficient as fat due to the high mobility of the water molecules. Water nuclei do not give up their energy to the lattice as quickly as fat, and therefore take longer to regain longitudinal magnetization resulting in a long T1 time. This illustrates that the composition of tissue has a pronounced effect on the longitudinal relaxation, i.e. T1.

Via a spin-spin interaction, spins lose their phase coherence, which results in a loss of transverse magnetization. T2 relaxation is temperature dependent. At a lower temperature molecular motion is reduced and the decay times are reduced. Fat has a very efficient energy exchange and therefore it has a relatively short T2. Water is less efficient than fat in the exchange of energy, and therefore it has a long T2.

Relaxation can be strongly influenced by administration of contrast agents, i.e. compounds with unpaired electron spins, which possess a magnetic moment that is two to three orders of magnitude larger than that of proton spins (see section 1.6). Before discussing contrast agents we will address methods that allow the measurement of relaxation times.

The inverse of relaxation time is called relaxation rate or relaxivity and has a unit of $[s^{-1}]$.

$$R1 = \frac{1}{T1} \quad [8]$$

$$R2 = \frac{1}{T2} \quad [9]$$

1.2.2 Measurement of T1

Of T1 measurements, the longitudinal magnetization is not detectable. The basic principle is to generate non-equilibrium longitudinal magnetization, wait for relaxation to occur and then apply a RF pulse to generate observable transverse magnetization. The two classical methods are the application of a saturating pulse or of an inversion pulse. Immediately after the pulse the longitudinal magnetization is given by $M_z(0) = 0$ or $M_z(0) = -M_0$, respectively. The system will return to equilibrium as a function of the time T evolved after the pulse,

$$M_z(t) = M_0 \cdot \left\{ 1 - \frac{M_0 - M(0)}{M_0} \cdot \exp(-t/T_1) \right\} \quad [10]$$

which becomes

$$M_z(t) = M_0 \cdot \{1 - \exp(-t/T_1)\} \quad [11]$$

for the saturation recovery and

$$M_z(t) = M_0 \cdot \{1 - 2 \cdot \exp(-t/T_1)\} \quad [12]$$

for the inversion recovery experiment provide the application of ideal saturation and inversion pulses. For the saturation recovery experiment, T_1 is the time at which the magnetization has recovered to $1 - e^{-1} = 0.67$.

An alternative method to assess T1 values is rapid pulsing, with the inter-pulse delay (= repetition delay) $TR \ll T1$. The transverse magnetization then becomes

$$M_{xy}(0) = M_0 \cdot \sin \beta \cdot \frac{1 - \exp(-TR/T_1)}{1 - \cos \beta \cdot \exp(-TR/T_1)} \quad [13]$$

where β being the pulse angle.

The optimal pulse angle is given by the Ernst angle

$$\cos \beta_{opt} = \exp(-T_R / T_1) \quad [14]$$

which for short TR values is much smaller than $\pi/2$. The principle of rapid pulsing is applied in the so-called gradient-recalled imaging or FLASH imaging methods [Haase *et al.*, 1987].

1.2.3 Measurement of T2

T2 accounts for the loss of phase coherence due to spin-spin interaction. It is measured using spin-echo pulse sequences, which compensate for the signal loss due to differences in magnetic susceptibility.

A basic spin echo sequence is the Carr-Purcell-Meiboom-Gill (CPMG) sequence (see chapter 1.4.3). T2 values are derived from the decay of the echo envelope in a CPMG sequence, which is governed by

$$M(t) = M(0) \cdot \exp(-t / T_2) \quad [15]$$

At a time $t = T_2$ the signal amplitude has decayed to $1/e = 0.33$ of the original value.

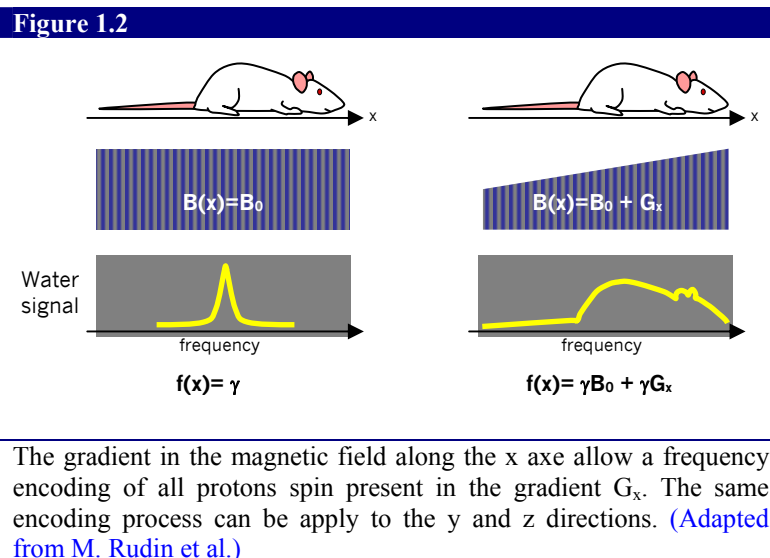
1.3 Principles of Imaging

1.3.1 Magnetic Field Gradient

A gradient in the magnetic field is what will allow to distinguish each spin from his neighbor image his position in the magnetic field. A magnetic field gradient is a variation in the magnetic field with respect to position. The most useful gradient in MRI is a one-dimensional linear magnetic field gradient. For example, when applied along the x-axis, the effective field seen by a proton at location X is defined as the sum of the static field B_0 plus the corresponding gradient field G_x , i.e.

$$B(x) = B_0 + G_x \cdot X$$

The magnetic gradient along the three x, y, and z directions are commonly labeled G_x , G_y , and G_z .



1.3.2 Frequency Encoding

The isocenter of the magnet is the point in the center of the magnet where $(x,y,z) = 0,0,0$. The magnetic field at the isocenter is B_0 and the resonant frequency is ω_0 . If a linear magnetic field gradient is applied to different spin containing regions, each regions experience different magnetic fields. Hence the NMR signal is dispersed along to the gradient field. The amplitude of the signal is proportional to the number of spins in a plane perpendicular to the gradient.

This procedure is called frequency encoding and causes the resonance frequency to be proportional to the position of the spin (see Figure 1.2).

1.3.3 Pulse sequences

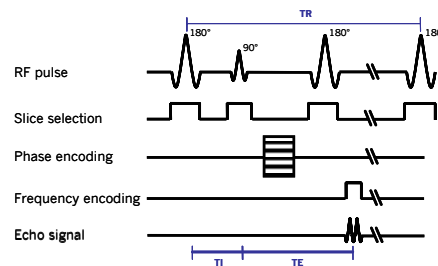
Pulse sequences are a preselected set of defined RF and gradient pulses, usually repeated many times during a scan, wherein the time interval between pulses, the amplitude and shape of the gradient waveforms will control NMR signal reception and affect the characteristics of the MR images.

A recommended shorthand designation of inter-pulse times and excitation pulse used to generate a particular image is to list the repetition time (TR), the echo time (TE) and, if using inversion recovery, the inversion time (TI) with all times given in milliseconds and if using a gradient echo sequence the flip angle.

Variations in the value of TR and TE have an important effect on the control of image contrast characteristics. Short values of TR (less than e.g. 1000 ms) and TE (less than e.g. 25 ms) are common in images exhibiting T1 contrast. Long values of TR (greater than e.g. 1500 ms) and TE (greater than e.g. 60 ms) are common in images exhibiting T2 contrast. Middle TR values (e.g. from 1000 to 1500 ms) and middle TE values (e.g. from 25 to 60 ms) are common for density weighted contrast. The values are depending on the field strength. TR is also a major factor in total scan time. As a rule, if the TR is sufficiently short, all tissues will show a range of only partial recovery of longitudinal magnetization (M_0), which will maximize T1 differences. As TR is increased, the overall signal increases, but T1-weighted contrast decreases. When inserting a delay between signal excitation and detection, signal from all tissues will be associated with varying degrees of T2-related spin dephasing. As TE is increased, the overall signal decreases, but T2-weighted contrast increases.

Inversion recovery (IR) This sequence involves a 180° . The inversion recovery sequence is specified in terms of three parameters, inversion time, TR and TE. The inversion recovery sequence has the advantage, that it can provide very strong contrast between tissues having different T1 relaxation times or to suppress tissues like fluid or fat (Figure 1.3).

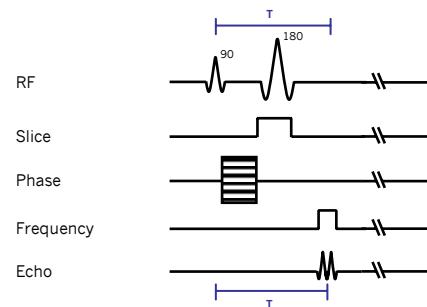
Figure 1.3



Pulse sequence timing diagram of an “Inversion Recovery” sequence.

The Carr-Purcell-Meiboom-Gill sequence A basic spin echo sequence is the Carr-Purcell-Meiboom-Gill (CPMG) (see Figure 1.5) sequence [Wehrli *et al.*, 1984].

Figure 1.5

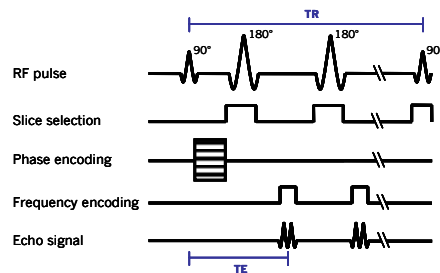


The Carr-Purcell-Meiboom-Gill sequence.

This type of sequence consist of a 90° RF pulse followed by successive 180° pulses and is useful for measuring T2 weighted images. It is a modification of the Carr-Purcell RF pulse sequence, with 90° phase shift in the rotating frame of reference between the 90° pulse and the subsequent 180° pulses in order to reduce accumulating effects of imperfections in the 180° pulses. Suppression of effects of pulse error accumulation can alternatively be achieved by switching phases of the 180° pulses by 180° .

Spin-echo sequence The spin echo pulse sequence is a commonly used pulse sequence. The pulse sequence timing can be adjusted to give T1-weighted, proton density, and T2-weighted images. The two variables of interest in spin echo sequences are the TR and the TE. All spin echo sequences include a slice selective 90 degree pulse followed by one or more 180 degree refocusing pulses.

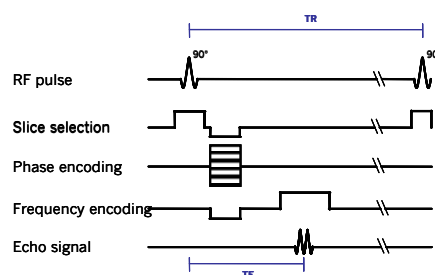
Figure 1.4



Pulse sequence timing diagram of an “Spin Echo” sequence.

Gradient echo sequence The gradient echo sequences show a wide range of variations compared to the spin echo sequences. Not only is the basic sequence varied by adding dephasing or rephasing gradients at the end of the sequence, but there is a significant extra variable to specify in addition to things like the TR and TE. This variable is the flip or tip angle of the spins. The flip angle is usually at or close to 90 degrees for a spin echo sequence but commonly varies over a range of about 10 to 80 degrees with gradient echo sequences. This so-called Ernst-angle is an angle less than 90° optimized to have the best signal-to-noise ratio considering a given TR. For the basic gradient echo sequence the larger tip angles give more T1 weighting to the image and the smaller tip angle give more T2* weighting to the images.

Figure 1.6



Pulse sequence timing diagram of an “Gradient Echo” sequence.

1.4 Contrast Mechanisms in MRI

Image contrast in MRI is based on differences in magnetic resonance signal between tissues. The determinants of signal and contrast in MRI are numerous. Spin density, magnetic susceptibility, diffusive properties of water, proton/spin exchange and all characteristics of the tissue that influence NMR signal are the parameters that can be manipulated for the purpose of contrast enhancement.

1.4.1 Spin density – Water proton density (ρ)

This is the number of resonating spins (protons) per unit volume in an NMR experiment. The maximum potential signal coming from any one given tissue is directly proportional to the fraction of protons that contribute to this signal. Most protons in human tissues are associated with water and most tissues typically consist of 60% to 80% water. Moreover, water protons outnumber by far other protons in organic components. As the tissue-water content is relatively constant, each tissue has its respective signal intensity. Yet, contrast among different tissues is weak

An alteration of the spin density to enhance the contrast would require significant changes in the water content. Hence, the diagnostic value of spin-density contrast is generally low.

1.4.2 The magnetic susceptibility (χ)

The magnetic susceptibility is the degree of magnetization of a material in response to a magnetic field. All forms of the matter like solid liquid or gas, possess the macroscopic property of magnetic susceptibility. From a general point of view, diamagnetic compounds have small negative susceptibility, paramagnetic substances have positive susceptibilities and superparamagnetic and ferromagnetic materials have large positive susceptibilities.

Diamagnetic material Most of biological or organic tissues as well as inorganic materials are diamagnetic. Diamagnetism is a very weak form of magnetism that is only exhibited in the presence of an external magnetic field. It is the result of changes in the orbital motion of electrons due to the external magnetic field. Diamagnetic substances do not have unpaired electrons; the magnetic moment of paired electrons is essentially zero. Therefore, diamagnetic susceptibility by itself has little effect in NMR and is of little interest as a contrast magnet.

Materials like water, copper, nitrogen, barium sulfate and most of the tissue constituents are diamagnetic.

Paramagnetic material Substances with positive susceptibility are known as paramagnetic and are attracted by magnets. Paramagnetism is the tendency of atomic magnetic dipoles, in a material that is otherwise non-magnetic to generate individual magnetic moments when an external magnetic field is applied. When the external field is turned off, magnetic moments will lose their alignment. Paramagnetic materials include oxygen and ions of various metals like aluminum, calcium, platinum and sodium. These ions have unpaired electrons, resulting in a positive magnetic susceptibility. The effect of paramagnetic materials on MRI is increase in the T1 and T2 relaxation rate.

Ferromagnetic material There is a third, rather broad class of materials that have extremely high, positive susceptibility. These materials are known as ferromagnetic. Ferromagnetism is a phenomenon by which a material can exhibit a spontaneous magnetization, and is one of the strongest forms of magnetism. Ferromagnetic materials generally contain iron, nickel, cobalt. When placed in a magnet field, the field strength is much stronger inside the material than outside. Ferromagnetic materials are also characterized by being made up of clusters (10^{17} to 10^{21} atoms) called magnetic domains, that all have their magnetic moments pointing in the same direction. The ability to remain magnetized in absence of magnetic field is a distinguishing factor compared to diamagnetic, paramagnetic materials.

Superparamagnetic material Superparamagnetic material consists of individual ferromagnetic domains of an elements that have paramagnetic properties in bulk. Their magnetic susceptibility is between that of ferromagnetic and paramagnetic materials. In an applied field these domains align with the field, setting up a very large and positive magnetization; but, in absence of external field, they lose the magnetization and return to random orientations similar to paramagnetic substances. Examples of a superparamagnetic material include iron containing contrast agents for bowel, liver, lymph nodes and brain imaging.

1.4.3 Diffusive properties of water

Diffusion is the process by which water molecules or molecular substances mix and migrate due to their random thermal motion. These diffusive processes mean that particles move from areas of high to areas of low concentration, leveling out concentration gradients. The distribution of vessels including capillaries within tissues is such that transport over macroscopic distances is accomplished by the blood circulation, while intercapillary distances are covered by molecular diffusion.

MRI provides a sensitive technique for measuring diffusion of some substances in particular water. MR imaging is sensitive to diffusion, because the diffusion of water molecules along a field gradient reduces the MR signal. In areas of lower diffusion the signal loss is less intense and the display from this areas is brighter.

1.4.4 Proton/Spin exchange

In MRI, signal strength is directly proportional to the total concentration of water protons (proton density). Protons in macromolecules and water molecules that are bound to macromolecules are normally not visible due to their very short T_2 relaxation times. T_2 relaxation time in macromolecules is much shorter than that of bulk water. In order to get a signal from these protons, magnetization transfer contrast techniques have to be applied, which saturates the magnetization of macromolecule-bound water protons, but ideally does not affect the magnetization of the protons of bulk water [Balaban *et al.*, 1992]. During the pulse sequence, the saturated protons may enter the free pool of protons of bulk water, or may transfer their longitudinal magnetization to free water protons which lead to a decrease of the MR signal of the bulk water. Any water molecules in contact with the protein might be capable of exchanging magnetization with the protein. Therefore saturating water molecules bound to the protein will affect the signal and the contrast between water in contact and not in contact with the protein.

One use of magnetization transfer is to increase the visibility of areas of demyelination (e.g. multiple sclerosis). In this case, protons bound to myelin will transfer their magnetization to bulk water, leading to a localized loss of signal proportional to the amount of myelin present in this area.

1.5 Contrast Enhancement using Contrast Agents

1.5.1 General requirement for contrast agent

Contrast agent (CA): the principle aim to use contrast agents in MR imaging is to enhance the contrast between different anatomical regions otherwise undistinguishable to the MR imaging techniques.

This often occurs when a lesion is too small and is lost because of partial-volume averaging with other tissues or if its tissue properties are too similar to these of surrounding tissues [Okuhata, 1999]. The presence of paramagnetic or superparamagnetic material affects the T1 and/or T2 relaxivity of the protons in water. Physiological and structural differences of neighboring tissues allow or prevent the accessibility of CA to these tissues. As a result, the concentration of CA will vary amongst tissues, resulting in an enhanced contrast [Gibby, 1988] [Sobol, 1994; Lauffer, 1990].

The first requirement for a good CA is the ability to interact magnetically with hydrogen nuclei (of water molecules) to influence their magnetic properties [Hendrick and Haacke, 1993]. This is related to the number of unpaired electrons in the outer electron shell of an atom that overwhelmingly determines its effect as a relaxation CA (see Table 1.3).

The second requirement is that MR contrast agent be capable of reversibly binding water molecules in order to provide a rapid exchange of water molecules between binding sites close to the CA and bulk water [Kirsch, 1991]. This rapid exchange of magnetic properties between near water molecule and bulk water is at the origin of the enhanced contrast.

Table 1.3

Element	Unpaired electrons	Net magnetization moment (magneton)	Electron spin Relaxation time (sec)
Transition metals			
Cr ²⁺	4	4.9	10 ⁻¹¹ -10 ⁻¹²
Mn ³⁺	4	4.9	10 ⁻¹⁰ -10 ⁻¹¹
Fe ³⁺	5	5.9	10 ⁻⁹ -10 ⁻¹⁰
Fe ²⁺	4	5.1	10 ⁻¹⁰ -10 ⁻¹¹
Lanthanides metals			
Gd ³⁺	7	7.6	10 ⁻⁸ -10 ⁻⁹
Eu ²⁺	7		10 ⁻¹² -10 ⁻¹³
Tb ³⁺	6	9.5	10 ⁻¹²

Metals which have unpaired electrons that interact with water molecules to enhance the magnetic relaxation of protons. The unit generally used for net magnetization moment is *the magneton*. 1 magneton = magnetic moment of one proton H⁺. [Hendrick and Haacke, 1993]

1.5.2 Theoretic consideration of relaxivity enhancement

Paramagnetism The large local fields of the moments of magnetic dipoles in paramagnetic substances can potentially enhance the relaxation rates of water protons bound to or in the vicinity of ions [Mendonca-Dias *et al.*, 1983; Lauffer, 1987]. It is the coupled interaction between the ions (lattice) and the protons that leads to changes in the relaxation. This provide a direct effect on T1 (energy exchange between spin and lattice) but also in the T2 (see Table 1.4).

Table 1.4

CA	Effect on T1	Effect on T2 or T2*	Number of atomic dipoles per molecule or particle
Paramagnetic material	Decrease	Decrease	1
Superparamagnetic particles	Little change	Marked decrease	10 ¹⁰
Ferromagnetic particles	Little change	Dramatic decrease	10 ¹²

The following table sums up the ability of different CA to influence the T1 or T2 relaxation time. (Adapted from [Hendrick and Haacke, 1993])

Superparamagnetism For superparamagnetic substances, a much greater influence occurs compared to paramagnetic materials due to the significantly larger magnetic moment [Wood and Hardy, 1993]. This results in more inhomogeneities (compared to paramagnetism) in the magnetic field that lead to a shortening of T2 and T2* that far exceed any degree of T1 reduction [Pochon *et al.*, 1997].

The theoretical explanation for the effect of contrast agents on tissue relaxation rates (R1 and R2) was given first by Solomon [Solomon, 1955] and Bloembergen [Bloembergen *et al.*, 1948]. The effect of a CA on tissue relaxation rates is in direct linear proportion to the concentration of the CA ([CA] in millimole per liter):

$$R1_{observed} = R1_{inherent} + r1 \times [CA] \quad [16]$$

$$R2_{observed} = R2_{inherent} + r2 \times [CA] \quad [17]$$

where *observed* and *inherent* denotes tissue relaxation properties with CA and without CA and r1 and r2 being the molar relaxivity of the contrast agent in the respective tissue.

The Solomon-Bloembergen equations are presented and described in detail in other articles [Kucharczyk *et al.*, 1991].

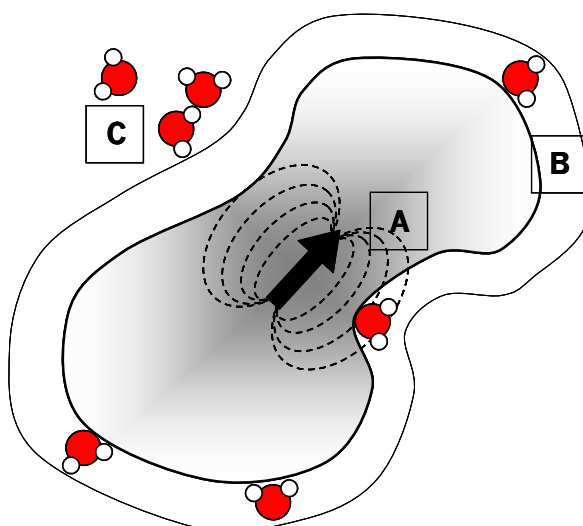
1.5.3 Inner sphere and outer sphere relaxation

When a small amount of paramagnetic compound is dissolved in water, water molecules exchange between three different molecular environments [Lauffer, 1987].

First, there is the bulk water, or regions sufficiently far from the CA which are not effected by the magnetic properties of the agent. The dipole-dipole intermolecular behavior between paramagnetic centers of the CA and hydrogen atoms of water molecules decreases rapidly as the distance separating the dipole increase. Any proton attached to a water molecule that is separated from the paramagnetic center by more than three other water molecules is practically unaffected by the magnetic moment of the paramagnetic material (C in the Figure 1.7). Other water molecules bind close enough to paramagnetic material have an ion-dipole interaction that have a very short half-life. This interaction lasts however long enough to ensure a strong interaction of proton with the electronic dipole. The water molecule binds to the paramagnetic ligand and the water is said to be coordinated and belongs to a hydration sphere (inner-sphere) (Figure 1.7A).

The third environment, often labeled as outer sphere, is defined as the transition region between the inner-sphere and the bulk water. This environment describes water molecules that diffuse close enough to interact with the paramagnetic center via intermolecular dipole-dipole coupling but are not otherwise bound to the paramagnetic agent (Figure 1.7B).

Figure 1.7



Adaptation from [Sobol, 1994]. The three water environment in the vicinity of a paramagnetic ligand. A=hydration (inner-sphere) environment; B=outer-sphere environment; C=bulk water

It is clear that the hydration water, being close to the paramagnetic center, would interact strongly with the electronic dipole, and thus its relaxation rate of these molecules should be greatly enhanced. The rapid exchange of water molecules bound to the CA and bulk water molecules enhances the paramagnetic effect beyond the volume of the CA.

1.5.4 *In vivo stability, excretability and toxicity*

After the intravenous injection, the concentration of the contrast agent increases, then starts to decrease as it is eliminated from the tissues. In general, a contrast enhancement is obtained by one tissue having a higher affinity or vascularity than another.

The CA must be absolutely non toxic for the patient [Oksendal and Hals, 1993]. The acute or chronic toxicity for an metal complex CA is related to its stability *in vivo* and its tissue clearance behavior. At doses required for MR relaxation rate changes, transition metals and the lanthanide ions are relatively toxic [Lauffer, 1990].

Therefore, these ions have to be chelated (see definition) in order to form an inert non-toxic complex for the organism. The chelation between the metal ion and ligand neutralizes the avidity of each partner for binding to proteins, enzymes, or membranes via electrostatic, hydrogen bonding interaction or covalent bonds.

Chelation: process of reversible binding of an organic ligand, the chelator or chelating agent, to a metal ion, forming a metal complex, the chelate.

A diagnostic agent should be efficiently eliminated from the body within minutes or few hours after administration and the stability is therefore required only for this period of time [Luckey and Venugopal, 1977]. With chelation of these ions, elimination rate is increased thereby reducing the chance of long term toxicity.

1.5.5 *CA in vivo distribution*

The *in vivo* distribution of CA is another approach to categorize the substances. Historically, the first class of CA distributed into the intravascular and interstitial space. These unspecific agents allow the evaluation of physiological parameters such as the status of BBB or the renal function. However, to improve diagnostic accuracy, compounds with tissue-specific distribution are needed [Oksendal and Hals, 1993]. Due to their physico-chemical properties, each CA has a specific behavior within the body.

Intravascular agents, also known as blood pool agents, remain in the blood for extended periods of time rather than diffusing quickly into the interstitial spaces [Okuhata, 1999]. The renal-specific agent accumulate in the kidneys due to their glomerular filtration [Rusinek *et al.*, 2004]. CA designed for hepatic imaging can be divided into nonspecific, extracellular space directed, reticuloendothelial system- (RES) selective, and hepatocyte-selective compounds. Based on their specificity, these CA provide either information on vascularization and perfusion or more "functional" information (RES CA) [Helmberger and Semelka, 2001]. For lymph-nodes imaging, many CA are available either to discriminate tumoral and normal parenchyma or to see cells of the immune system [Ishikawa and Anzai, 2002; Weissleder *et al.*, 1990]. Finally, using MRI to localize malignant tumors need the use of specific agent that accumulates only in malignant tissues [Shahbazi-Gahrouei *et al.*, 2001].

1.6 T1 Contrast Agents

T1 contrast agents enhance contrast by shortening T1 relaxation. Because they increase signal intensity in T1 weighted images they are therefore also called “Positive contrast agent”. They are typically small molecular weight compounds containing paramagnetic substances which make them good T1 relaxation agents (see section 1.3.1). Most T1 agents in use are Gadolinium (Gd) chelates.

These agents produce predominantly spin-lattice relaxation effects because of the fast exchange of the water molecules from a close vicinity to the bulk water [Lauffer, 1987]. However, paramagnetic materials causes both T1 and T2 shortening (see Table 1.4), but at low concentrations, the T1 shortening dominates the signal intensity.

1.6.1 Gadolinium compounds

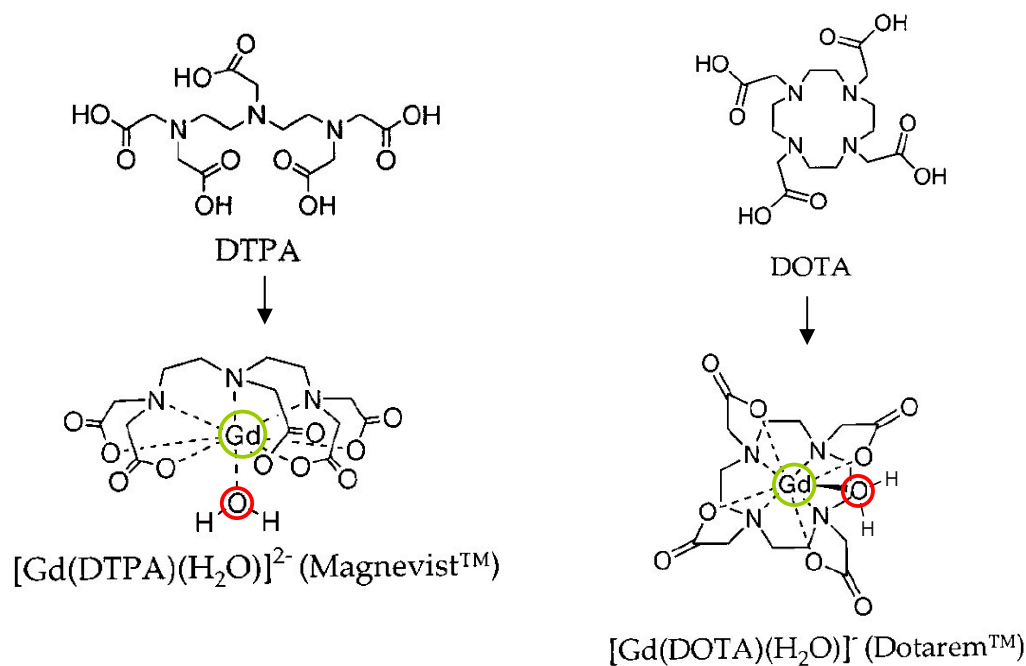
All Gd chelates are paramagnetic compounds which shorten mainly the T1 relaxation time of local water molecules increasing their intensity on T1-weighted images [Caravan *et al.*, 1999].

Structure Gd chelates associated with proper ligands actually remain chelated in the body and are excreted intact. Ligands such as DTPA (diethylenetriamine pentaacetic acid) or DOTA (1,4,7,10-tetraazacyclododecane-N,N',N'',N'''-tetraacetic acid) form complexes stable enough so that, for the period that the agent is in the body, there is no detectable dissociation (see Figure 1.8).

Due to the large size of the metal ion, lanthanides favor high coordination numbers with water molecules. All gadolinium(III)-based chelates approved for use in MRI are nine-coordinate complexes with the chelating ligand occupying eight binding sites at the metal center, the ninth coordination site is accessible by a solvent water molecule.

Stability and toxicity The free gadolinium ion is unsuitable for clinical use due to high toxicity, however, the metal chelate is metabolically inert. Gd chelates are hydrophilic and thus do not penetrate cells. There are no nitrogen groups or intercalating groups to attack DNA molecules. The metal ion is buried in the cage protected by the multidentate ligand; it is unlikely to bind to donor groups in proteins and enzymes. The structure is not susceptible to nucleophile or electrophile attack [Lauffer, 1987].

Figure 1.8



Commonly, the chelation of Gd(III) with diethylenetriamine pentaacetic acid (DTPA) or 1.4.7.10-tetraazacyclododecane-N,N',N'',N'''-tetraacetic acid (DOTA), form a strongly paramagnetic, stable complex. The interaction between the Gd atom and a free water molecule is illustrated with colors.

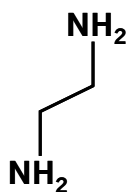
1.6.2 Dendrimers

Dendrimers are three-dimensional (not planar), oligomeric structures prepared by reiterative reaction sequences starting from smaller “core” molecules, as shown schematically in Figure 1.9. The highly branched, nearly monodisperse structure of dendrimers has led to a number of interesting molecular attributes for this relatively new class of macromolecule [Kobayashi and Brechbiel, 2004].

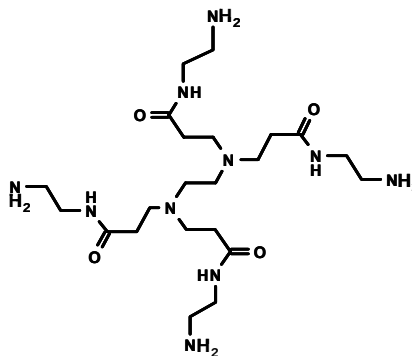
The potential advantages of Gd chelate dendrimer conjugates include the fact that dendrimers, such as the Starburst polyamidoamine (PAMAM) dendrimers (see Figure 1.9C), have uniform surface chemistry, narrow molecular weight distribution and minimal shape variation.

Figure 1.9

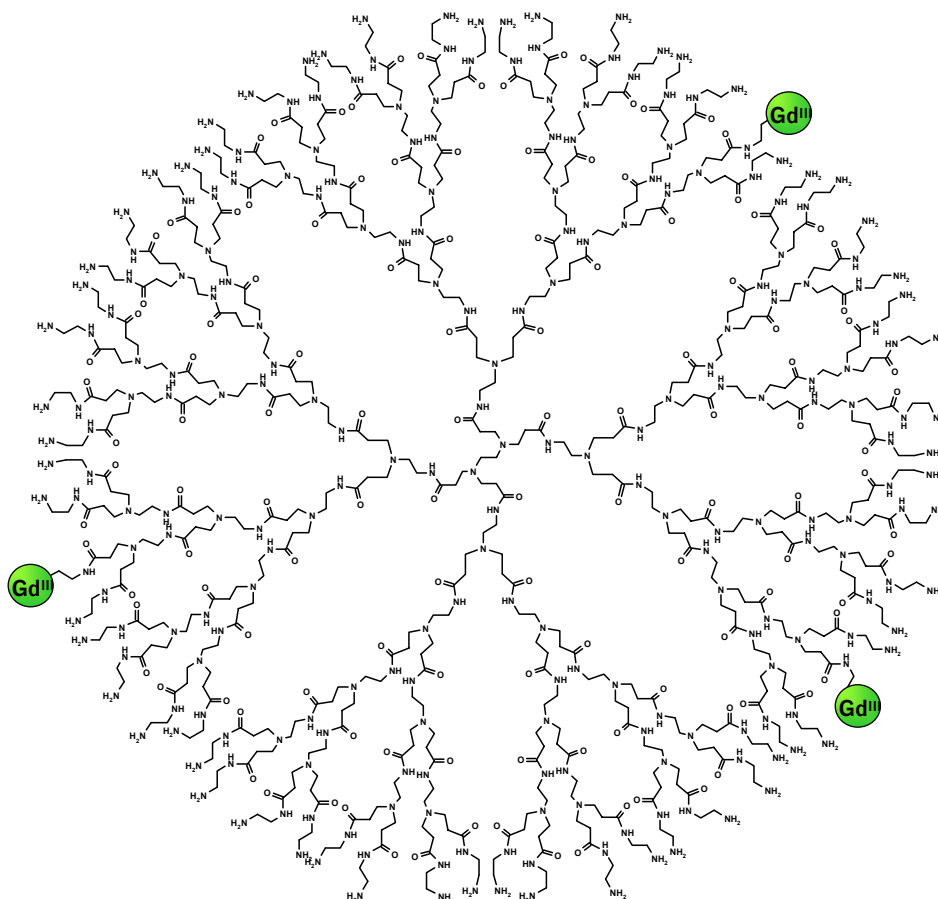
A



B



C



A represents the core molecule. B is a dendrimer of first generation. C is a schematic representation of the 4th generation on which Gd compounds have been fixed.

1.6.3 In vivo distribution

This class of T1 contrast agents represents the dominant use of MRI contrast media in radiology. After intravenous injection, the bolus rapidly distributes into the entire blood plasma pool and distribute nonspecifically throughout the plasma and interstitial space of the body [Hendrick and Haacke, 1993] with the exception of the brain where the agent does not penetrate the intact BBB and thus stays entirely in the plasma compartment of the capillary bed [Oksendal and Hals, 1993]. The agents are excreted by the kidneys with an elimination half-life of 1.5h. Concerning the best known extracellular Gd-containing CA, Gd-DTPA, standard doses are 0.1 mmol/kg of body weight. Regardless of the type of Gd-based extracellular CA, these compounds have a relatively low rate of side effects, and all of them can be bolus injected.

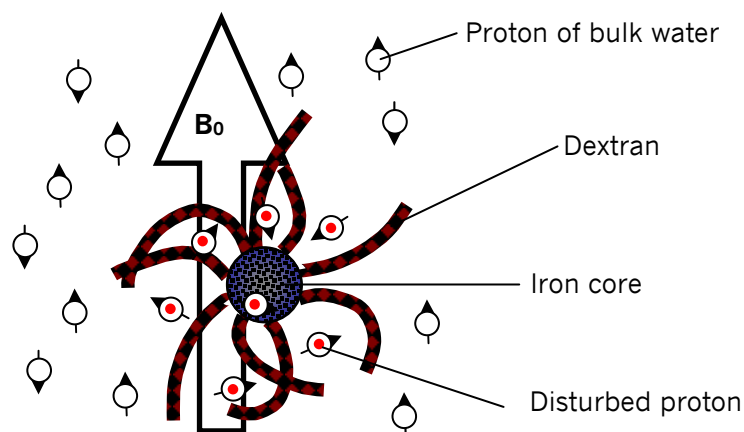
1.7 T2 Contrast Agents

SPIOs and USPIOs: Small Particles of Iron Oxide and Ultra Small Particles of Iron Oxide
They are commercially available small particulate aggregates of iron oxides. These T2 CAs lead to a loss of signal intensity due to increased transverse relaxation. Areas with high CA contents appear dark on MR images, they are therefore also called “negative contrast agents”.

1.7.1 Ferumoxides

Structure Iron cores are composed of magnetically active iron oxide crystals which range from about 1 to about 50 nm in diameter [Groman *et al.*, 1989]. The core may be alternatively coated or associated by the mean of hydrogen bonds with a polysaccharide (e.g. dextran), a protein or a polypeptide [Bulte *et al.*, 1993] [Bach-Gansmo, 1993]. With coating, the overall particle diameter ranges from about 1 to about 500 nm. The coating can serve as a base to which various biological molecules can be attached. Polymer coatings grafted onto the iron oxide core during synthesis are necessary to provide stability of the iron oxide in aqueous solutions and in vivo [Nicolle *et al.*, 2002]. The type of surface coating and the geometric arrangement of the polymer on the iron oxide core determine not only the overall size of the colloid, but also play a significant role in biokinetics and biodistribution (Figure 1.10).

Figure 1.10



Dextran-Coated superparamagnetic iron oxide particles induce microscopic magnetic field inhomogeneities that lead to a rapid dephasing of proton spins (red dots) and loss of imaging signal.

Stability and toxicity Surface charge is known to play an important role in blood half-lives of colloids and polymers [Oksendal and Hals, 1993]. It is generally agreed that a strong positive and negative charge decrease circulation time. The biodistribution of iron oxide preparations is also determined by particle size. Most iron oxides have a relatively short blood half-life (minutes) and their primary application is for imaging of liver, spleen and the gastro-intestinal tract [Helmberger and Semelka, 2001]. Long-circulating iron oxides (hours) [Pochonet *et al.*, 1997], however, are very useful for imaging of the vascular compartment (magnetic resonance angiography), and for perfusion imaging [Ostergaard, 2004], neurofunctional imaging [Bradley, 2004], imaging of lymph nodes, receptor imaging, and target specific imaging [Laurent *et al.*, 2004] (Table 1.5).

Iron oxides have been shown to degrade *in vivo* with iron mobilization and utilization according to natural iron pathways [Emerit *et al.*, 2001]. Iron is a useful component of cytochromes, oxygen-binding molecules (hemoglobin, myoglobin) and some enzymes [McCord, 1998].

Table 1.5

Property	AMI-25/ENDOREM	AMI-227/SINEREM	MION
Fe (mg/ml)	11	20	8.25
Mean particle size	60-150	11.5	8
R1 in buffer (mM/s)	24	21	16.5
R2 in buffer (mM/s)	107	44	34.8
Plasma Half-life	10 min*	>24 h (human)	>4 h

Properties of various Superparamagnetic Iron-oxide based Contrast agents
 * Proposed value in man; no information was available about the plasma half-life of Endorem in rodents

However, iron can also damage tissues by catalyzing the conversion of superoxide and hydrogen peroxide to free radical species that attack cellular membranes, proteins and DNA [Gutteridge *et al.*, 1982]. Once inside the cells, particles are clustered within lysosomes. Degradation of iron oxides into iron and oxygen is presumed to occur in intracellular lysosomes of macrophages under the influence of a variety of hydrolytic enzymes, low pH and proteins participating to iron metabolism.

1.7.2 *In vivo* distribution

Medium sized and large particles (> 30nm diameter) tend to accumulate in the spleen and lung while small particles (< than 30nm) accumulate preferably in the liver, bone marrow and lymph nodes. USPIO have a potential to improve differentiation of metastatic from inflammatory lymph nodes while normal lymph nodes appear black on T2* weighted images due to a massive uptake of USPIO [Ishikawa and Anzai, 2002] [Shah *et al.*, 2003].

Metastatic lymph nodes remain unchanged in signal intensity due to the lack of phagocytotic activity. Another application is liver imaging: CAs are either specifically targeted to hepatocytes (Mg or Gd-based compounds) or are accumulated in the reticuloendothelial system (RES) of the liver (Kupffer cells) and the spleen (e.g. SPIO) to allow discrimination between normal tissues and tumors.

2 NEAR INFRARED IMAGING

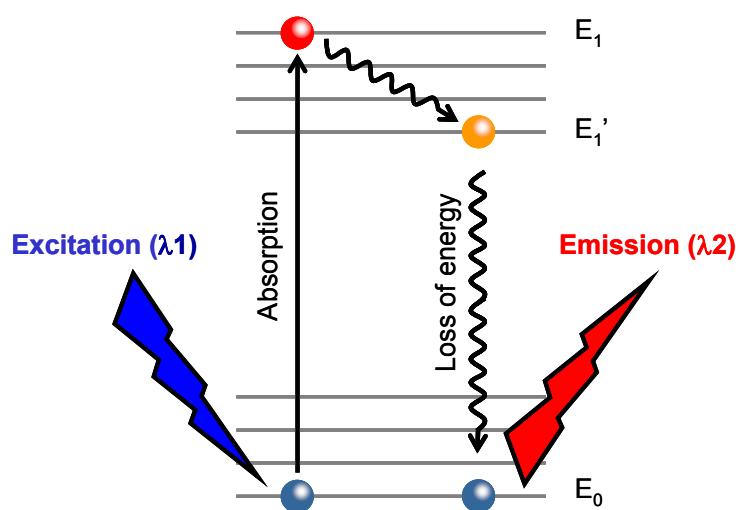
The second section is firstly dedicated to fluorescence optical imaging in general and then focuses on the applications of using near infrared light. General fluorescence principles such as light excitation and fluorescence emission are described in the chapter **2.1** followed by their implication in experimental protocols to monitor fluorescence *in vivo* (**2.2**). The description of cyanine dyes, which are commonly used contrast agents for near infra-red imaging, is the subject of chapter **2.3**.

2.1 Fluorescence

2.1.1 Excitation-Emission

Fluorescence is a property of molecules that involves electronic transitions. Absorption of photon of the appropriate energy causes a transition from the molecular ground state $E_0(v=0)$ which for the majority of molecules is a singlet state, to an excited state $E_1(v=n)$, correspondingly also a singlet state (Fig.2.1).

Figure 2.1



Light excitation at wavelength λ_1 provoke the energy absorption by electrons which jump from the energy state E_0 to E_1 . After a certain time (pico sec) the loss of energy occurs in two steps: a non radiative loss toward E_1' and the fluorescence emission when returning to the ground state E_0 . The photon emission occurs always with a wavelength $\lambda_2 > \lambda_1$.

Energy is dissipated via radiation less transitions to the vibrational ground state of $E_1(v=0)$. Relaxation to the ground state occurs by emission of a light photon, which is lower energy (longer wavelength) than the exciting photon, i.e. the amount of energy emitted as fluorescence is always less than the amount of energy absorbed. The energy difference between the absorbed and emitted photons ends up as molecular vibrations (heat). In fluorescent materials, the excited state has always the same spin as the ground state (singlet).

The excitation and fluorescence frequencies ν_{ex} and ν_{fl} are defined as

$$h \cdot \nu_{ex} = E_1(v = n) - E_0(v = 0)$$

and

$$h \cdot \nu_{fl} = E_1(v = 0) - E_0(v = 0)$$

respectively, where h is Planck's constant and ν the vibrational quantum number

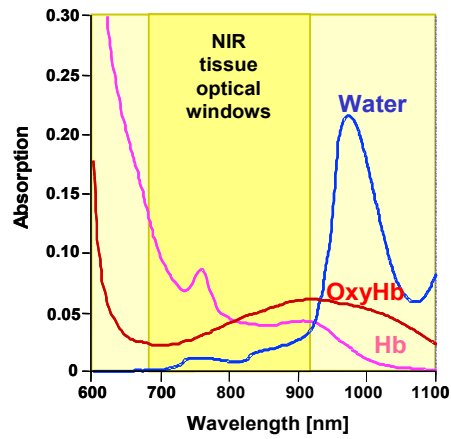
The quantum yield of a fluorescent substance is defined by

$$\text{Quantum yield} = \frac{\# \text{ photons re-emitted}}{\# \text{ photons absorbed}}$$

The absorption and emission of energy can only occur at precise wavelengths, which are characteristic for a given molecule. Thus, each fluorescent molecule is defined by its own distinct absorption and emission energy spectrum. The distribution of wavelength-dependent intensities that cause fluorescence is known as the fluorescence excitation spectrum, and the distribution of wavelength-dependent intensities of emitted energy is known as the fluorescence emission spectrum.

2.1.2 Interaction of NIR radiation with biological tissues

Infrared (IR) radiation is electromagnetic radiation of a wavelength longer than visible light, but shorter than microwave radiation. Infrared radiation has wavelengths between 700 nm and 1 mm. Infrared is absorbed more strongly than microwaves (wavelength from 10^{-3} to 0.1 m), but less strongly than visible light. The result of infrared absorption is heating of the tissue since it increases molecular vibrational activity. Because of its longer wavelength and the low absorbance of tissue intrinsic chromophores such as oxy- and deoxyhemoglobin, melanin and fat, infrared radiation penetrates tissue further than visible light and propagates by multiple scattering through several centimeters of tissue, enabling deep (> 1 cm) tissue imaging [Sevick *et al.*, 2002]. Moreover, working at near-infrared (NIR) wavelengths between 700 and 1100 nm limits biological tissues autofluorescence [Frangioni, 2003]. Figure 2.2 is showing the autofluorescence spectra of the principal components of biological tissue upon illumination with NIR radiation.

Figure 2.2

NIR fluorescence of major tissue components. To avoid problems of tissue unspecific autofluorescence, the NIR tissue optical window is between 700 and 900 nm.

2.2 In Vivo NIRF Imaging

Fluorescence has proven to be a versatile tool for many applications. It is a powerful technique for studying molecular interactions, biochemistry, cell biology and physiology. Fluorescence detection has three major advantages over other light-based investigation methods: high sensitivity, high speed, and safety:

- The point of safety refers to the fact that samples are not affected or destroyed in the process, and no hazardous byproducts are generated.
- Sensitivity is an important issue because the fluorescence signal is proportional to the concentration of the substance being investigated. Using fluorescence, one can monitor very rapid changes in concentration.
- Because it is a non-invasive technique, fluorescence does not interfere with a sample. The excitation light levels required to generate a fluorescence signal are low, reducing the effects of photo-bleaching; and living tissue can be investigated with no adverse effects on its natural physiological behavior.

Although the spatial resolution (1mm) is limited when compared with other imaging modalities e.g. MRI, NIRF tomography provides access to a variety of physiological parameters that otherwise are not accessible [Hielscher *et al.*, 2002].

Main optical imaging technologies currently used are fluorescence reflectance imaging (FRI) and fluorescence mediated tomography (FMT).

2.2.1 Fluorescence Reflectance Imaging

FRI is the simplest method: a NIR light source with the appropriate spectral intensity illuminates the specimen and the reflected fluorescence is detected. Optical bandpass filter are installed to avoid spectral overlap between the excitation and the emission wavelengths [Mahmood *et al.*, 1999]. These systems allow potentially simultaneous imaging of two or more dyes [Mahmood *et al.*, 2002] and real-time quantitative assessment of the fluorescent signal.

2.2.2 Fluorescence Mediated Tomography

FMT is a tomographic imaging modality capable of quantitatively displaying deep near-infrared fluorescence (NIRF) signals in three-dimensional volume [Ntziachristos *et al.*, 2003]. The emitted fluorescence that propagated through tissues is collected, quantified and then combined to obtain the distribution of fluorophores in deep tissues. A tomographic image is reconstituted after the data are mathematically processed. Recent results show that NIRF signal from tumor like structures can propagate about 10 cm in breast or lung tissues and more than 5 cm in the adult brain [Ntziachristos *et al.*, 2002].

2.2.3 Elements for fluorescence detection

Four essential elements of fluorescence detection systems can be identified: 1) an excitation source, 2) a fluorophore, 3) wavelength filters to isolate emission photons from excitation photons, and 4) a detector that registers emission photons and produces a recordable output, usually as an electrical signal or a photographic image. Regardless of the application, compatibility of these four elements is essential for optimizing fluorescence detection.

2.3 NIRF Contrast Agent

Because there is little NIR fluorescence contrast generated by most tissues, most of *in vivo* studies administer exogenous contrast agent (CA). All of the techniques are based on the same concept: expose the specimen to NIR light, detect the emitted fluorescence coming out of the tissue and use the absorption spectra of the light absorbing molecules present in the tissue to interpret the detected light levels as changes in CA concentrations.

2.3.1 Theory

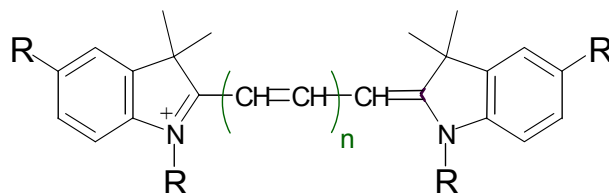
For successful *in vivo* imaging with NIR contrast agents, careful attention must be paid to parameters, which can influence the signal to background ratio including [Sevick *et al.*, 2002]:

- selection of excitation/emission wavelengths and quantum yield: optimal excitation and detection wavelength have to be determined; excitation and detection wavelength have to be chosen such that the best fluorescence quantum yield of the probe is reached. Studying carefully the excitation spectrum can also avoid problem of tissue autofluorescence (see Figure 2.2).
- photo bleaching threshold: under high-intensity illumination conditions, the irreversible destruction or photo bleaching of the excited fluorophore becomes the factor limiting fluorescence detectability. The most effective remedy for photo bleaching is to maximize detection sensitivity, which allows the excitation intensity to be reduced. Detection sensitivity is enhanced by low-light detection devices such as CCD cameras, as well as by high-numerical aperture objectives and the widest bandpass emission filters compatible with satisfactory signal isolation. Alternatively, a less photo labile fluorophore may be substituted in the experiment.
- biodistribution and target binding affinity: *In vivo* imaging requires that the contrast agent is delivered to the target and is retained by the target while non-bound material is cleared from the circulation [Frangioni, 2003].

2.3.2 Cyanine dyes

Structure Cyanine dyes are structurally defined by a conjugated chain of an odd number of carbon atoms linked between two nitrogen centers forming a polymethine chromophore:

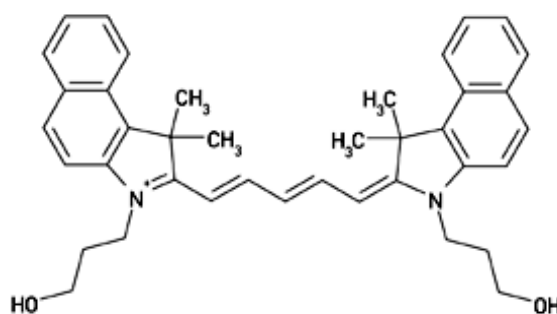
Figure 2.3



Cyanines molecular structure; n can vary from 1 to 7

With cyanine dyes, a broad chemical derivatization is possible. By varying the number of odd carbon atoms, the spectrum of the probe changes and the whole spectral range between visible to NIR wavelengths can be covered. Moreover, these dyes show high absorbance coefficients and very good fluorescence efficiency (i.e. high quantum yield). The most commonly used dye for NIRF imaging is the Cyanine 5.5 (see Figure 2.4).

Figure 2.4



Molecular structure of the cyanine 5.5

Toxicity After intravenous injection, the dye is stable and remains in the blood circulation until excretion. It seems there is no renal elimination of the initially absorbed dye in an unchanged form. Apparently the dye accumulates in the liver and kidneys for detoxification and elimination, causing no inconsiderable damage to the fine structures of these organs [Uhlenbroock, 1965].

3 ORGANIZATION OF THE NERVOUS SYSTEM

In order to better understand the sections on mechanisms of brain inflammation, chapter three describes the general organization and function of the central nervous system. Neurons that generate and conduct nervous impulse (**3.1**) and glial cells that permit neurons to work in optimal conditions are described. The role of the blood brain barrier is discussed in the chapter **3.2** by detailing endothelium architecture and the function of tight junctions.

3.1 Cells of the Central Nervous System

3.1.1 Neurons

Neurons are the main compound of the central nervous system (CNS) and the peripheral nervous system (PNS). Neurons vary considerably in structure and size throughout the nervous system and within a given brain region. Its task is to relay signals to a specifically targeted cell [Ramón y Cajal, 1995]. The neuron cell body contains the nucleus and other intracellular organelles common to non-neuronal as well as neuronal cells. Neurons have branches (dendrites) to which other neurons form synapses and axons that make connections with other neurons. They often look like branches or spikes extending out from the cell body. It is primarily the surfaces of the dendrites that receive chemical messages from other neurons. Dendrites act like receiving stations for excitation and inhibition signals. One extension is different from all the others: the axon. Although in some neurons, it is hard to distinguish from the dendrites, in others it is easily distinguished by its length. The purpose of the axon is to transmit an electro-chemical signal to other neurons, sometimes over a considerable distance. At the very end of the axon is a synapse. It is there that the electro-chemical signal that has traveled the length of the axon is converted into a chemical message that activates the next neuron.

3.1.2 Myelin and nerve conduction

To analyze events in the outside world or within the body, and to transmit information from cell to cell, nerve cells use electrical and chemical signals. Myelin is the material that insulates axons and speeds the conduction of nerve impulses. The nerve that transmits the impulse can be compared to an electrical wire with the myelin sheath being the insulation around the wire. The myelin chemical composition is very particular and varies from the CNS to the PNS. This is a substance rich in protein (15-30%), lipids (70-85%) that forms layers around the nerve fibers and acts as an electrical insulation due to its lipophilic composition, thereby excluding polar and conducting particles such as water and ions. The Table 3.1 gives an idea about the several lipidic compounds of the rat myelin. The most frequent proteins encountered in the CNS are PLP (Proteolipid Protein), MBP (Myelin Basic Protein) and MAG (Myelin Associated Glycoprotein).

Table 3.1

Substance	Myelin	White matter	Grey matter
Lipid (% dry)	70%	55%	33%
Cholesterol (% lipid)	28%	28%	22%
Cerebroside (% lipid)	23%	20%	5%
Galactopeptids (% lipid)	28%	29%	7%
Plasmalogens (% lipid)	12%	11%	9%
Phospholipids (% lipid)	43%	46%	70%

Composition of myelin in the white and grey matter of human CNS. ([The Human Brain by Nolte J. 5th Edition](#))

Myelin is present in both the CNS and the PNS. Myelin is formed in the PNS by Schwann cells and in the CNS by oligodendrocytes.

The myelin layer is segmented and there are small areas or “nodes” that are naturally unmyelinated (nodes of Ranvier). As chemical ions pass in and out of the axons membrane, the electrical current they generate is conducted down the nerve, and jumps from node to node. Myelin prevents the current from leaking out of the nerve at inappropriate points and decreases the electrical resistance of the nerve. This helps make sure the nerve impulse is conducted efficiently.

3.1.3 Glial cells

Glial cells were first described in 1846 [[Virchow, 2005](#)]. In subsequent years, Ramón y Cajal focused his attention on glial cell functions like secretion of trophic molecules and the current spread during conduction of nerve impulse [[Ramón y Cajal, 1995](#)]. During these investigations, he draw precise figures of different glial cells, their distribution throughout the nervous system and their morphology. Glial cells act as a supporting system for the neurons and their dendritic and axonal processes; they also have a primary role in a wide range of normal functions and reactions to injury, including inflammation repair, fluid balance, and energy metabolism. In the CNS among the neurons, glial cells are usually subdivided into several distinct categories [[Ketteyman and Ransom, 1995](#)] [[Ransom, 1991](#)].

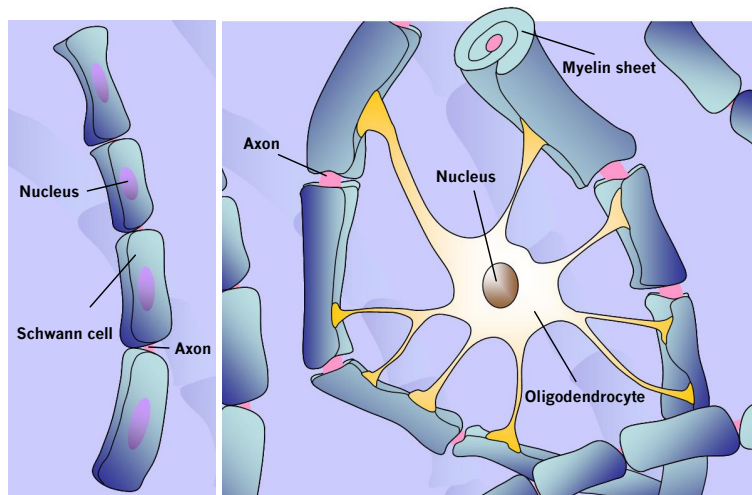
Macroglia comprise:

Astrocytes make contact with capillaries and neurons. The major astrocytic processes are directed toward neurons and their process and synapses, where they are believed to act as metabolic buffer or detoxifiers and suppliers of nutrients. Astrocytes play a significant role during infectious and autoimmune disease and are the principal cells responsible for repair and scar formation in the brain.

Oligodendrocytes are predominant in the white matter. Oligodendroglial cytoplasmic processes wrap around the axons of neurons to form myelin in a manner analogous to the Schwann cells in the PNS (Figure 3.1). Injury to oligodendroglial cells is a feature of acquired demyelinating disorders (e.g. multiple sclerosis)

Radial glial cells play an essential role in the developing mammalian CNS by guiding neurons growth.

Figure 3.1



Structure of an myelin-insulated axon. Oligodendrocytes synthesize myelin which surround axons to form Schwann cells.

Microglia is represented only by *microglial cells* resembling macrophages in the blood and probably arise from them. They serve as a CNS macrophage system.

The distribution of neurons and glial cells through the nerve system is well organized.

The CNS (the brain, spinal cord and optic nerves) is made up of several different components:

- The gray matter contains the cell bodies of the nerves.
- The white matter contains nerve fibers coated with myelin.
- The glial cells that form a supporting network.

PNS nerve cells perform two major functions:

- Sensory neurons collect information about the body's internal and external environment and convey it to the CNS.
- Motor neurons carry instructions on what to do from the CNS to the glands and muscles

3.2 Blood Vessels and Blood Brain Barrier

Blood vessel and capillaries are formed by endothelial cells. These cells are organized in a flat epithelium (endothelium) and form a cylindrical structure: the capillary lumen (see Figure 3.2).

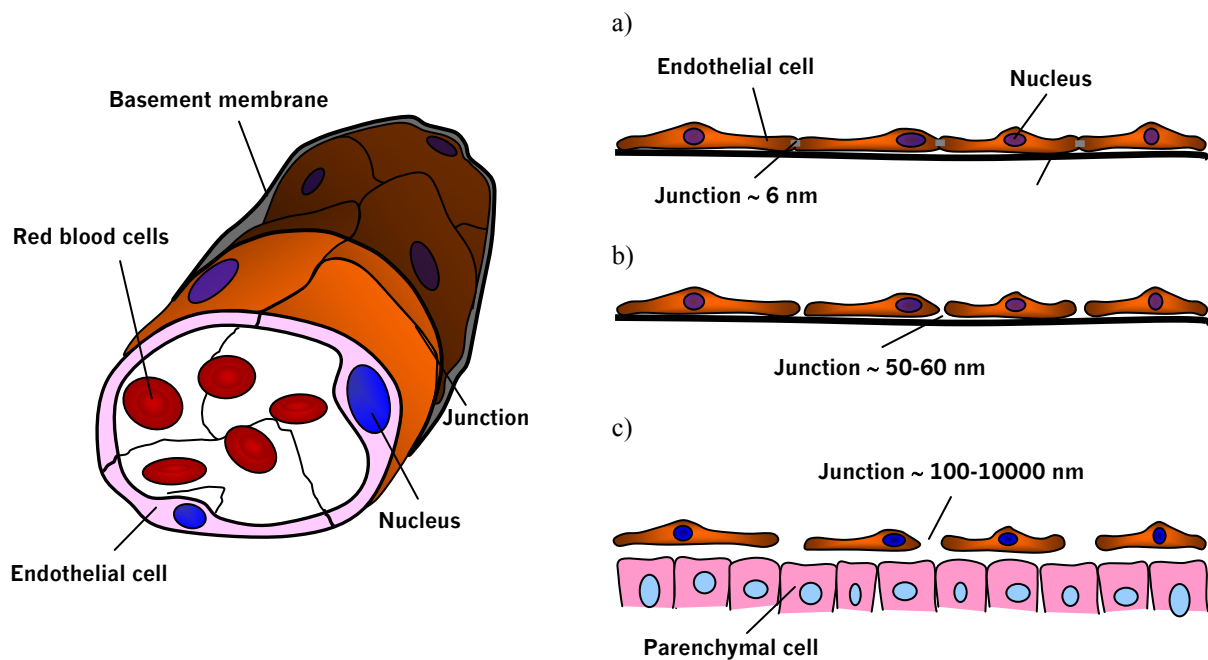
3.2.1 Endothelium

Blood Brain Barrier: zone that delineates the vascular lumen from brain parenchyma. The barrier layers consist of endothelial cells with adjacent cells forming the tight junctions (*zonulae occludentes*). In addition, the BBB is composed of the basement membrane and astrocytic end-feet contacting the tight junctions from the abluminal side.

In contrast to vessel walls in the periphery, only a few molecules can cross the intact BBB freely by diffusion [Abbott, 2002]. While water and lipophilic substrates such as O₂ and CO₂ can diffuse freely along their concentration gradient, uptake of nutrients like glucose and amino acids depends on transporter systems, while other larger molecules might be taken up by specific receptor mediated transcytosis [Ballabh *et al.*, 2004; Gloor *et al.*, 2001].

Thus, a particular epithelium is lining all blood vessel in the body: the endothelium. Endothelium is the largest “organ” in the body, its surface is equivalent to 6 tennis court in a 70kg man and weight about 1800g (> liver) with a mass that approximates five normal hearts. The trillion cells that compose the endothelium are in close contact and form a slick layer that prevents blood cell interaction with the vessel wall as blood moves through the vessel lumen (see Figure 3.2). The endothelium plays a critical role in the mechanics of blood flow, the regulation of coagulation, leukocyte adhesion, and vascular smooth muscle cell growth, and also serves as a barrier to the transvascular diffusion of liquids and solutes. For years the endothelium was thought of as an inert single layer of cells that passively allowing the passage of water and other small molecules across the vessel wall. However, this dynamic tissue performs many other active functions, such as the secretion and modification of vasoactive substances and the contraction and relaxation of vascular smooth muscles.

Figure 3.2



- a) Continuous capillaries, including most tissues, such as muscle, lung, and skin
 b) Fenestrated capillaries, including kidney, intestine, and some endocrine and exocrine glands
 c) Sinusoid capillaries, including liver, spleen, and bone marrow. It is noted that this illustration expresses only the morphological pores contributing to diffusive permeability. Actual trans-capillary exchanges are modified by vesicular transports with variable sizes up to 20–30 nm
 Adapted from [Okuhata, 1999]

Within the brain, the association between blood vessel endothelium and astrocyte membrane form together the so-called blood-brain barrier (BBB). This is the specialized system of capillary endothelial cells and astrocytes that protects the brain from foreign substances or harmful substances like hormones or neurotransmitters in the blood stream, while supplying the brain with the required nutrients for proper function. Unlike peripheral capillaries that allow relatively free exchange of substance across cells, the BBB strictly limits transport into the brain through both physical (tight junctions) and metabolic (enzymes) barriers [Huber *et al.*, 2001]. Proteins, ions and hydrophilic molecules cannot pass through the BBB; lipophilic molecules such as alcohol and gases can [Mayhan and Heistad, 1985]. Thus the BBB is often the rate-limiting factor in determining permeation of therapeutic drugs into the brain [Robinson, 1987]. BBB breakdown is assumed to be a key component in CNS associated pathologies [Perry *et al.*, 1997].

The BBB barrier can be damaged by the following events:

- hypertension (high blood pressure)
- hyperosmolarity (a high concentration of a substance in the blood)
- exposure to microwave as well as radiation
- exposure to infectious agents
- injury to the brain like trauma, ischemia, inflammation and pressure

3.2.2 Tight junctions

Tight junctions are the connections between epithelial and endothelial cells that comprise various tissues of the body [Huber *et al.*, 2001]. They regulate the passage of molecules across these natural barriers [Mayhan, 2001]. As part of the body's normal activity, tight junctions selectively open and close in response to various signals both inside and outside of cells. This allows the passage of large molecules or even entire cells across the tight junction barrier. Large molecular weight drugs need to pass through these tissue barriers in order to get to their sites of action [Rapoport, 2000].

Tight junctions consist of proteins, (e.g. claudins, occludins) and junctional adhesion molecules that are anchored in the membranes of two adjacent cells and interact with each other to hold the cells together and prevent other molecules from passing between them [Wolburg and Lippoldt, 2002].

Tight junctions are found in all tissues, but those of particular relevance to drug delivery include: nasal tissue, gastrointestinal tissue, blood vessels and blood-brain barrier.

4 INFLAMMATION IMMUNE MECHANISMS

Basic mechanisms of inflammation leading to immune responses are the topic of the section four. Following a general description of cells of the immune system and the way they interact (4.1), processes of acute and chronic inflammation are discussed (4.2). The importance of chemical mediators involved in cell communication that permit coordination of the immune response is explained in the chapter 4.3.

4.1 Basis of the Immune System

4.1.1 Cells of the immune system

T lymphocytes are the mediators of the cellular immunity (\neq humoral immunity cf. B lymphocytes). They contribute to the immune defenses in two major ways. Some help regulate the complex workings of the immune system, while others are cytotoxic and directly contact infected cells and destroy them.

The regulatory T cells are "helper/inducer" T cells. They are needed to activate many immune cells, including B cells and other T cells. Another subset of regulatory T cells acts to turn off or suppress immune cells. Cytotoxic T cells help the body in eliminating cells that have been infected by viruses as well as cells that have been transformed by cancer. They are also responsible for the rejection of tissue and organ grafts.

T cells constitute 60 to 70% of peripheral lymphocytes. But T lymphocytes are also found in lymph nodes and the spleen. Each T cell is genetically programmed to recognize a specific cell-bound antigen by means of an antigen-specific T cell receptor (TCR). This TCR receptor is always noncovalently linked to a cluster of polypeptide chains: the CD3 molecular complex. Some other co-receptors expressed in the membrane of T cells are linked to a specific function: CD4+ for helper T cells and CD8+ for cytotoxic T cells.

T cells cannot be activated by soluble antigens; presentation of processed, membrane-bound antigens by macrophages or other antigen-presenting cells (APCs) is mandatory for induction of cell-mediated immunity.

B lymphocytes B cells work mainly by secreting soluble substances known as antibodies (immunoglobulins). On antigenic stimulation, B cells form large plasma cells that secrete immunoglobulins, which are the mediators of humoral immunity.

B lymphocytes constitute 10 to 20% of the circulating peripheral population. They are also present in bone marrow, lymph nodes and spleen, and extralymphatic organs such as the gastrointestinal tract. B cells recognize antigens via the B cell antigen receptor complex. Immunoglobulin M (IgM), present on the surface of B cells constitutes the antigen-binding component of the B cell receptor. As with T cell, each B cell get activated by binding a soluble unique antigen on their receptor and is programmed to make one specific antibody.

Phagocytes are large white cells that can engulf and digest foreign invaders. They include monocytes, which circulate in the blood, and macrophages, which are found in tissues throughout the body, as well as neutrophils, cells that circulate in the blood but move into tissues where they are needed.

Macrophages are versatile cells; they act as scavengers, they secrete a wide variety of powerful chemicals, and they play an essential role in activating T cells. Neutrophils are not only phagocytes but also granulocytes: they contain granules filled with potent chemicals. These chemicals, in addition to destroying microorganisms, play a key role in acute inflammatory reactions. Macrophages play important roles both in the induction and in the effector phase of immune responses:

- they are first required to process and present the antigen to immunocompetent T cells
- they are important effector cells in certain form of cell-mediated immunity
- they can also play a role in the humoral immunity by phagocytosing microbes that are covered by IgG

Natural killer cells (NK cells) At least two types of lymphocytes are killer cells: cytotoxic T cells (CD8+) and NK cells. To attack, cytotoxic T cells need to recognize a specific antigen, whereas NK cells do not. Both types contain granules filled with potent chemicals, and both types kill on contact. The killer binds to its target, aims its weapons, and delivers a burst of lethal chemicals.

These cells represent approximately 10 to 20% of the peripheral blood lymphocytes and do not bear TCR or cell surface immunoglobulins. NK cells do not present the CD3 receptor.

4.1.2 Cytokines, messengers of the immune system

The induction and regulation of the immune responses involve multiple interactions among all the immune cells. Some interactions depend on cell-to-cell contact some others are mediated by short-acting soluble mediators, called cytokines. Cytokines are diverse and have a wide spectrum of effects. Despite several different cells produce cytokines, these molecules are the principal instrumentation of T cells.

Cytokines: small protein molecules that are the core of communication between immune system cells, and even between immune system cells and cells belonging to other tissue types. They are actively secreted by immune cells. Their action is often local, but sometimes can have global effects on the whole body.

There are a lot of known cytokines that have both stimulating and suppressing action on lymphocyte cells and immune response (see Table 4.1). Cytokines act by binding to their cell-specific cytokine receptor. This receptor is located in the cell membrane and allows a signal cascade to start in the cell that eventually will lead to biochemical and phenotypical changes in the target cell.

A chemokine is a cytokine that has a chemoattractant effect for monocytes and may also cause cellular activation of specific functions related to host defense.

Binding to specific receptors on target cells, cytokines recruit many other cells and substances to the site of immune activity. Cytokines encourage cell growth, promote cell activation, direct cellular traffic, and destroy target cells.

Table 4.1

Names	Abbreviation	Examples
Interleukins	IL	IL-1, IL-2, etc
Interferons	IFN	IFN α , IFN β , IFN γ
Tumor Necrosis Factors	TNF	TNF α , TNF β
Growth Factors	GF	NGF, EGF
Colony stimulating Factors	CSF	M-CSF, G-CSF, GM-CSF
Chemokines	-	RANTES, MCP-1, MIP-1 α

The nomenclature of cytokines partly reflects their first-described function and also the order of their discovery. There is no single unified nomenclature, and individual cytokines may belong to two groups (e.g. the chemokine IL-8) [Roitt *et al.*, 2005].

4.2 Mechanisms of Inflammation

4.2.1 Acute inflammation process

The cause of acute inflammation may be due to physical damage, chemical substances, micro-organisms or other agents. The acute inflammatory response is a very common, complex and stereotyped response to recent or ongoing injury. Three main processes occur:

- Increased blood flow due to dilation of blood vessels (arterioles) supplying the region. This implies that acute inflammation can just take place in vascularized tissues.
- Increased permeability of the capillaries, allowing fluid and blood proteins (exudate) to move into the interstitial spaces. The exudate carries proteins, fluid and cells from local blood vessels into the damaged area to mediate local defenses.
- Migration of neutrophils (and perhaps a few macrophages) out of the venules and into interstitial spaces.

These events are essentially the same whatever the cause and wherever the site. However, it is important to notice that they do not only lead to beneficial effects. Desired aspects of fluids exudates are dilution of toxins by removing them, entry of antibodies and/or drugs in the wound, fibrin formation to trap pathogens, more efficient supply of nutrients and oxygen to neutrophils and finally the drainage of the fluid exudates into the lymphatics organs allowing the stimulation of the immune response. On the other hand, the release of lysosomal enzymes by inflammatory cells may also have harmful effect such as digestion of healthy tissues; the swelling of damaged tissues can arm normal tissues surrounding the inflammation area and sometimes, the excessive inflammatory response (e.g. hypersensitivity) provokes more tissue destructions than the pathogen itself.

Acute inflammation is short-lasting, only a few days. Longer lasting processes are referred to as chronic inflammation.

4.2.2 Chronic inflammation

If the agent causing acute inflammation is not removed, the acute inflammation may progress to the chronic stage. In this case, the character of the cellular exudate changes, with lymphocytes, plasma cells and macrophages replacing the neutrophils. Chronic inflammation is a complex response to prolonged problems, orchestrated by T-helper lymphocytes. It involves recruitment and activation of T and B lymphocytes, macrophages, eosinophils, and/or fibroblasts.

4.3 Chemical and Cellular Mediators of Inflammation

4.3.1 Chemicals mediators

The spread of the acute inflammatory response following injury to a small area of tissue suggests that chemical substances are released from injured tissues, spreading outwards into uninjured areas. These chemicals, called endogenous chemical mediators, cause vasodilatation, emigration of neutrophils, chemotaxis and increased vascular permeability (see Table 4.2).

Table 4.2

Chemical mediator	Source	Effect
Histamine	Mast cells, leukocytes and platelets	Increase vascular dilatation and permeability
Lysosomal compounds	Neutrophils	Increase vascular permeability and activate complement system
Prostaglandins	Many cell types	Increase vascular permeability and platelet aggregation
Serotonin	Mast cells	Potent vasoconstrictor
Lymphokines	Lymphocytes	Chemotactic
Complement system	Plasma	Chemotactic, cytolytic activity, opsonisation*
Kinin system	Plasma	Increase vascular permeability, vasodilatation and smooth muscle contraction
Coagulation system	Plasma	Conversion of fibrinogen to fibrin promoting clotting of blood

List of chemical mediators playing a role in the inflammation process.

* process whereby opsonins make an invading microorganism more susceptible to phagocytosis

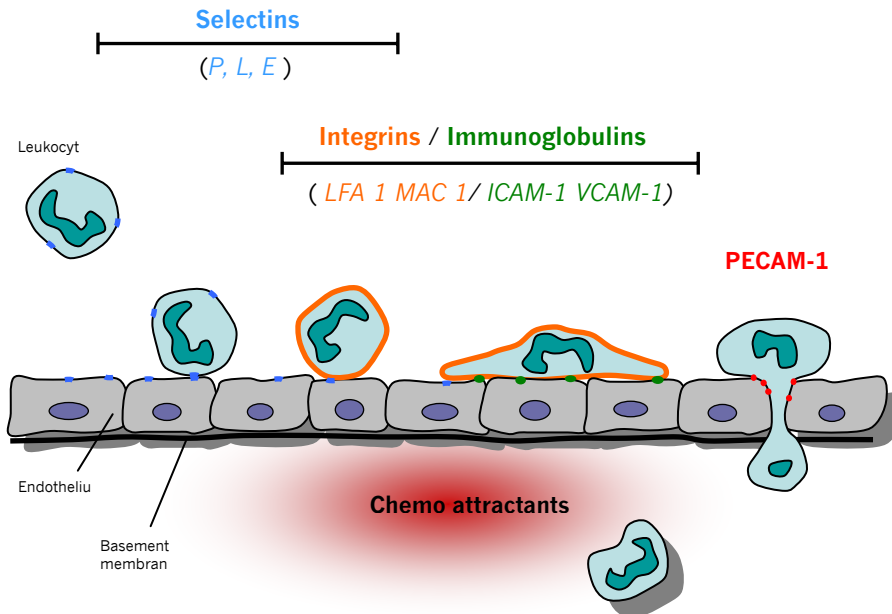
4.3.2 Leukocytes activation and extravasation

An other critical function of inflammation is the delivery of leukocytes to the site of injury. The sequence of events from the lumen of a blood capillary to the interstitial tissue, called extravasation, can be divided into the following steps: see Figure 4.1.

Leukocytes first roll on the inner part of the endothelium. The adherence is due to the affinity between the selectin molecules, present on the surface of leukocytes, to their respective selectin ligands which are situated on the surface of endothelial cells.

Figure 4.1

Rolling → **Activation** → **Adhesion** → **Transmigration**



Different steps of recruitment of leukocytes on an inflammation site.
(Derived from "Pathologic basis of disease", Cotran Kumar Collins, Ed. Robbins).

Leukocytes then become activated. The slowed leukocytes have now the opportunity to respond to the signaling molecules held at the endothelial surface. Particularly important are the large group of chemokines, which activate certain populations of leukocytes that have the appropriate receptors.

Activation upregulates the affinity of the leukocyte integrins which engage the cellular adhesion molecules on the endothelium (e.g. ICAM-1) to cause first adhesion and initiate a programme of migration.

Then leukocytes transmigrate across the endothelium. This is an active process which involves both cell types (leukocytes and endothelial cells) and occurs near the junctions between endothelial cells. By the help of enzyme secretion, leukocytes can digest and pierce the basement membrane to migrate into the tissue toward chemoattractants coming from the source of injury.

It is important to notice that in specialized tissues such as the brain, in case of non-damaged BBB where the endothelium is connected by continuous tight junctions, it is clear that lymphocytes migrate across the endothelium via vacuoles, and the junctions do not break apart [Roitt, Brostoff, and Male, 2005].

4.3.3 Phagocytosis

Phagocytosis is mediated by macrophages and polymorph nuclear leucocytes. Phagocytosis consist on the ingestion and digestion of microorganisms, insoluble particles, damaged or dead host cells, cell debris, activated clotting factors. There are several stages of phagocytosis:

Chemotaxis: movement of cells against a concentration gradient of chemotactic factors.

Adherence: receptor-ligand interaction that guide the extension of macrophage's pseudopods around the particle (bacteria for instance)

Pseudopodium formation: protrusion of membranes to flow round the "prey".

Phagosome formation: fusion of the pseudopodium with a membrane enclosing the "prey" leads to the formation of a structure termed a phagosome.

Phago-lysosome formation: the phagosome moves deeper into the cell, and fuses with a lysosome, forming a phago-lysosome. These contain hydrogen peroxide, active oxygen species (free radicals), peroxidase, lysozyme and hydrolytic enzymes. This leads to digestion of the phagolysosomal contents, after which they are eliminated by exocytosis. The speed of phagocytosis can be increased by coating the organisms by molecules termed opsonins, this is the phenomenon of opsonization.

5 MULTIPLE SCLEROSIS AND EAE MODEL

Under healthy conditions, the immune system has no access to the normal brain. Autoimmune neurodegeneration processes occurring in multiple sclerosis (MS) are particular cases. The pathology as well as the etiology of the disease are discussed in chapter **5.1**. To study this disease and evaluate potential treatments, an animal model of experimental autoimmune encephalomyelitis (EAE) has been developed (**5.2**). Brain inflammation processes occurring in EAE that reflect changes observed in MS are summarized in chapter **5.3**.

5.1 Multiple Sclerosis

5.1.1 Definition

Multiple sclerosis (MS) is an inflammatory disease of the CNS of unknown etiology characterized pathologically by the occurrence of areas of destruction of the myelin (demyelination) followed by gliosis throughout the brain.

In many cases, early disease manifestations are phasic with relapses during which patients often present episodes of neurological and/or cognitive dysfunction and followed by phases of improvement or even apparent complete clinical recovery [Miller, 1998]. In case of a progressive disease course, some deficits might persist and even aggravate with time. In fact, MS is a complex and heterogeneous disease with a phenotype that is not unitary. Not only disease courses vary among relapsing remitting, primary progressive and secondary progressive, but also clinical symptoms as well as domains of cognitive dysfunction [Julien and Ferrer, 1989].

Gliosis: The production of a dense fibrous network of neuroglia; includes astrocytosis, which is a proliferation of astrocytes in the area of a degenerative lesion.

5.1.2 Pathology

The pathological hallmark in MS is a circumscribed lesion beginning with destruction of the myelin sheaths of the nerve fibers and ending with the formation of a sclerotic plaque. These plaques occur predominantly in the white matter of the brain and spinal cord. They are sometimes found in the grey matter of the CNS but rarely in the grey matter of the PNS [Allen *et al.*, 1981].

Characteristic histological features are perivascular inflammation, demyelination and axonal loss. Cellular analysis of lesions show evidences that the inflammatory cells present in MS plaques play an important role in the lesion development. These cells are mainly T lymphocytes [Babbe *et al.*, 2000] [Huseby *et al.*, 2001] [Calopa *et al.*, 1995] [Hellings *et al.*, 2002] but some B cells, macrophages and plasma cells may also be found [Prineas and Connell, 1978; Prineas and Wright, 1978] [Nyland *et al.*, 1982]. Many immunoglobuline-containing cells are found in the plaques [Esiri, 1977; Esiri, 1980]. There is also good evidences to indicate that circulating immune complexes [Tachovsky *et al.*, 1976] [Goust *et al.*, 1978] and circulating T cells sensitized to proteins of the myelin are of importance

[Traugott *et al.*, 1979] [Traugott *et al.*, 1983a] [Turner *et al.*, 1980] and similar cells may be found in the CSF [Kam-Hansen, 1980].

However, as demonstrated by Trapp and colleagues [Trapp *et al.*, 1999], different demyelinating processes can be distinguished. These processes can range from demyelination caused by inflammatory process [Bitsch *et al.*, 2000] that is followed by remyelination [Lassmann *et al.*, 1997], to inflammatory demyelination with irreversible axonal death. The latter process is known as Wallerian degeneration. Demyelination followed by regeneration may lead to compromised or even failing nerve conduction [Raine and Wu, 1993] that can be related to a slowing of the physical or mental abilities of patients. In the case of axonal loss, deficits may persist.

5.1.3 Etiology

Auto-immune disease MS is more and more believed to be an autoimmune disease. The prefix “auto” means “self.” Autoimmunity means that the immune system is reacting against normally occurring antigens in the person’s body, as if these antigens were foreign [Bruck and Stadelmann, 2003]. It is not known what, in patients with MS, causes T cells to become activated but it is postulated that viral infections, genetic predisposition, environmental factors, and autoimmunity are all considered as contributing factors in the etiology of MS [Julien and Ferrer, 1989].

In the case of MS, the target of the immune attack is believed to be a component of myelin in the central nervous system, probably one or few of main protein composing the myelin (see section 3.1.2). Certain T cells become sensitized to myelin and enter the CNS [Steinman, 2001] [Stinissen and Raus, 1999] [Neumann *et al.*, 2002]. Once in the CNS, these T cells not only injure myelin, but secrete chemicals that damage nerve fibers (axons) and recruit more damaging immune cells to the site of inflammation [Barnett and Prineas, 2004]. During active disease, demyelination is associated with an inflammatory reaction that is orchestrated by activated lymphocytes, macrophages and endogenous glial cell (astrocytes and microglia) [Benveniste, 1997] [Minagar *et al.*, 2002] [Raivich and Banati, 2004].

Symptoms and distribution As mentioned previously, myelin not only protects nerve fibers, but is also essential for their proper function. When myelin sheath of the nerve fiber is destroyed or damaged, the ability of the nerves to conduct electrical impulses to and from the brain is disrupted, producing the various symptoms of MS such as abnormal sensations,

vision problems, and weakness [Berg *et al.*, 2000] [Barnett and Prineas, 2004]. Symptoms of MS are unpredictable and vary from person to person and from time to time in the same person. Symptoms can vary widely because the damage can occur anywhere in the brain, spinal cord or optic nerve. The principal consequences of these hallmarks are motor weakness and incoordination of the lower limbs. Other characteristics like sensory symptoms, ataxia and bladder symptoms appear in respectively 87, 82 and 71% of the cases. Patients generally complain because of fatigue and cramps. The affection of the optic nerve lead to visual symptoms in 49% of the patients.

This demyelinating disease of the CNS generally afflicts persons between 20 and 50 years old, affecting more women than men.

Therapy and areas of research There is currently no cure for MS. However, over the past several years, first effective treatments for the disease have become available. In contrast to non-specific immunosuppression [Hauser *et al.*, 1982] [Kanwar, 2005], which was the mainstay of MS treatment for many years, these newer medications, called immune modulators, target various components of the immune attack in MS [Fujino *et al.*, 2003]. While these treatments have shown promise, they are still only partially effective at decreasing the incidence of recurrent attacks that characterize relapsing-remitting MS; yet they have minimal effects, if any, on the progressive forms of the disease.

Efforts to reverse the damage caused by MS and restore function in people with MS must focus on the repair of myelin, oligodendrocytes, and neurons in the CNS. Some neural repair occurs naturally [Billinghamurst *et al.*, 1998]. Spontaneous healing of MS lesions has been observed following stimulation of oligodendrocytes in the area, or recruiting young oligodendrocytes from more distant area, in order to synthesize new myelin at the damaged site. Researchers are now working to identify the molecular players that are used by the body to activate the oligodendrocytes in order to stimulate additional repair. Similarly the role of growth factors (proteins) for myelin repair is being evaluated.

Replacement of damaged cells is an alternative approach to treat MS [Bulte *et al.*, 2002]. Possible cell sources include: skin-derived cells, bone marrow and umbilical-cord blood cells, fetal cells, adult brain cells, and Schwann cells from the PNS. The usefulness of these replacement cells will depend on finding or creating the signals needed to stimulate their transformation and growth into healthy new cells.

These efforts will not be successful, however, unless a way is found to stop the immune system from damaging the CNS tissue in the first place. Much of the ongoing research in MS is directed towards finding answers to questions about the role of the immune system in the development of MS. Scientists have begun to identify the sites or receptors on the T cells that bind to the myelin. The precise identification of these receptor sites may help lead to the development of more specific immunosuppressant therapies that destroy only these sensitized T cells while leaving other cells intact. That is why, method to image *in vivo* T cells localization during the course of MS would be extremely informative on the illness development and evolution.

5.2 The EAE Rodent Model

EAE (experimental autoimmune encephalomyelitis): is an animal models for MS which has been developed to elucidate the underlying mechanisms of neuro-inflammation. Established animal models of acute and chronic-relapsing EAE have led to important insight into the pathophysiology of the immune disease.

5.2.1 Description

EAE and related demyelinating diseases affect the brain and spinal cord, similar in many aspects to MS. Like MS, EAE is a demyelinating disease: it destroys the myelin. EAE can be induced in rats, mice, guinea pigs, rabbits, and monkeys [Gold R. *et al.*, 2000]. Like MS, it takes several clinical forms, including relapsing-remitting and progressive-relapsing. The time course and pathology of the disease depend on the species and the type of antigen.

5.2.2 Inoculation

EAE can be induced only in specific species by injecting homogenized spinal cord or myelin fragments. In the Lewis rat, at least three myelin proteins can induce EAE, myelin basic protein (MBP) [Ben Nun *et al.*, 1981], proteolipid protein (PLP) [Yamamura *et al.*, 1986], or myelin-oligodendrocyte glycoprotein (MOG) [Linington *et al.*, 1993] in combination with an immune-exciting agent, called an adjuvant (an agent which, while not having any specific antigenic effect in itself, may stimulate the immune system, increasing the response to a vaccine). Alternatively, EAE can be induced by injection of CD4⁺ T cells that have been activated *in vitro* (adoptive transfer EAE) [Zamvil *et al.*, 1985]. In this case, the time course of the disease runs in a more synchronous mode. Moreover, this protocol highlights the importance of T cells for disease induction.

Although not being identical to all pathophysiological aspects of the human disease, EAE models nevertheless reproduce many aspects of MS [Gold *et al.*, 2000]. While active EAE in Lewis rats induces a strong inflammatory response, it does not lead to chronic axonal damage as found in human MS. Active immunization of congenic Lewis rats (DA, BN strains) or mice (SJL, C57/Bl6 strains) leads to a relapsing-remitting time course and persistent damage of axons and is therefore more similar to the human pathology. Therefore, EAE models can be used to streamline the development and validation of novel imaging approaches suited for patient/therapy management and for testing novel therapeutic strategies.

5.2.3 EAE animal studies inform about MS

Much of our current knowledge about the disease damage (pathology) and immune responses underlying MS has been gained from studies of animals with EAE. Information derived from microscopic and biochemical examination of the brain, blood, and spinal cord of animals with EAE includes:

- identifying sites in the central nervous system that are more likely to develop MS lesions (damaged areas) also known as plaques
- finding out which immune cells are involved in the formation of plaques and how they interact
- developing experimental treatments or manipulations that can stop or reverse the demyelinating process

In the past, MRI has been employed as a valuable tool to detect and characterize clinical or neurological changes. Unfortunately, conventional MRI provides only low pathological specificity and correlations between lesion volume, atrophy, and lesion localization and clinical symptoms or cognitive measures are only moderate [Berg, *et al.*, 2000] [Rovaris *et al.*, 1998].

5.3 Brain Inflammation in MS and EAE

Several diseases of the central nervous system (CNS) are caused or at least accompanied by inflammatory processes. These processes comprise acute inflammatory events, which are supported by infiltration of brain tissue by different types of leucocytes but also by the transformation of brain residing microglia to an activated form and later also to macrophages. Immune defense in the CNS generally follows a typical layout in which the different cells of the immune system play their specific role. Immune responses are generally induced by the presence of a foreign antigen.

5.3.1 Immune privilege of the normal brain

The CNS presents some differences in comparison to other organs. First, due to the BBB, immune cells, antibodies and immunological mediators have little access to the normal brain [Hickey, 1991]. Yet, there are some hematogenous cells (see definition), in particular monocytes/macrophages and T lymphocytes, present in the CNS under normal conditions [Hauser *et al.*, 1983b]. T lymphocytes can traverse the normal BBB, when they are in an activated state [Wekerle *et al.*, 1991] [Hickey *et al.*, 1991]. These data suggest that it is a small pool of peripheral activated T cells that enter the CNS for immune survey and are, thus, allowed to search for specific antigens or pathogens.

Hematogenous cells: originating in the blood or spread through the bloodstream

Another factor promoting an immune response in the CNS is the active suppression of the expression of major histocompatibility (MHC) antigens in the nervous system. Antigen recognition by T lymphocytes requires the presentation of the small peptides of the antigenic protein by antigen presenting cells in the context of MHC antigen. Thus, in the absence of MHC-antigens T lymphocytes cannot recognize their target and thus, do not activate the mechanisms would lead to inflammation [Vass *et al.*, 1986].

Thirdly, other molecules like adhesion molecules, that are essential to in the cell-cell contacts during the migration of inflammatory cells [Bevilacqua, 1993; Springer, 1994] have a low expression on endothelial cells of cerebral vessels as well as on local tissue elements [Lassmann *et al.*, 1986].

Finally the CNS is equipped with a particular tissue macrophage, the microglia [Gehrmann *et al.*, 1995] [Gehrmann *et al.*, 1993]. In the normal brain microglia seems to be immunologically inert. Microglia can become activated by a variety of immunological and non-immunological stimuli. Different levels of activation appear to exist, which may transform the cells in pure scavengers of fully activated immunological effector cells [Lassmann, 1997]. Furthermore these cells can produce both, immunostimulatory as well as immunosuppressive cytokines [Kiefer *et al.*, 1995].

5.3.2 Induction of initial brain inflammation

In the case of EAE, immune system has to recognize the pathogen or autoantigen that is sequestered in the nervous system. That implies, that immune cells have to get access to the normal nervous system or that the antigens have to be presented in a way that allows recognition.

In the first hypothesis, activated T cells can pass the normal BBB. Thus, peripheral stimulation of the immune system will allow a selected population of T cells to enter the CNS and to search for their respective antigen. To enter the CNS, activated T cell are slowed down and attached to endothelium wall due to adhesion. When the antigen or a cross reactive antigen is present in the CNS compartment, it will be presented to the T lymphocytes on a population of meningeal and perivascular tissue macrophages, which constitutively express MHC antigen even normal conditions [Vass *et al.*, 1986] [Hickey *et al.*, 1991]. If we admit that T cells cannot pass the normal BBB, astrocyte and microglia should be involved to present the antigen to circulating T cells. The initial antigen recognition in the perivascular space triggers a cascade of secondary events that lead to the development of the brain inflammation. A key role in this process is played by cytokines that are produced by either hematogenous cells or by local tissue elements.

In any hypothesis, the initiation of the immunological/inflammatory response is initiated by antigen presenting cells (APC) (e.g. pericytes) that present characteristic peptide-motifs of the antigen together with other surface signals to cells of the immune system. The antigen-specific autoimmune T cells first contact a naive intact BBB and are able to extravasate through the BBB due to their activated status. This is the first step of BBB disruption. The cells which initiate disease are predominantly myelin-reactive CD4⁺ T-helper cells [Swanborg, 1995]. These cells are retained in the CNS due to presentation of appropriate antigen (most likely by endogenous microglia) and undergo further activation. When antigen

is recognized a cascade of events is started which leads to inflammation and elimination of the pathogen, however which may be associated with additional tissue damages. This lead to the recruitment of non-antigen-specific lymphocytes and activated macrophages from the blood into this site, accompanied by further disruption of the BBB.

5.3.3 Amplification of the inflammatory response

The recruitment of immune cells is mediated by a variety of chemotactic factors (chemokines) secreted into the circulation and of adhesion proteins (selectins, integrins) presented at the luminal surface of activated endothelial cells (see section inflammation). Chemokines play an important role in the secondary recruitment of leukocytes into the established inflammatory focus [Baggiolini and Dahinden, 1994]. In brain, inflammatory chemokines are not only produce by hematogenous cells but also and predominantly by local cells such as astrocytes [Tani and Ransohoff, 1994]. Liberated in the extracellular and perivascular space, they apparently modulate the inflammatory reaction by attracting additional monocytes. In comparison to cytokines, the synthesis of chemokines in the lesion is much more prominent and less controlled [Schluesener and Meyermann, 1993].

5.3.4 Mechanisms of immune-mediated tissue damage in brain lesion

Infiltrating macrophages and intrinsic microglia take part in the inflammatory process by phagocytosis of myelin, leading to demyelination [Gehrmann *et al.*, 1993; Bauer *et al.* 1994]. Immune effector cells, such as monocytes/macrophages, granulocytes or cytotoxic T cells also produce a variety of toxic factor, that are required for the destruction and elimination of foreign pathogens (myelin in our example of EAE). These include cytotoxic cytokines (TNF- α , lymphotoxin) perforin or complement factors, proteolytic and lipolytic enzymes and oxygen radicals. These toxic factors, however, not only destroy foreign pathogens but may also damage local tissue elements. In the CNS the myelin/oligodendroglia complex appears to be particularly vulnerable to the action of these toxic inflammatory mediators [Griot *et al.*, 1990] [Scolding *et al.*, 1990] [Selmaj and Raine, 1988].

5.3.5 Physiopathology of MS brain lesions

The earliest change observed in the lesions examined in our model was widespread oligodendrocyte apoptosis in tissue in which macrophages, activated microglia, reactive astrocytes, and neurons appeared normal [Barnett and Prineas, 2004]. However, the local accumulation of activated CD4⁺ and CD8⁺ T cells around small venules, with CD4⁺ cells predominating is relevant of a starting inflammation [Hauser *et al.*, 1986]. The primary demyelination observed in MS results from damage to the myelin sheath and/or oligodendrocytes. Macrophage/microglia are active participants in myelin breakdown; phagocytosis of myelin proteins in the lesions by these cells is a reliable indicator of ongoing demyelinating activity [Bauer *et al.*, 1994]. At a later stage in the disease process myelin degeneration is associated with perivascular inflammation involving of T cells, B cells, plasma cells and activated macrophages [Prineas and Wright, 1978] [Prineas, 1975].

Gliosis is also a predominant feature of MS, and is characterized by astrocyte proliferation, hypertrophy and increase synthesis of glial fibrillary acidic protein, an astrocyte-specific protein [Bignami *et al.*, 1972]. This reaction is thought to contribute to the formation of dense glial scars in the CNS, leading to motor and sensory impairment. Recent findings with magnetic resonance imaging indicate that considerable subclinical disease occurs, and BBB breakdown is an early event in lesion development [Thompson *et al.*, 1992] [Gay and Esiri, 1991], which may be a crucial for the pathogenesis of new lesions in MS.

A typical relapse is characterized by an abrupt loss of oligodendrocytes throughout a circumscribed and relatively small volume of tissue. The formation of these new lesions occur within hours: oligodendrocytes throughout the affected tissue appear apoptotic and ramified microglia with thickened processes appear in increased numbers [Gay *et al.*, 1997]. Although apoptosis typically allows dead cells to be removed without inciting an inflammatory reaction, [Henson *et al.*, 2001] [Fadok *et al.*, 1998] [De Simone *et al.*, 2003] the multiple sclerosis lesion might be an exception in view of the relatively huge quantity of apoptotic plasma membrane, in the case of this altered myelin, generated by each dying oligodendrocyte. Inflammation is associated with postapoptotic necrosis, which occurs when normal clearance mechanisms of apoptotic cells are overwhelmed [Henson *et al.*, 2001] [Barnett and Prineas, 2004]. T cell, early activated macrophages [Aboul-Enein *et al.*, 2003] and myelin phagocytes are rare or absent in the apoptotic zone but are present elsewhere in the lesion. After 1 or 2 days, oligodendrocytes disappear, most presumably phagocytized by the now amoeboid

microglia present in the tissue. The tissue appears vacuolated because of the presence of widespread intramyelinic edema, which usually accompanies oligodendrocyte loss [Graeber Blakemore, Graham DI, Lantos PL, eds. *Greenfield's Neuropathology*. 7th ed. London: Arnold 2002].

5.3.6 Clearance of inflammation

Finally during clearance of inflammation, inflammatory cells, that have entered the brain during inflammation, have to be removed from the lesion during recovery. Most of the apoptotic cells are T lymphocytes and the peak of T cells apoptosis correlates well with the clearance of the inflammatory lesion [Schmied *et al.*, 1993]. There is some evidences that the population of autoantigen-specific T lymphocyte that is removed by programmed cell death in the brain [Tabi *et al.*, 1994; Bauer *et al.*, 1995].

Lassman *et al.*, have studied recently that migration routes of macrophages that have taken up brain proteins in inflammatory demyelinating lesion and found evidence for a drainage pathway through the spinal meninges into the epidural lymphatic vessels and the para aortal lymph nodes. In addition, some macrophages were also found to migrate through the walls of inflamed vessels through the circulation and could then be identified in the spleen.

6 IN VIVO MRI OF BRAIN IMPAIRMENT

The noninvasive measurement of brain impairment can be performed by MRI (6.1) by focusing on the injuries induced by the progression of MS or EAE. The chapter 6.2 presents the possibilities to image structural changes such as blood brain barrier leakage or demyelination processes. Beyond tissues imaging, new protocols in MRI allow a spatial resolution at the single cell level. Chapter 6.3 describes the possibilities to label specific cells and to visualize them by MRI.

6.1 MRI Visualization of Brain Inflammation

Imaging of inflammatory events in the brain can be based on targeting various processes along the immune response. Because the CNS presents some differences compared to other organs, specific events of the pathophysiological cascade have to be identified and tagged.

First, due to the BBB, immune cells, antibodies and immunological mediators have little access to the normal brain [Hickey, 1991]. Yet, there are some hematogenous (coming from the blood) cells present in the CNS under normal conditions [Hauser *et al.*, 1983b]. T lymphocytes can traverse the normal BBB, when they are in an activated state [Wekerle *et al.*, 1991; Hickey *et al.*, 1991; Hickey, 1991]. These data suggest that it is a small pool of peripheral activated T cells that enter the CNS for immune survey in search for specific antigens or pathogens.

Secondly, other molecules like adhesion molecules, that are essential in the cell-cell contacts during the migration of inflammatory cells [Bevilacqua, 1993] [Springer, 1994] have a low expression on endothelial cells of cerebral vessels as well as on local tissue elements [Sobel *et al.*, 1990] [Raine *et al.*, 1990] [Lassmann *et al.*, 1991].

Two ways are thus available to visualize inflammatory events in the brain either targeting antigens or immune cells or by targeting secondary markers of inflammation.

Targeting antigens or immune cells: The immune cells themselves or immune chemical receptors (e.g. cytokine receptors) could serve as primary imaging targets, since their activation or presence within inflammation areas in the brain is directly linked to the disease process and to the damage of brain tissue.

Targeting secondary markers of inflammation: Imaging of neuro-inflammation has emerged from the visualization of processes down-stream of the initial inflammatory events, i.e. structural/micro-structural changes in brain tissue. Markers of vascular edema, demyelination and blood brain barrier damage have been extensively applied both in preclinical and clinical studies. Despite the fact that their specificity for the pathophysiology of MS remains questionable, these readouts have played, and still do so, a tremendous role for the *in vivo* assessment of inflammatory diseases of the CNS due their robustness and broad availability.

6.2 Imaging of Structural Changes

6.2.1 Assessment of BBB Leakage: Gd-Enhancing Lesions

It has been detailed in the section 3.2 that the BBB play the role of a high selective filter that protect the brain parenchyma from circulating agent potentially dangerous for the brain and is responsible for the homeostatic regulation of the brain microenvironment. In the case of brain inflammation, BBB integrity is disturbed: transcytosis of leukocytes from the circulation into the brain parenchyma and their associated inflammatory processes can interfere with the integrity of the BBB. This damage is specific for leukocyte infiltration under inflammatory conditions since the trans-endothelial migration of immune cells during immune surveillance does not lead to BBB damage [Gloor *et al.*, 2001]. Moreover, BBB breakdown can occur as a consequence of direct mechanic (hemorrhage) or ischemic damage of endothelial cells. The breakdown of the BBB can be visualized by MRI during early lesion development [Thompson *et al.*, 1992] [Gay and Esiri, 1991], which may be a crucial event in the pathogenesis of new lesions in MS [Abbott *et al.*, 1999]. In most cases, low molecular weight CAs such as Gd-DOTA or Gd-DTPA are used, which are approved for clinical use since almost two decades. These CAs are administered intravenously at a typical dose of 0.1 mmol/kg (clinical single dose). The intact BBB is impermeable for these molecules but in areas of acute inflammation, CA can leak out of the blood vessels into the interstitial space, where it leads to an enhancement of longitudinal and transversal relaxation rates and therefore to a change in MR signal intensity.

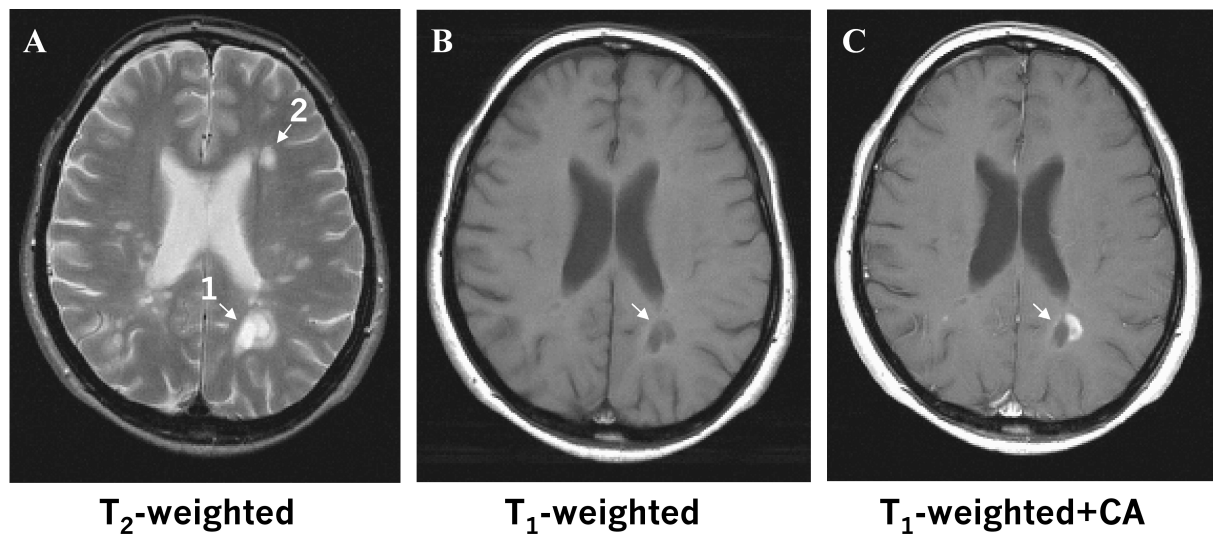
However, the visualization of increased BBB permeability provides a sensitive but not very specific marker for acute inflammatory processes. It should also be remembered that correlative studies of Gd-enhancement and cellular infiltration cannot provide the ultimate prove for a one-to-one correlation, because tissue samples are always taken from areas which show clear signal abnormalities in the MR images; hence the available data are biased. The occurrence of inflammatory events of neurological relevance, i.e. infiltration of immune competent cells into brain parenchyma, might not be associated with structural damage. At least for the rat EAE model it was shown that areas of macrophage infiltration were not affected by BBB damage as measured by administration of Gd-DOTA [Rausch *et al.*, 2003] or that BBB damages has occurred only transiently and the BBB has been reconstituted at the

time point of the measurement. Such tissue areas have been defined “normal-appearing white matter”.

6.2.2 T_2 -Hyperintense Lesions and Multi-Component- T_2 -Mapping

Enhanced T_2 relaxation times are one of the most characteristic hallmarks of MS lesions. T_2 is a sensitive but rather unspecific imaging readout [Barkhof and van Walderveen, 1999]. Combined MRI and histopathological analysis has shown that T_2 -hyperintensity can be observed during the acute, subacute and chronic demyelinated or even remyelinated state of lesions [Bruck *et al.*, 1997]. Physiologically, T_2 -prolongation can be observed as a consequence of vascular edema, which results from a redistribution of water from the vasculature into the tissue. Occurrence of a vascular edema is an important indicator of acute inflammatory processes accompanied by acute or persistent BBB damage (Figure 6.1).

Figure 6.1



MR-images showing MS-lesions of different characteristics. (A) T2-weighted image. Two lesions are marked by arrows. (B) Same slice acquired with a T1-weighted sequence prior to administration and (C) after administration of a low molecular weight CA (Gd-DOTA). Only lesion 1 from the T2-weighted scan appears hypointense on the T1-weighted scan and takes up CA. Lesion 2 does not enhance CA. This set of images demonstrates the variable relationship of lesion type and MR parameters.

At least two components contribute to the overall T_2 -values measured in affected tissue: a long T_2 -component (70-95ms) of (bulk) water in cytoplasmic and extracellular spaces and a short T_2 -component (10-55ms) associated with water molecules bound within myelin membranes. Protons of cerebrospinal fluid (CSF) have T_2 -times of the order of 1s [MacKay *et al.*, 1994]. Although not prominent in the T_2 -maps, the short T_2 -component might play the relevant role for the distinction between acute inflammation and persistent degeneration. As shown for MS lesions in patients and in animal models of EAE [Stewart *et al.*, 1993], a decrease of the fast T_2 -component has been observed for chronic lesions; this is interpreted as loss of myelin and reflects a chronic impairment of tissue function.

6.2.3 Magnetization Transfer Contrast

Magnetization transfer imaging can be used to assess the degradation of myelin in the brain of MS patients or in animal models [Henkelman *et al.*, 2001] [Graham and Henkelman, 1997]. The technique probes the transfer of longitudinal magnetization between to molecular partners that are coupled via chemical exchange, magnetic cross-correlation, or spin diffusion. For water exchange in biological tissue the process studied is the transfer of longitudinal magnetization between protons that are bound to immobile (macromolecular) surfaces such as the myelin sheath of axons (see section 3.1.2) and free protons.

MTRs have been extensively used in clinical MS trials. Compared to BBB damage and edema, reduction of MTR has been associated to permanent loss of white matter integrity or at least to transient demyelination. Similar assumptions have been made for tissue damage due to ischemia [Ordidge *et al.*, 1991]. However, as already discussed, even quantitative measurements of MTRs or of exchange rate constants cannot provide direct information on the reduction of myelin or other membrane elements. Degradation of these structures should be associated with a reduced amount of bound water, which, however, is invisible in MRI. The indirect visualization by imaging the interaction of bound and free water protons by the magnetization transfer effect underlies one severe limitation: changes in the empirical rate constant k (or in MTRs) can be due to changes in the density of the bound protons or the alteration of the effective exchange rate. Hence, a strict biophysical link between the empirical MRI-derived parameters to tissue degradation is not possible. Nevertheless, the assumption that reductions in MTR qualitatively reflect tissue damage is plausible, and the readout is considered of diagnostic value.

6.2.4 T_1 -Hypointense Lesions

Chronic lesions can appear hypointense on post-contrast T_1 -weighted images [Barkhof and van Walderveen, 1999] [Truyen *et al.*, 1996], and were therefore termed 'black holes'. It has been proposed that this signal change is associated with hypocellularity, demyelination, axonal loss and/or the presence of reactive astrocytes [van Walderveen *et al.*, 1998]. Hence, T_1 -hypointensity should indicate severe, irreversible damage of brain tissue, actually neurodegeneration, which should be more closely related to the disability status as compared to the inflammation marker vascular edema or BBB damage. From a diagnostic point-of-view, however, T_1 -hypointensity is considered just a qualitative measure for the presence or absence of a lesion. Since several different pathological processes can lead to this form of signal loss (or a decrease of the T_1 -relaxation time corresponding to an increase in R_1 -relaxivity), it is almost impossible to measure the status of a lesion or to predict its future development.

6.3 Cell Labeling

In the previous section we focused on visualizing aspects of immune cell recruitment, i.e. on the expression of antigens by endothelial cells in the affected region. *In vivo* tracking of immune cells per se would provide another relevant readout to evaluate inflammatory processes in the brain.

As already discussed, there are two classes of immune-cells: lymphocytes, which orchestrate the tissue response to inflammation and macrophages, which eliminate the antigen expressing pathogen and are responsible for massive tissue destruction. The majority of *in vivo* labeling studies focused on macrophages taking advantage of their phagocytotic activity. Macrophages recognize nano-particles of a certain size as foreign antigens, and incorporate them into their lysosomes. This mechanism is rather established for labeling cells of the monocyte phagocytic system of the liver with SPIOs nanoparticles. Efficient labeling of the different types of macrophages (e.g. lymphnode or blood-borne monocytes) requires sufficient exposure time for phagocytotic label uptake. Nanoparticles should not be cleared rapidly by Kupffer-cells in the liver, circulation time should be of the order of several hours. USPIOs were originally designed for the demarcation of benign from malignant lymphnode lesions. However, due to their plasma half-life of 5 hours, it could be demonstrated that these particles also allow visualization of blood-borne macrophages in animal models of stroke and EAE [Rausch *et al.*, 2001] [Dousset *et al.*, 1999c] [Dousset *et al.*, 1999a] [Dousset *et al.*, 1999b].

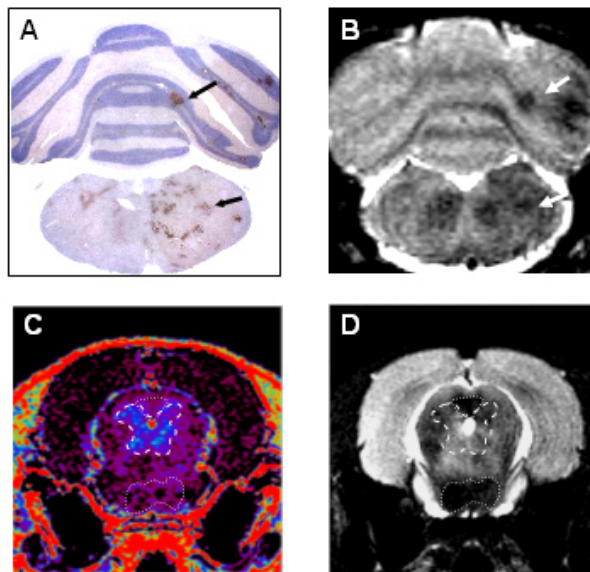
6.3.1 Macrophages tracking by MRI

Visualization of infiltrating macrophages offers several advantages over imaging of downstream processes such as BBB damage. First, the primary demyelination observed in MS results from damage to the myelin sheath and/or oligodendrocytes. Macrophage/microglia are active participants in myelin breakdown; phagocytosis of myelin proteins in the lesions by these cells is a reliable indicator of ongoing demyelinating activity [Bauer *et al.*, 1994].

Secondly, acute inflammatory activity is a transient process. In the rat EAE model it could be demonstrated that the infiltration of macrophages is closely linked to behavioral disability as reflected by a neurological score. BBB damage, on the other hand, appears to be a more persistent effect, which extends over several days [Floris *et al.*, 2004]. This suggests that the BBB is leaky during several phases of the inflammatory cascade including the early

interaction of leucocytes with endothelial cells, the opening of tight junctions due to transcytosis and potentially also tissue repair mechanisms. There is also experimental evidence that the presence of labeled macrophages is not necessarily associated with BBB damages (see Figure 6.2).

Figure 6.2



Comparison of parametric images from one animal of the EAE group. A) ED-1 stain demonstrating macrophages in the cerebellum and the medulla of an animal with acute EAE. B) The T2 image displays hypo-intense areas, induced by accumulation of USPIO. C) and D) Corresponding slices from another animal with EAE demonstrating the mismatch of Gd- and USPIO-enhancements. Enhancement of Gd-DOTA is visible in structures of the midbrain. The discrepancy of spatial localization of USPIO and Gd-DOTA enhancement is demonstrated by the dotted and dashed lines. The area marked by the dotted line accumulated USPIO but no Gd-DOTA. The reverse situation can be observed in the area marked by the dashed line.

A detailed analysis of Gd- and USPIO-enhancing lesions in a chronic relapsing rat EAE model has demonstrated a significant spatial mismatch between BBB permeability and monocyte infiltration [Rausch *et al.*, 2003]. Qualitatively, Gd-enhancement also appeared more diffuse as compared to the distribution of USPIO-labeled cells, possibly because low molecular weight CAs passively diffuse within the interstitium. However, during the acute phase of EAE there was also a clear mismatch in that some areas that showed either accumulation of USPIO or Gd-DOTA. During the chronic phase, only USPIO-induced enhancement has been observed. Although the EAE model cannot be translated in a one-to-

one fashion to human MS, these findings raise the question whether BBB damage can in fact serve as a reliable readout for acute-inflammation. This reservation is even more justified, since BBB damage as measured by Gd-extravasation is often also poorly correlated with neurological function and disease outcome [Kappos *et al.*, 1999]. Whether the correlation between the lesion load as derived from USPIO-enhancing lesions, reflecting a high macrophage concentration and correspondingly high inflammatory activity, and the clinical status of MS patients will reveal a better prognostic value of the MRI readout remains to be shown.

6.3.2 Non-phagocytotic cells labeling

Non-phagocytotic immune-cells cannot be tracked *in vivo* using MRI as easily as macrophages because those do not take up nanoparticles from the circulation. Visualization of early forming lesion in EAE would allow to characterize the local accumulation of activated CD4⁺ and CD8⁺ T cells around small venules in inflamed areas [Hauser *et al.*, 1983a]. During the next stages, the myelin degeneration is associated with perivascular inflammation consisting of T cells, B cells, plasma cells and activated macrophages [Prineas, 1975]. Imaging of such cells requires harvesting cells from a donor animal followed by *ex vivo* labeling. The feasibility of T cell labeling by USPIOs has been demonstrated: cells were incubated for several hours in medium containing the CA [Yeh *et al.*, 1995]. However, this approach turned out to be not very efficient as the incorporation of CA by pinocytosis occurs at a rather low rate. Improved methods are based on conjugating nanoparticles with transfection agents, such as the trans-acting activator domain (TAT) of the human immunodeficiency virus [Dodd *et al.*, 2001], poly-L-lysine [Frank *et al.*, 2002], or lipid-based transfection agents such as Fugene [Arbab *et al.*, 2004a], which serve as translocation signals and enhance the particle uptake. Alternatively, magnetodendrimers (see section 1.7.2) can be used, which tightly interact with the cell membrane [Bulte *et al.*, 2002]. Up to now, *in vivo* tracking of labeled T cells has not been used extensively. The reason for that might be the relatively low sensitivity of MRI itself and the complex preparation of the cell cultures. Several factors have to be considered in this respect: first, T cells have to be myelin-specific. For observation of bystander T cells, huge amounts of labeled cells must be administered because only a low fraction of these cells would enter the brain. Secondly, clonal expansion will lead to label dilution and finally, the specificity of T cells should not be affected by the labeling procedure.

Today, the advantage of the MR approach is high temporo-spatial resolution and the potential translatability to humans. It can be anticipated that imaging of monocyte infiltration and eventually also lymphocyte recruitment will have a profound influence on the diagnosis and management of MS patients.

7 OBJECTIVES AND OUTLINE OF THE THESIS

Cellular and molecular imaging is a rapidly evolving field. MR and optical approaches are constantly improved to explore the molecular processes of diseases. In consequence, there is a great need of developing new methods to make these technological advances profitable. Recently, it has become possible to detect single cells by NMR with the help of contrast agents [Dodd *et al.*, 1999] and to monitor cell migration *in vivo* [Bulte and Kraitichman, 2004]. A better understanding of immune cell migration in neuropathological diseases (e.g. multiple sclerosis) would allow a quicker and improved diagnosis. Being non-invasive, MR and optical imaging permit longitudinal studies of immune cell activity during brain inflammation or after treatment with anti-inflammatory drugs.

7.1 Tracking tagged macrophages by MRI: a tool to evaluate drug effects

The first objective of this thesis is to use nonspecific CAs for MR imaging to focus on the detection of preliminary labeled immune cells. Macrophages which are professional phagocytotic cells, are easily labeled by circulating iron particles and can be observed *in vivo* after rat transient ischemia [Rausch *et al.*, 2002a] or FTY treatment of EAE [Rausch *et al.*, 2004]. It is known that the brain inflammation in the EAE model is initiated by T lymphocytes [Traugott *et al.*, 1983b], thus the second objective is to evaluate the possibility of labeling T cells for *in vivo* tracking by MRI. As lymphocytes have no natural phagocytotic activity, primary cultured T cells have been labeled *in vitro* in order to be transferred adoptively in EAE animals before measurement.

7.2 New methods to label T lymphocytes for MR and NIRF imaging

As the visualization of iron-tagged T lymphocytes by MRI was not possible because of dilution of tagged cells in the blood and the weak inherent sensitivity of the MRI method, the third aim of the thesis was to visualize T cells and track them by using a more sensitive technique, such as near infrared imaging. Fluorescence reflectance imaging is complementary to MRI because it can detect fluorescent markers at the molecular level [Ntziachristos *et al.*, 2003]. T lymphocytes have been labeled with the cyanine 5.5 dye coupled to the Tat peptide and re-injected in the blood circulation of EAE animals. Before performing *in vivo* imaging, the toxicity and the pharmacology of the newly designed probe has been evaluated *in vitro*.

7.3 Outline of the thesis

The experimental section is composed of the following manuscripts, which have been published or are in preparation for submission:

Berger C, Hiestand P, Kindler-Baumann D, Rudin M and Rausch M.

Analysis of lesion development during acute inflammation and remission in a rat model of EAE by visualization of macrophage infiltration, demyelination and blood-brain-barrier damage.

NMR Biomed, 2006 Jan 12

Berger C, Hiestand P, Kindler-Baumann D, Rudin M and Rausch M.

Longitudinal assessment of cerebral lesions by USPIO-enhanced MRI in EAE rats: assessment of treatment efficacy of FTY720 in acute and chronic relapsing EAE.

Novartis Internal Study Report (RD-2004-01566)

Berger C, Rausch M, Schmidt P, and Rudin M.

Feasibility and limits of magnetically labeling primary cultured T cells with ferumoxides coupled with commonly available transfection agents.

Mol Imaging (2006)

Berger C, Gremlich H-U, Schmidt P, Kneuer R, Cannet C, Rausch M and Rudin M.

Tracking of Cy5.5-TAT labeled T lymphocytes by quantitative near-infrared imaging during acute brain inflammation in a rat model of experimental autoimmune encephalomyelitis.

(in preparation)

These manuscript are presented in the chapters **8.1, 8.2, 9.1** and **9.2** respectively.

The aim of the **chapter 10** (overall conclusion) is to present results in the general context of molecular imaging. It reports recent investigations in this domain and compare them to our results to orient further investigation related to the subject.

EXPERIMENTAL SECTION

8 MACROPHAGES LABELING FOR MRI

8.1 Macrophage Tracking during EAE Brain Inflammation

Analysis of Lesion Development during Acute Inflammation and Remission in a Rat Model of EAE by Visualization of Macrophage Infiltration, Demyelination and Blood-Brain-Barrier Damage

8.1.1 Abstract

In vivo tracking of macrophage migration is feasible by labeling cells with ultra small particles of iron oxide (USPIO). Here, we demonstrate that it is possible to monitor distinct patterns of macrophages migration during the early states of inflammation in a rodent model of chronic relapsing experimental autoimmune encephalomyelitis (EAE). As previous MRI studies showed that EAE inflammation processes are clearly linked to macrophages infiltration in the brain, a longitudinal protocol for macrophages visualization was designed, where USPIOs were injected repeatedly during the acute phase of the disease, the remitting phase and the first relapse. Besides USPIO-enhanced MRI, blood brain barrier (BBB) damage, magnetization transfer ratios (MTR) and neurological impairment were assessed as classical markers for central nervous system (CNS) inflammation and tissue damage. During the acute phase, animals showed severe paralysis of the hind paws, intense accumulation of macrophages in brain tissue and some diffuse patterns of BBB disruption. While USPIO-accumulation completely disappeared after the acute phase, residual damage of the BBB remained detectable in some lesions during the remitting phase. During the first relapse, the accumulation of USPIO loaded cells was less pronounced but still detectable. The time course of MTR, which is used as a marker for myelin loss, was linked to the infiltration of macrophages during the acute phase.

8.1.2 Introduction

In vivo tracking of inflammatory cells in animal models or humans is of large interest for diagnosis or staging of neuroinflammatory diseases such as multiple sclerosis (MS) and for testing new therapeutic approaches. Beyond conventional magnetic resonance based markers such as imaging of blood-brain-barrier (BBB) defects, edema or atrophy, readouts with greater pathophysiological specificity are under investigation, one being USPIO-enhanced MRI. USPIOs are ultra-small particles of iron-oxide that are taken up by activated macrophages after systemic administration [Dousset *et al.*, 1999b] [Rausch *et al.*, 2002a] [Rausch *et al.*, 2002b]. This method has already been used in several experiments showing inflammation of the brain and other organs. Dousset *et al.* [Dousset *et al.*, 1999b] have shown that *in vivo* CNS macrophage cellular imaging can be achieved on Experimental Autoimmune Encephalomyelitis (EAE) by using USPIOs. In particular for the brain, histological correlation between iron particles and perivascular macrophages showed that USPIOs are almost exclusively located within macrophages. In addition, after an exposure time of about one day, USPIO do not penetrate the intact BBB passively in EAE or stroke [Rausch *et al.*, 2003] [Rausch *et al.*, 2002b].

It is assumed that macrophages are to a large extent responsible for tissue damage in inflammatory and degenerative diseases of the Central Nervous System (CNS) [Steinman, 1996]. Detailed analysis of their accumulation has been carried out by immunohistochemistry (IHC) in animal models and in patients with MS [Bruck and Stadelmann, 2003] [Kerschensteiner *et al.*, 2004b]. In preclinical research, the model of EAE is used to study the processes leading to tissue damage and the effects of anti-inflammatory drugs [Steinman, 1999].

As demonstrated by Floris *et al.* [Floris *et al.*, 2004], the time course and spatial pattern of cell infiltration is a highly dynamic process in EAE animals and might be used as a fingerprint for brain areas undergoing acute tissue damage. In the present study, we were in particular interested in studying whether repeated USPIO injections allow distinction of the inflammatory episodes from those devoid of acute cell infiltration (remitting periods) and to compare these data to conventional imaging readouts. Imaging macrophage infiltration in

EAE animals at multiple time points would also allow studying the development of individual lesions with respect to inflammation, demyelination and tissue repair. Such a longitudinal imaging protocol would allow differentiating areas, which undergo multiple episodes of inflammation from newly forming lesions. In the present study, USPIO were administered at three time points (the acute phase, the remitting phase and first relapse) in each animal to study ongoing infiltration of macrophages. The elimination half-life of USPIO used here is of about 5h [Dousset *et al.*, 1999c] and the time during which USPIO labeled macrophages remain visible in MR images is in the order of two to three days post-injection [Rausch *et al.*, 2001]. Therefore, at intervals of 5 days between each injection, contrast in MR images is not sensitive to USPIO which have been injected during an earlier imaging session.

USPIO accumulation was in addition compared to Gd-DOTA enhancement, allowing visualization of BBB damage, to magnetic transfer ratio imaging (MTR), which allows detection of demyelination and to neurological readouts.

8.1.3 Material and Methods

Animal Model Experimental Autoimmune Encephalomyelitis (EAE) in the Lewis rat is characterized by an acute monophasic attack after immunizing with xenogenic CNS proteins (i.e. guinea-pig spinal cord tissue). It is possible to prolong the disease course in Lewis rats and induce a relapsing pattern by slightly increasing the concentration of encephalitogenic antigens (which generate inflammation of the brain) and/or *Mycobacterium tuberculosis* in the inoculum [Feurer *et al.*, 1985]. In this experiment, brain inflammation is monitored only during the acute phase up to the first relapsing phase.

Inbred (RT1^l) female Lewis rats (N=10) from Charles River (Sulzfeld, Germany) were kept in a climate-controlled room with 12 hour light/dark cycles, housed in sawdust-lined cages with 4 to 5 rats per cage, and given standard rodent chow and water *ad libitum*.

Rats weighing 150-165 grams were lightly anesthetized with isoflurane (Abbott, Baar/Zug, Switzerland) and immunized intradermally (i.d.) into each hind foot pad with a 100 µl

suspension consisting of 1 part (volume:volume) guinea pig spinal cord (Gp-sc) emulsified in 0.9% NaCl to 1 part complete Freund's adjuvant (CFA; Difco, Detroit, MI, US) supplemented with *M. tuberculosis* strain H37RA (Difco). The final inoculum per rat consisted of about 66 mg Gp-sc and 2 mg mycobacterium.

For the MRI experiments, the rats were anaesthetized using 1.5% isoflurane in nitrous oxide (2:1) and the tail vein was cannulated with a catheter (0.5×25 mm) (Becton-Dickinson, Basel, Switzerland) for infusion of contrast agent. The animals were placed on a support where body temperature was maintained at 37°C using warm air. Total MRI scanning time was 45 min per rat. All experiments were in strict concordance to the Federal law for animal protection.

All animals were scanned at three time points by MRI. MRI acquisitions were performed on two days during each of the three EAE phases, i.e. 11-12 days post immunization (dpi) for the acute phase, 18-19 dpi (remitting phase) and 24-25 dpi (first relapse). Additionally, neurological scoring was carried out on every day after immunization. A measurement of animal body weight was done at days 0, 7, 14 and 21 after immunization.

Neurological scoring Neurological examination was performed daily and animals were graded according to disease symptoms: 0 = normal; 1 = flaccid tail; 2 = hind limb weakness or ataxia; 3 = complete hind limb paralysis, often accompanied by incontinence.

Imaging protocol MRI experiments were carried out on a Bruker Biospec 7T/15 cm system (Bruker, Karlsruhe, Germany) using a birdcage head coil with 35 mm inner diameter for RF transmitting and receiving. The protocol comprised a T2-weighted fast-spin-echo scan (TR=4500, TE=73, RARE-factor=12, NEX=4, MTX=256×192) and a T1-weighted scan (TR=600, TE=8, NEX=4, MTX=256×128). In a third scan, T1-imaging (same parameters as before) was combined with magnetization transfer suppression (MTS). A Dante pulse sequence for MTS (pulse power = 16 μ T, number of pulses = 256, offset frequency = 5000 Hz) was used. After an intravenous injection of 0.2 ml (1mmol) Gd-DOTA per animal (Dotarem®, Guerbet, Aulnay-sous-Bois, France), one T1-weighted scan was started five minutes after the contrast agent injection. The geometrical parameters were the same in all scans: FOV = 3.5×3.5 cm, slice thickness = 1 mm and interslice-distance = 0.28 mm.

For labeling of macrophages, 0.3 mL per animal of Sinerem® (AMI-227, Guerbet, Aulnay-sous-Bois, France) was injected into the tail vein of each animal 24h prior to every MRI acquisition at a dose of 300 $\mu\text{mol Fe/kg}$. Each rat received this bolus of USPIO before each MRI measurements i.e. during acute phase (at 11 or 12 dpi), remitting phase (at 18 or 19 dpi) and first relapse (at 24 or 25 dpi). Every MRI sessions were performed on all animals. The administration and scanning protocol was adopted from previous studies on EAE and stroke [Rausch *et al.*, 2002b], [Rausch *et al.*, 2003], [Rausch *et al.*, 2001] and was optimized to detect labeled cells without background signal from USPIO, which had not been captured by phagocytic cells.

Image analysis BioMAP 3 software (developed in-house based on IDL 6, an application development software; Research Systems Inc., Col., USA) was used for image analysis. For quantitative assessment of disease-related signal changes, regions of interest (ROIs) have been defined, which comprised areas of hypo-intense signal in T2-weighted images during the acute phase. As demonstrated in our previous studies [Rausch *et al.*, 2003] [Rausch *et al.*, 2002b] [Rausch *et al.*, 2001], dark areas correspond to lesions infiltrated by labeled macrophages. ROIs were only defined for the medulla oblongata since inflammation occurred systematically in this part of the brain. Signal alteration in Gd-DOTA enhanced maps (Enh-maps) as well as MTR values were analyzed for these ROIs. Gd Enh-maps and MTR maps were calculated for the three phases of the disease (i.e. acute, remitting and first relapse) based on the ROIs defined for the acute phase. Due to the inherent variability of the immunization effect (i.e. concentration and virulence of the encephalitogenic antigens), lesion patterns can differ between experiments. As animal never showed USPIO enhanced areas in the cortex in this experiment, the parietal cortex was used as a control region for inter- and intra-subject comparison.

To measure the lesion volume during the remitting and the first relapse phase, ROIs based on USPIOs hypo-intense areas were also determined for these EAE episodes. Total lesion volume was calculated by adding the areas of all ROIs (acute, remitting and first relapse) multiplied by the interslice distance. Enh-maps were calculated from the signal of the pre- (S_{pre}) and post-contrast (S_{post}) T1-weighted scans according to

$$Enh = \frac{S_{post} - S_{pre}}{S_{pre}}$$

MTR-maps were calculated from the T1-weighted scans with (S_{MTR}) and without MTS-preparation (S_0) by

$$MTR = \frac{S_0 - S_{MTR}}{S_0}$$

Statistical analysis Statistical comparisons were made by using Microsoft Excel applying the two-tailed Student t-test. Differences larger than $p < 0.05$ were reported as significant.

8.1.4 Results

Neurological assessment Animals showed neurological impairment up to level 3 between 10 and 12 days post immunization (dpi, Figure 1A) with 100% disease incidence paralleled by a loss of weight during the same period (Figure 1B). The acute phase was followed by a remitting phase between 15 and 20 dpi during which neurological status improved almost completely and body weight recovered.

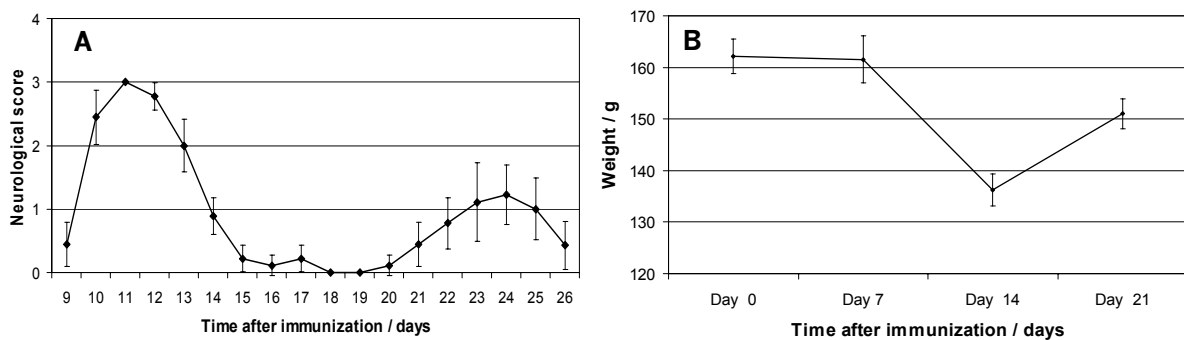


Figure 1: A) Neurological score of animals during the different phases of EAE. Animals display neurological impairment during the acute phase and the first relapse, while they show almost complete remission between the two periods. The acute inflammatory phase ranges from 9 to 15 dpi, the remitting phase from 15 and 20 dpi, and the first relapse from day 21 to 26 post immunizations. **B)** The body weight of animals was monitored on days 0, 7, 14 and 21. Animals display significant loss of body weight during the acute phase. Animals recovered weight during the remitting phase. Values are shown as mean \pm standard deviation.

During the first relapse (21 to 26 dpi), neurological impairment was characterized by an average level of 0.85.

MRI Tissue infiltrated by USPIO labeled macrophages is visible on T₂-weighted images as hypointense areas. Representative images are shown for each EAE phase in the Figure 2. The lesion volume as defined by the area of macrophage infiltration in the medulla oblongata is shown in Figure 3A. Infiltration of labeled macrophages could be detected during the acute phase. During the remitting phase, no USPIO enhanced lesions became apparent in the brain. During the first relapse, only weak signs of USPIO enhancement were observed in 3 out of 9 animals (one animal died during MRI scan of the first relapse), which were located in sub-cortical areas (not shown in the Figure 2). These USPIO enhanced lesions were not necessarily collocated with lesions that were formed during the acute phase. Although an USPIO-lesion volume of 20 up to 60 mm³ produce almost constantly the same high degree of neurological impairment (see Figure 3A), there was no linear correlation during the first relapse (Figure 3B).

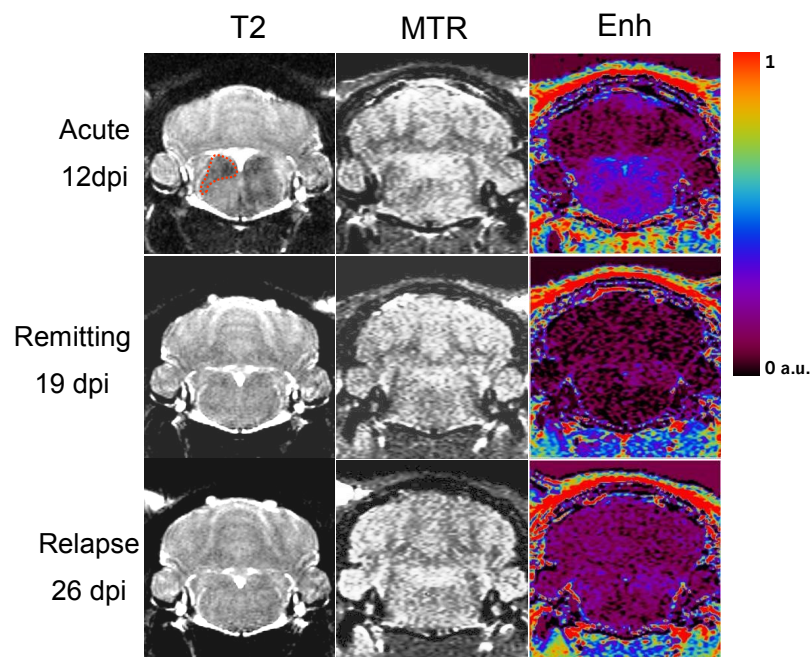


Figure 2: MRI brain scans of EAE animals during acute phase i.e. 11,12 dpi (first row), remitting phase 18, 19 dpi (second row) and first relapse 24, 25 dpi (third row). Left column: USPIO-enhancement. Tissue infiltrated by labeled macrophages appears hypo-intense on T₂-weighted images. Middle column: MTR maps. There are no large changes visible in the images (ROI based analysis revealed only changes in the order of 10%; see Figure 3). Right column: Enhancement of Gd-DOTA in brain tissue as a marker for BBB damage. Areas of Gd-DOTA extravasation in the medulla appear blue on the Enh-maps. Enhancement of Gd-DOTA in the medulla is more diffuse as compared to USPIO enhancement.

Enhancement of Gd-DOTA in brain tissue was primarily observed during the acute phase of the disease (Figure 2, right column). Even if areas of Gd-DOTA enhancement appeared more diffuse probably due to the passive diffusion of Gd-DOTA within the edema, these areas were matching those of USPIO-enhancement. However, in some animals (images not shown), areas of the medulla oblongata showed only uptake of either USPIO or Gd-DOTA. A quantitative analysis of BBB-damage is shown in Figure 3C. During the acute phase, the extravasation of Gd-DOTA was significantly increased in USPIO enhanced lesions as compared to the frontal cortex ($p=0.003$), which was used as reference. During the remitting period, the integrity of the BBB recovered but Gd-DOTA-extravasation was still larger than in the cortex ($p=0.007$). The first relapse was not related to a second increase of BBB permeability but a further recovery.

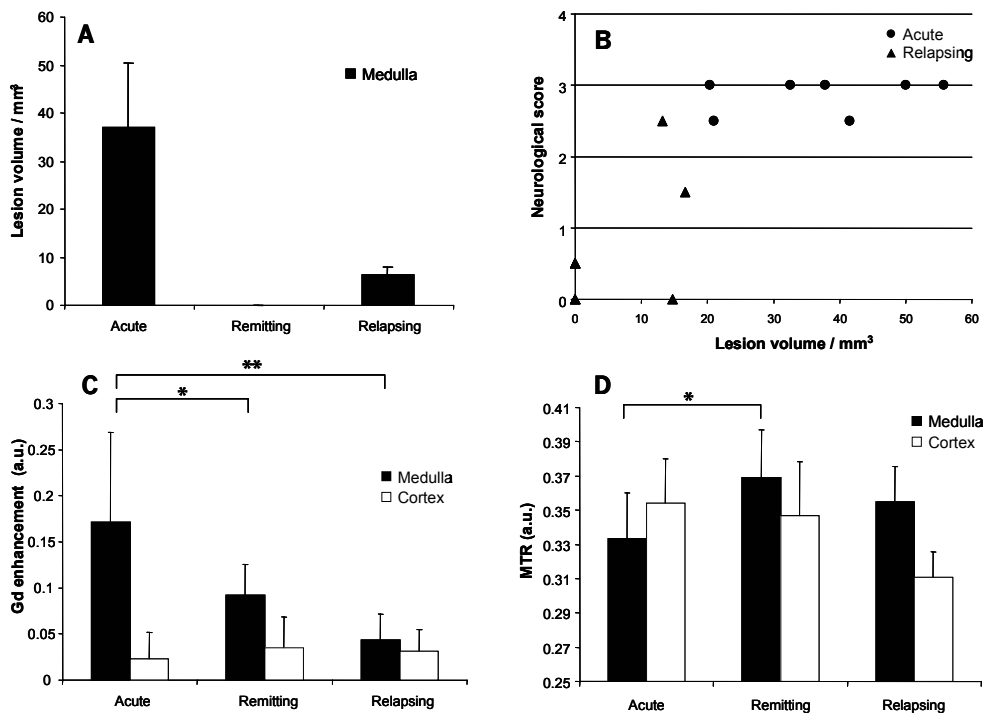


Figure 3: **A)** Lesion volume for the medulla. Values are shown for the three episodes of the disease, which are the acute phase, the remitting phase and the first relapse. **B)** Correlation among different animals between USPIO-lesion volume corresponding to macrophages infiltration and neurological state of EAE animals. Data from the acute phase (circles) and first relapse (triangles) where lesions were visible are shown (7 animals of 10 present a lesion volume equal to zero). Data from the remitting phase are not shown, since animals had neither USPIO-enhancement nor neurological symptoms. **C)** Quantitative analysis of Gd-enhancement from T1-weighted MRI data. Quantitative analysis was carried out for the ROIs, which were defined on the T2-weighted images and represented USPIO-enhancing areas. (with * = $p < 0.05$ and ** = $p < 0.01$) **D)** Quantitative analysis of MTR data. Analysis was carried out for the same ROIs as in C. Values are shown as mean \pm standard deviation.

Figure 3D shows a quantitative analysis of MTR values. MTR of the medulla is slightly reduced compared to MTR values in the cortex of EAE animals during the acute phase. In the remitting phase MTR of the medulla recovered significantly compared to acute phase and did not decrease again during the first relapse. Despite the fact that we have never observed USPIO accumulation in the cortex, a significant decrease in MTR ($p = 0.00178$) was found for the cortical ROI between the acute phase and the first relapse.

8.1.5 Discussion

MRI and neurological impairment were used to study neuro-inflammatory and neuro-degenerative processes in EAE rats. An estimation of the body weight of EAE rats was relevant for the general healthy states of animals. In contrast to earlier studies [Rausch *et al.*, 2003] [Floris *et al.*, 2004] which focused on a particular stage of the disease, animals have been scanned multiple times allowing the longitudinal observation of macrophage infiltration and BBB-damage during the different stages of the disease in individual animals.

Animals showed the typical pattern of chronic EAE: acute phase – remitting phase – 1st relapse. However, unlike in human MS, episodes of active inflammation clearly decrease in severity after the acute phase, which was observed around day 11 after immunization. The three phases could clearly be identified from the neurological state of animals (weakness, hind limb paralysis): animals showed a loss of weight during the inflammatory episodes and a recovery of body weight and neurological state during the remitting phase. Infiltration of macrophages was also exclusively observed during episodes with active inflammation i.e. acute phase and first relapse: lesions showing clear signal attenuation in T2-weighted scans during the acute phase, which disappeared during the remitting phase. Regarding MRI data, it is impossible to distinguish if USPIO have been degraded within the lysosomes of macrophages and have lost their superparamagnetic characteristics or if labeled macrophages have left the area of inflammation. However, data suggest that there is no infiltration of macrophages during the remitting phase of the disease. This observation indicates that acute infiltration of macrophages can be detected by systemic administration of USPIO and that the elimination time of this contrast agent or labeled of macrophages is sufficiently short to

distinguish episodes of inflammation and remission. This non-invasive MRI readout for cell migration is superior to immunohistochemistry since it allows studying the fate of inflammatory lesions over time. In this experiment lesions within the medulla, which have emerged during the acute phase, did not undergo a second infiltration by macrophages during the first relapse. This observation suggests that infiltration by macrophages within these lesions ends with the onset of neurological remission.

We attribute this decrease in the T2 signal to iron-labeled recruited blood-born macrophages because no free diffusion of USPIO across tight junctions can be expected. Typically, BBB capillaries have 4-6 nm fenestrations [Mandler, 2002]. During the acute inflammation processes, tight junction pores can increase to a diameter of up to 20 nm [Rapoport, 2000] which does not allow USPIO particles (30 nm) to cross the BBB. Even if the BBB is disrupted and allows serum components to passively diffuse across tight junctions (i.e. forming edema), the absence of neutrophils and red blood cells within the CNS suggests that even the impaired BBB actively controls the recruitment of inflammatory cells into the CNS [Wolburg *et al.*, 2004]. Moreover, it has been shown recently that the migration of mononuclear cells across the BBB during EAE inflammation leaves tight junction intact [Wolburg *et al.*, 2005]. Hence, there is much evidence that USPIOs are specific markers for blood-born macrophages and should not freely diffuse across tight junctions followed by uptake by resident microglia.

USPIO-lesion load and neurological symptoms were also analyzed on a single-subject level in order to assess the relevance of macrophage infiltration for the development of paresis of the sensory-motor system. Since spinal cord and brain stem are important structures for transmission of ascending and descending neuronal signals, neurological impairment should coincide with lesions within these sites. Although USPIO uptake coincided with neurological impairment on a qualitative level, no quantitative correlation was found between these parameters. In particular during the acute phase, high neurological impairment was found with a wide range of lesion load as defined by the area of USPIO enhancement. Nevertheless, a minimal lesion load leading to an onset of symptoms was observed, which was in the order of 15mm³. This threshold cannot be explained by the present imaging data. It is known, however, that rats display a high grade of brain plasticity, which might compensate for axonal damage because a certain amount of residual fibers remains intact [Wiessner *et al.*, 2003]. Moreover, reorganization of corticofugal fibers was observed in a model of focal EAE of

spinal cord already a few days after induction of an inflammatory lesion [Kerschensteiner *et al.*, 2004a].

MTR is related to the amount of myelin, which is subject to degradation by macrophages in EAE. Quantitative changes of this parameter indicate either demyelination or myelin re-synthesis. In this study, the time course of MTR followed that of USPIO accumulation. Hence, as expected from the pathophysiology of EAE, myelin degradation seems to be closely linked with the infiltration of macrophages. MTR reduction was more pronounced during the acute phase, since the present EAE model rarely leads to pronounced relapses. Moreover, the fast recovery of MTR-values after the acute phase suggests a possible remyelination, which was also reported for MS lesions [Raine and Wu, 1993]. However, the normalization of MTR values during the remitting phase could be also explained by resorption of vascular edema and normalization of T1-values since the MTR-effect is to some extent sensitive to longitudinal relaxation of bulk water [Rudin and Sauter 1992].

The measurement of BBB damage revealed similar results as reported earlier [Rausch *et al.*, 2003]: although there was a mismatch of USPIO and Gd-DOTA enhancement for some potential inflammatory lesions, both parameters provided useful results on the time course of the disease. Interestingly, USPIO-enhancing lesions disappeared after the acute inflammatory episode, while BBB damage of these lesions recovered more slowly. Although several studies have demonstrated a close link between macrophage infiltration and BBB damage, it must be assumed that opening of the tight junctions persists also after termination of leukocyte transmigration [Floris *et al.*, 2004] [Morrissey *et al.*, 1996].

In conclusion, this approach for in vivo cell labeling allows longitudinal monitoring of acute infiltration of macrophages, which are of high relevance for tissue damage in EAE and MS by repeated USPIO administration and MRI measurements. Combined with MTR analysis and Gd-enhancement mapping, USPIO administration can be used several times during the disease course to monitor the evolution of pathological hallmarks of EAE. As in an earlier study, we have found a mismatch of USPIO and Gd-DOTA enhancement, while there was a closer link between USPIO-accumulation and MTR reduction.

8.2 Monitoring Macrophage: a Tool to Evaluate Drug Effects

Longitudinal Assessment of Cerebral Lesions by USPIO-Enhanced MRI in EAE Rats:

Assessment of Treatment Efficacy of FTY720 in Acute and Chronic Relapsing EAE

8.2.1 Abstract

The efficiency of the anti-inflammatory drug FTY720 on experimental allergic encephalomyelitis (EAE) was evaluated using longitudinal magnetic resonance imaging measurements. The anti-inflammatory drug FTY720 was used for treatment of rats in a model of chronic relapsing EAE at a dose of 0.3mg/kg/day. MRI and neurological readouts were used to study the burden of disease in treated and untreated animals. Animals were studied at three time points: acute phase, remitting phase and first relapse. Our results show that untreated animals showed severe paralysis of the hind paws, intense accumulation of macrophages in brain tissue and areas of blood brain barrier (BBB) disruption in contrast to FTY720 treated animals, which displayed no signs of inflammatory activity or neurological impairment during the treatment period. These observations were made for the acute phase and the first relapse. Termination of treatment after the acute phase led to fast onset of symptoms. Moreover, there is some evidence that treatment with FTY720 before or during a relapse might cause partial loss of blood-brain-barrier integrity. We conclude that FTY720 administration can reduce demyelization and BBB disruption during leading to prevention of inflammatory events in EAE rats.

8.2.2 Introduction

Experimental allergic encephalomyelitis (EAE) is a commonly used animal model, which mimics in several aspects human multiple sclerosis [Steinman, 1999] [Raine and Traugott, 1984]. EAE can be induced in several species by administration of myelin antigens, most often myelin basic protein (MBP), or myelin reactive CD4+ cells. The immune response triggered in EAE involves activation of several cell types. While T lymphocytes trigger inflammatory process by secreting chemokines that promote leukocytes infiltration, monocytes are thought to be the primary cell type that causes tissue damage [Steinman, 1996; Izikson *et al.*, 2000].

The aim of this study was to further evaluate the *in vivo* immunomodulatory effects of FTY720, a novel sphingosine-1 phosphate (S1P) receptor agonist [Brinkmann *et al.*, 2002] by conventional and target specific MRI techniques. FTY720 is a myriocin analogue that alters homing of lymphocytes from the peripheral blood to secondary lymphoid organs. FTY720 acts by signaling EDG-6, a lymphoid specific G-protein coupled receptor, which increases the intrinsic mobility of lymphocytes [Kahan, 1998; Brinkmann *et al.*, 2001]. Hence, the cells respond more readily to lymphocyte-homing chemokines, which are continuously expressed in secondary lymphoid organs. The homing to these lymphoid organs decreases the levels of freely circulating lymphocytes and hence the number of activated lymphocytes recruited by inflamed tissue will be reduced.

MRI allows *in vivo* assessment of several aspects of EAE or MS related pathological processes including early inflammation, tissue degradation and scar formation: contrast enhanced T1-weighted imaging using extra cellular contrast agents allows to detect areas of increased blood brain barrier (BBB) permeability as an early indicator for leukocytes infiltration [Katz *et al.*, 1993]. T2-weighted scans are sensitive to elevated levels of tissue water, as found in edematous tissue and also across sclerotic lesions [Miller *et al.*, 1998] but are generally of low histo-pathological specificity [Barkhof and van Walderveen, 1999]. In later stages of the lesion development, magnetization transfer imaging (MTI) can provide specific information about demyelization. MTI is a technique based on the transfer of longitudinal magnetization from protons of bulk water to relatively immobile myelin-bound

protons by continuous or pulsed off-resonance excitation [Clark *et al.*, 1991]. Signal attenuation is related to the local amount of myelin and other water macromolecules and hence allows to distinguish between transient edema formation and chronic degeneration of white matter tracts [Dousset *et al.*, 1992]. Macrophages can be labeled by systematically administrated ultra small particles of iron oxide (USPIO), which will remain for multiple days in the lysosomes, where they induce a significant increase of the local longitudinal and transversal relaxation rate and hence lead to a prominent signal increase in T1 and a signal decreases T2 weighted images [Dousset *et al.*, 1999b] [Rausch *et al.*, 2002a] [Rausch, *et al.*, 2003].

In vivo tracking of macrophages by MRI represents an attractive approach to study the efficacy of anti-inflammatory drugs. Recently, the immunosuppressive effect of FTY720 in the EAE model could be demonstrated by USPIO-enhanced MRI for prophylactic and chronic treatment regimes [Rausch *et al.*, 2004]. In the present study, we were in particular interested in studying the development of individual lesions from the acute inflammatory episode over the remitting phase to the first relapse by USPIO-enhanced MRI. As demonstrated by Floris [Floris *et al.*, 2004] and colleagues, the temporal development of pathological imprints in EAE is highly dynamic and appearance of lesions can be change with the state of the disease. The longitudinal imaging protocol employed here allows to distinguish the reoccurrence of lesions in areas of inflammatory history from the formation of new lesions and can therefore provide valuable information on the effect of anti-inflammatory drugs.

The macrophage-tracking approach was complemented by imaging of BBB disruption and myelin degradation using magnetization-transfer-imaging as further biomarkers for the assessment of neuro-inflammatory processes.

8.2.3 Material and Methods

Animal Model Actively-induced EAE in the Lewis rat is typically characterized by an acute monophasic attack after immunizing with xenogenic CNS proteins and is widely exploited for drug evaluation using a prophylactic treatment regimen (dosing starts at immunization). To assess drug effects using therapeutic treatment (dosing begins during established EAE), one can prolong the disease course in Lewis rats and induce a relapsing pattern by slightly

increasing the concentration of encephalitogenic Ag and/or *Mycobacterium tuberculosis* in the inoculum [Feurer *et al.*, 1985]. All studies were conducted in accordance with Swiss federal regulations for animal protection.

Inbred (RT1¹) female Lewis rats from Charles River (Sulzfeld, Germany) were kept in a climate-controlled room with 12 hour light/dark cycles, housed in sawdust-lined cages with 4 to 5 rats per cage, and given standard rodent chow and water *ad libitum*. After at least one week of adaptation, they were randomly distributed into experimental groups and individually numbered with a tail mark.

Rats weighing 150-165 grams were lightly anesthetized with isoflurane and immunized intradermally (i.d.) at the dorsal tail root with a 100 µl suspension consisting of 1 part (volume:volume) guinea pig spinal cord (Gp-sc) emulsified in 0.9% NaCl to 1 part complete Freund's adjuvant (CFA; Difco, Detroit, MI) supplemented with *M. tuberculosis* strain H37RA (Difco). The final inoculum per rat consisted of about 66 mg Gp-sc and 2 mg mycobacterium.

FTY720 was provided as a powder (Novartis Pharma AG, Basel, Switzerland) and dissolved in distilled water. The drug was freshly prepared and given *per os* (p.o.) once daily by gavage at a dosing volume of 5 ml/kg body weight.

For MRI experiments, the rats were anaesthetized using 1.5% isoflurane in nitrous oxide (2:1) and the tail vein was cannulated for infusion of contrast agent. The animals were placed on a support where body temperature was maintained at 37°C using warm air. Total MRI scanning time was 45 min per rat. All experiments were in strict adherence to the federal law for animal protection.

The experimental design comprised three groups: immunized rats treated p.o. with vehicle (water; 'vehicle', n = 9) or FTY720 0.3 mg/kg per day ('FTY-acute'; n = 7) during the acute phase (days 0-15) or FTY720 0.3mg/kg per day ('FTY-chronic'; n = 7) during the chronic phase (days 15-27). Each of the animals was scanned at three time points in the MRI: acute phase (11, 12 and 13 dpi). The remitting phase was measured during days 18 and 19 dpi and the first relapse on day 25, 26 and 27 post immunization.

Additionally, neurological scoring and determination of body weight was carried out on every day after immunization.

Neurological scoring Neurological examination was performed daily and animals were graded according to disease symptoms: 0 = normal; 1 = flaccid tail; 2 = hind limb weakness or ataxia; 3 = complete hind limb paralysis, often accompanied by incontinence.

Imaging protocol The protocol comprised a T2-weighted fast-spin-echo scan (TR=4500, TE=73, RARE-factor=12, NEX=4, MTX=256×192), a T1-weighted scan (TR=600, TE=8, NEX=4, MTX=256×128) and a magnification-transfer-prepared T1-weighted scan with the same parameters. A Dante-pulse-sequence for magnetization-transfer-suppression (pulse power = 16 μ T, number of pulses = 256, offset frequency = 5000 Hz) was used. After injection of 0.2 mL Gd-DOTA (Guerbet, Paris), the T1-weighted scan was prepared with a delay of five minutes. The geometrical parameters were the same in all scans: FOV = 3.5×3.5 cm, slice thickness = 1 mm and interslice-distance = 0.28 mm.

For labeling of macrophages AMI-227 (Guerbet, Paris) was injected at a concentration of 300 μ Mol Fe/kg into the tail vein of the animal 24h prior to the MRI measurement. The administration and scanning protocol was adopted from previous studies on EAE and stroke [Rausch *et al.* 2003] [Rausch *et al.* 2002] [Rausch *et al.*, 2001] and was optimized to detect labeled cells without background signal from USPIO, which had not yet been captured by phagocytotic cells.

Image analysis For image analysis BioMAP 3 (in-house development based on IDL 5.4 Research Systems Inc., Col., USA) was used. Enhancement-maps were calculated from the signal of the pre- and post-contrast T1-weighted scans according to

$$Enh = \frac{S_{pre} - S_{post}}{S_{pre}}$$

MTR-maps were calculated from the T1-weighted scans with and without MTS-preparation by

$$MTR = \frac{S_0 - S_{MTR}}{S_0}$$

For quantitative assessment of EAE-related signal alteration, hypo-intense areas in T2-weighted images reflecting accumulation of labeled macrophages were marked by region of interest (ROI). Those were only defined in the medulla since inflammation occurs

systematically in this part of the brain. For the animals of the *FTY-acute* group, areas of inflammation could not be identified during the treatment (acute phase) and ROIs have therefore been designed on images recorded during the remitting phase. For the two other groups (*vehicle* and *FTY-chronic*), the ROIs were selected on the basis of the acute phase pictures. As none of the animals showed inflammation in the cortex, a reference area for control measurement has been drawn in the cortex. Signal alteration in MTR- and Enh-maps were analyzed for these areas.

Statistical analysis Statistical comparisons were made in Microsoft Excel using a two-tailed t-test. Differences with $p < 0.05$ were reported as significant.

8.2.4 Results

Neurological assessment Animals of the *vehicle* treated group showed neurological impairment up to level 3 between 10 and 12 dpi (black curve in Figure 1a) with 100% disease incidence paralleled by a loss of weight during the same period (Figure 1b). The acute phase was followed by a remitting phase between 15 and 20 dpi during which neurological status improved almost completely and body weight recovered. During the first relapse (20 to 27 dpi), neurological impairment was characterized by an average level of 1.

For the *FTY-acute* group, no neurological impairment (red curve in Figure 1A) and no loss of weight (Figure 1B) were observed during the treatment period. One day after termination of treatment (day 13), neurological impairment began to increase up to level 2 between 15 to 17 dpi (red curve in Figure 1). This severe impairment was followed by a remitting phase (days 19-20) and a relapsing phase (21 to 27 dpi), which was similar to the vehicle group.

For the *FTY-chronic* group, acute and remitting phases were identical to the pattern of the vehicle group (Figure 1a and b). However, under FTY720 treatment from (days 16 to 27), animals did not enter a relapsing phase (20-27 dpi) (yellow curve in Figure 1) and all animals recovered weight faster as vehicle-treated animals (Figure 1b).

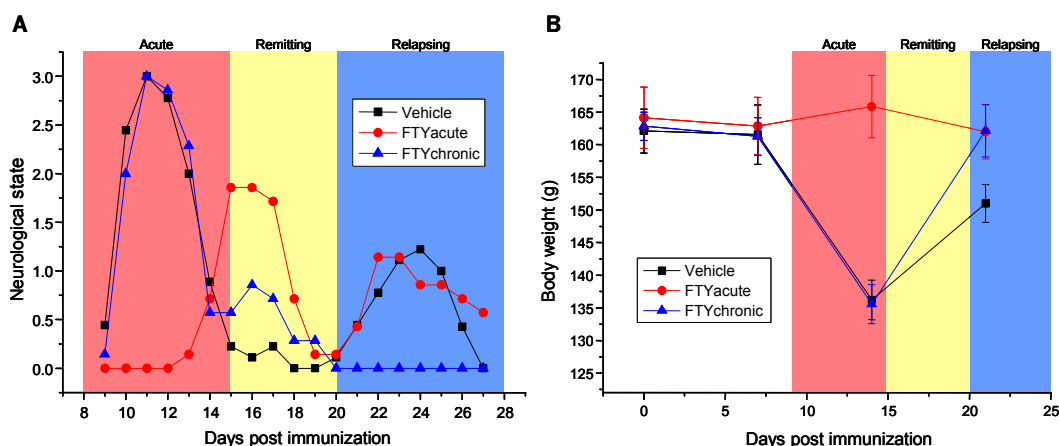


Figure 1A: Neurological state of animals during the different phases of EAE. The vehicle group displays the three characteristic disease episodes of EAE model: the acute inflammatory phase from 9 to 15 dpi, the remitting phase from 15 and 20 dpi, and the first relapse from day 20 to 27 post immunizations. FTY720 treatment leads to diminished symptoms during the treatment phase. Note that prophylactic treatment of the *FTY720-acute* group started already with day 0. The *FTY-acute* group displays delayed occurrence of symptoms starting 2 days after termination of treatment. **B:** Body weight evolution from day 0 to day 21. Animals, which were not treated during before and during the acute phase display significant loss of body weight during this inflammatory episode. Recovery of body weight is improved in the *FTY-chronic* group compared to vehicle treated animals.

MRI T2-weighted scans showed areas of signal attenuation induced by USPIO labeled macrophages during the acute phase and first relapse. Figure 2 shows representative images of lesions in the medulla and cerebellum for the three experimental groups. Infiltration labeled macrophages became most apparent during the acute phase for the *vehicle* and *FTY-chronic* group. At this time point no infiltration of labeled macrophages could be seen for the *FTY-acute* group. Almost no USPIO-enhancing lesions became apparent in these areas during the remitting phase for the *vehicle* and *FTY-chronic* group. Only animals of the *FTY-acute* group showed infiltration of labeled macrophages during this phase. Figure 3 shows a quantitative analysis of lesion volume, demonstrating that macrophage infiltration in the medulla is most prominent during the acute phase of the disease: in the vehicle treated animals lesion volume was largest during the acute phase. A reduction of lesion volume was found for the remitting period. Infiltration by macrophages was either found in sub-regions of lesions of the acute phase or in areas without inflammatory history. During the relapsing phase a second increase of lesion volume was observed for the *vehicle* but not for the *FTY-chronic* group. Only a very low lesion volume was observed during the treatment periods in the respective animals.

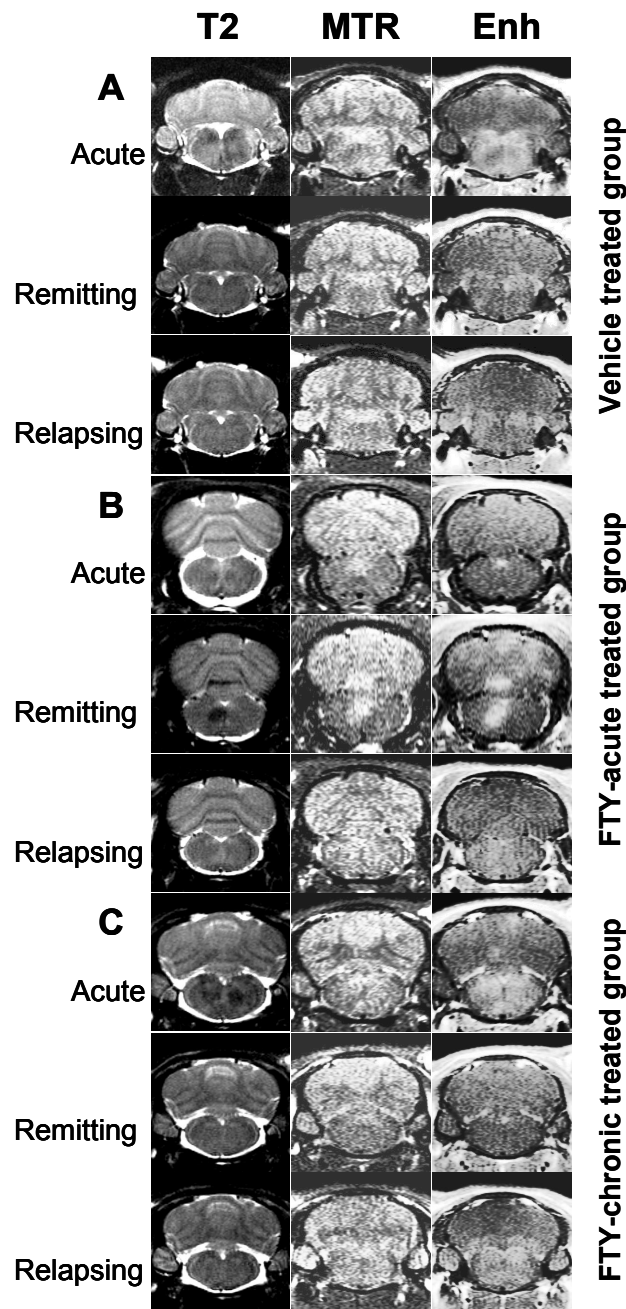


Figure 2: T2-weighted images and MTR-/Enh-maps showing the medulla of individual animals followed over the three episodes. A: Animal of the vehicle-group. Dark areas are visible during the acute phase in T2-weighted scans. Increased BBB-permeability can be observed in the same areas. MTR shows no prominent alterations. B: Animal for the FTY-acute group. A USPIO enhancing lesion can be observed during the remitting phase (note that the nomenclature is derived from the normal time course of the disease). C: Animal of the FTY-chronic group. A similar lesion pattern as in A can be observed.

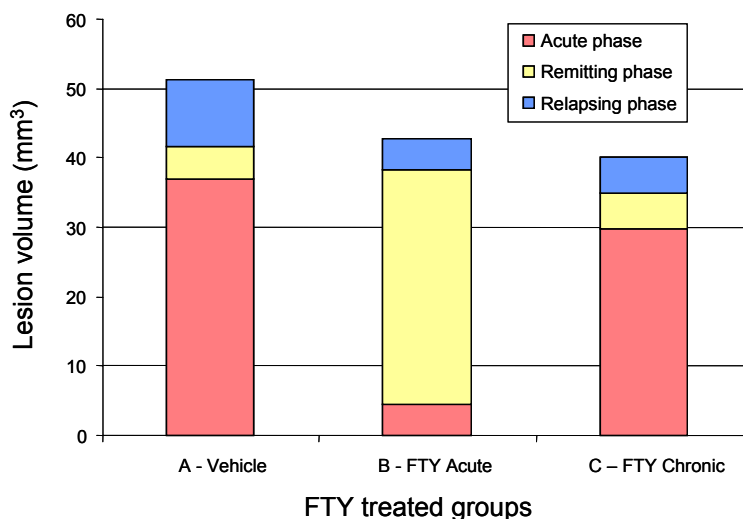


Figure 3: Lesion volume during the different phases of EAE. The lesion size was derived from the area covered by USPIO labeled macrophages.

Figure 4a shows a quantitative analysis of MTR values. During the acute phase MTR was significantly decreased ($p < 0.001$, mean MTR=0.34) in the *vehicle* treated animals as compared to the *FTY-acute* group (mean MTR=0.39). In the remitting phase MTR of the vehicle treated group and the *FTY-chronic* recovered to MTR=0.36. However, at this time point a reduction (not significant at $p < 0.05$) of MTR as compared to the treatment period was observed for the *FTY-acute* group. During the first relapse a slight decrease of MTR was observed for the *vehicle* treated group, which was significantly lower as compared to the *FTY-acute* and *FTY-chronic* group. In particular, the *FTY-chronic* displayed a further recovery of MTR during the treatment period.

Enhancement of Gd-DOTA (indicative for BBB disruption) was visible close to hypointense areas found in the T2-weighted images but there was no one-to-one correspondence. During the acute phase a significant increase of Gd-DOTA extravasation was observed in untreated rats (*vehicle* and *FTY-chronic*) as compared to the *FTY-acute* group. During the remitting period, BBB integrity recovered for the vehicle treated animals and the *FTY-chronic* group. Animals of the *FTY-acute* group, however, showed a clear increase of BBB disruption during this episode. The first relapse was not paralleled by a second increase of BBB permeability. Instead, a further decrease for vehicle treated animals and a clear reduction of Gd-DOTA extravasation was observed for the *FTY-acute* group. However, a slight increase of BBB permeability was observed for the *FTY-chronic* group, leading to a significant larger extravasation compared to the vehicle group.

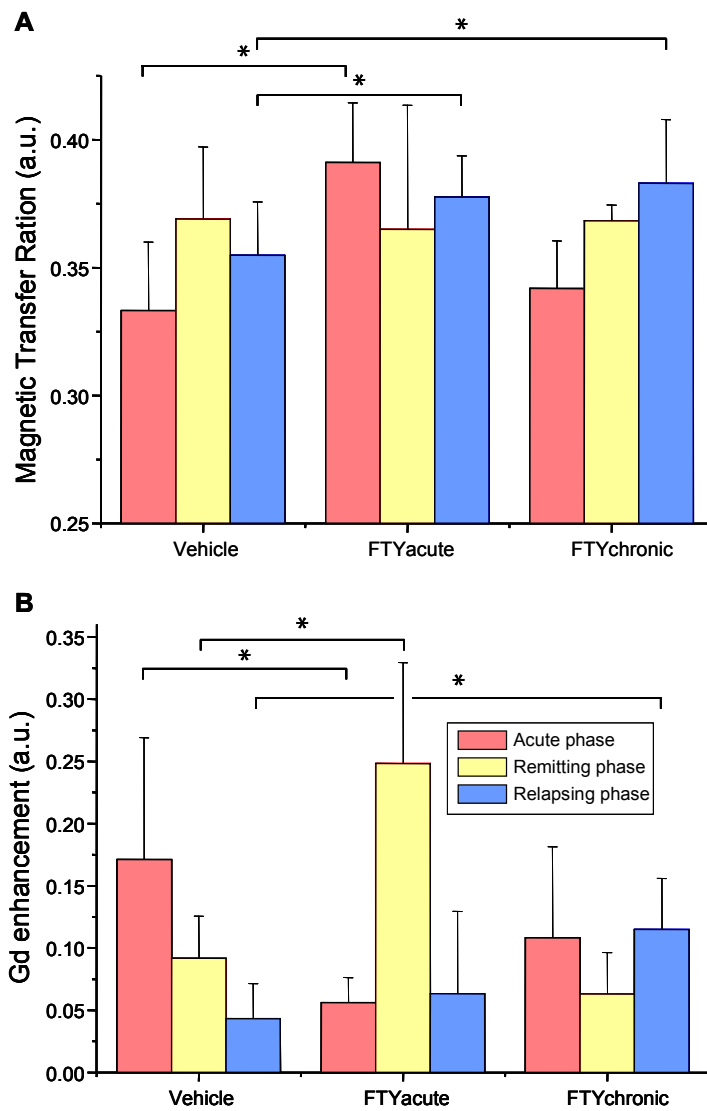


Figure 4: Quantitative analysis of parametric MRI data. Quantitative analysis was carried out for the ROIs, which were defined in the T2-weighted images. **A:** Magnetization Transfer Ratio MTR. **B:** Enhancement of Gd-DOTA.

8.2.5 Discussion

MRI, neurological impairment and body weight were used in this study to assess the effect of FTY720 on neuroinflammatory and neurodegenerative processes in EAE rats. In contrast to prior studies, animals have been scanned multiple times allowing the longitudinal observation of macrophage infiltration, de- and re-myelination and BBB-damage during the different states of the disease in individual animals. The type of immunization (guinea pig myelin to Lewis rats) that has been used in this study is generally regarded as model of acute EAE, however, by adding a larger amount of Freund's adjuvant to the emulsion a first relapse can be induced. Although inflammation is variable in its extent and location in the EAE model used here, previous studies have shown that the medulla is generally affected by inflammatory processes [Rausch *et al.*, 2003] [Dousset *et al.*, 1999] [Rausch *et al.*, 2003]. For this reason, the analysis of FTY720 activity was focused on this brain structure.

Animals, which were not treated at any time-point showed the typical pattern of chronic EAE: acute phase – remitting phase – 1st relapse. These phases could clearly be identified from the physiological and imaging data: animals showed a loss of weight during the inflammatory episodes and a regain of body weight during the remitting phase. A similar pattern was found for the neurological symptoms. Infiltration of macrophages was also exclusively observed during active inflammation: lesions showing clear signal attenuation in T2-weighted scans during the acute phase had normal signal intensity some days later during the remitting period (from a methodological perspective, this observation demonstrates that USPIO-labeling of macrophages is ideally suited to take multiple snapshots of ongoing cell infiltration being not sensitive for past inflammatory events).

Prophylactic treatment with FTY720 in the *FTY720-acute* group led to a general abolishment of macrophage infiltration, weight loss and neurological impairment. However, after termination of acute treatment, all symptoms, which were observed in the *vehicle-group*, began to develop. Hence, it must be assumed that FTY720 blocks inflammatory acutely but does not lead to a persistent homing or desensitization of lymphocytes: activation factors that remain in the blood circulation might be responsible for a continuous activation of T cells, which can enter the brain if no homing-signals were induced. This finding does not allow the conclusion that termination of treatment with FTY720 in humans will lead to an immediate onset of symptoms after termination of treatment, since the appearance of auto-reactive T

lymphocytes is not necessarily linked to acute presentation of the antigen and activation factors in MS.

MTR is related to the amount of myelin, which is subject to degradation by macrophages in EAE. Variations of this readout indicate either demyelization or myelin re-synthesis. The comparison between myelin quantity in the brain of treated and non-treated animals demonstrate, whether FTY720 can affect the activity of macrophages. The difference of MTR-values during the different groups and phases of the disease were lower compared to the results of prior studies carried on the same animal model [Rausch *et al.*, 2003]. This might be due to the fact that immunization in this experiment led to a lower degree of axonal degeneration. In addition, the EAE model used here is primarily a model for neuro-inflammation and not for neuro-degeneration or demyelination [Meeson *et al.*, 1994]. Administration of low molecular contrast agent such as Gd-DOTA allows assessment of BBB disruption. As already shown before, infiltration of macrophages and damage of the BBB did not correlate entirely in space and time. A spatial mismatch was observed for the acute phase in untreated animals. A further decrease of BBB integrity was found for animals of *FTY-chronic* group during the treatment phase. The physiological background of this BBB disruption is unclear and cannot be assigned to residual BBB damage induced during the acute phase and no acute inflammatory processes: the example shown in Figure 4c demonstrates that there is no Gd-DOTA extravasation during the remitting phase and no infiltration of macrophages during the first relapse. It can therefore not be excluded that FTY720 might interfere with BBB integrity in tissue that has already passed an initial inflammatory event. Methodological issues might be the reason why this effect has not been observed before: in the last study [Rausch *et al.*, 2003] a large ROI has been defined for the medulla of the *FTY-chronic* group, since these animals had not been scanned during the acute phase and therefore the areas of macrophage infiltration were not known. Here, however, specific ROIs could be defined for the medulla according the distribution of lesions during the acute phase.

In conclusion, the present study demonstrates that FTY720 can prevent inflammatory events in EAE rats and confirms the results of prior studies. In the EAE model used here, termination of treatment after the acute phase leads to the delayed development of symptoms. Furthermore, there is some evidence that FTY720 during a relapse leads to increased BBB disruption in areas which had already passed an inflammatory event.

9 TAGGING T CELLS FOR BIOMEDICAL IMAGING

9.1 T Cells Labeling for MRI: an *In Vitro* Study

Feasibility and Limits of Magnetically Labeling Primary Cultured Rat T Cells with Ferumoxides Coupled with Commonly Available Transfection Agents

9.1.1 Abstract

Visualization and quantification of inflammatory processes is of high importance for early diagnosis for a multitude of diseases. MR imaging using iron-oxide (FeO) nanoparticles as contrast agents allowed studying macrophage infiltration during inflammation in a variety of tissues. Macrophages are effectors of the immune response, their appearance being orchestrated by activated T lymphocytes. Therefore, tracking of labeled T lymphocytes, which initiate the immune process, should enable earlier detection of tissue inflammation. In this study, we investigate the feasibility of specifically labeling harvested T cells by using dextrane-coated FeO nanoparticles and commonly available transfection agents (TAs). Physico-chemical properties of the newly formed FeO/TA vesicles were determined as well as their cell toxicity and their T cell activation potential. Labeling efficiency of each FeO/TA combination was evaluated by measuring the transverse MRI relaxation rate R_2 , by X-ray spectroscopy and magnetic selection. Toxicity and labeling efficacy differed significantly among TAs. The best results were achieved by using poly-amine TAs and in particular by using poly-L-lysine at a concentration of 1.5 $\mu\text{g/ml}$ administered in combination with 22.5 μg iron/ml. Using this protocol up to 60% of harvested T cells could be labeled. Microscopic investigation revealed FeO/TA nanoparticles localized within the cytoplasm of the cells but also sticking to the outer membrane surface.

9.1.2 Introduction

The migration of immune-competent cells to sites of tissue inflammation is a key element in the immune response of the body. Visualization and quantification of these processes is critical from a diagnostic point of view, for the understanding of inflammatory disease, and for the evaluation of potential therapeutic interventions. A number of imaging approaches has been proposed to monitor cell migration in vivo [Bulte and Kraitchman, 2004] [Mempel *et al.*, 2004]. All of them involve specific labeling of the cells/cell types to be studied using either exogenous labels with radionuclides, MRI contrast agents or fluorescent dyes as reporter groups, or by genetically modifying cells to constitutively express a reporter gene [Allport and Weissleder, 2001]. Among the different imaging approaches evaluated for studying cell migration MRI is particularly attractive due to its superior spatial resolution, which is at least one order of magnitude higher than e.g. for nuclear and optical imaging.

Inflammation involves a massive accumulation of immune-competent cells, in particular macrophages, in the affected tissue. The infiltration of labeled macrophages can be monitored noninvasively by MRI following systemic administration of ferumoxides (FeOs), i.e. ultrasmall superparamagnetic iron oxide particles coated with dextran (USPIO), as demonstrated e.g. in the rat experimental autoimmune encephalomyelitis (EAE) model [Rausch *et al.*, 2004]. Due to their high phagocytotic activity, blood-borne monocytes efficiently internalize nanoparticulate matter and, hence, a substantial fraction of the macrophages that enter the inflamed tissue are labeled. In the rat EAE model, the use of USPIOs, initially developed for imaging of the liver lesions [Ferrucci and Stark, 1990], provided an almost 100% sensitivity for lesion detection [Dousset *et al.*, 1999b].

Macrophages are effectors of the immune-mediated injury in inflammation [Raivich and Banati, 2004], thus visualization and quantification of the migration of these labeled inflammatory cells to specific brain areas is of high diagnostic relevance due to the enhanced probability of detecting active demyelinating disease [Rausch *et al.*, 2003]. Macrophage infiltration is orchestrated by other inflammatory mediators such as T lymphocytes, which attract circulating monocytes by secretion of cytokines. Correspondingly, labeling T cells [Stinissen and Raus, 1999] might provide a tool to detect inflammatory events at an even earlier time point, potentially prior to the occurrence of significant tissue damage. The use of USPIOs for MR imaging [Weissleder *et al.*, 1990], their ability to tag T cells [Bulte *et al.*,

1996], and the possibility to track iron-tagged T cells *in vivo* using MRI [Yeh *et al.*, 1995] have been demonstrated. The sensitivity of the technique allows detecting single T cells labeled with ferumoxides *in vitro* [Dodd *et al.*, 1999]. In contrast to macrophages T cell cannot be labeled *in situ* by systemic administration of contrast agents due to lack of phagocytotic activity. Instead they have to be harvested and labeled in cell culture. Several methods to increase the efficiency of cell labeling using dextran-coated FeOs have been reported. One approach uses the Tat-peptide (Tat: transactivator of transcription) of the human immune deficiency virus-1 (HIV-1) to introduce tagged nanoparticles into the cells [Josephson *et al.*, 1999] [Lewin *et al.*, 2000]. A more frequently used method is based on complexing FeOs with polycationic transfection agents (TAs) to form complexes that should enter cells [Frank *et al.*, 2002]. TAs are positively charged macromolecules commonly used to shuttle foreign DNA into mammalian cells by formation of TA-DNA complexes [Xu and Szoka, 1996]. There are two principal classes of TAs available: lipid-based agents such as lipofectamine, Lipofectamine2000, FuGENE6, and polyamine polymers like poly-L-lysine (PLL) or poly-ethyleneimine (PEI). These polymers differ in size, charge, and molecular mass, which will affect transfection parameters and labeling efficiency. To achieve efficient labeling, the optimal ratio of FeO to TA that leads to the formation of stable FeO/TA complexes needs to be determined [Arbab *et al.*, 2004a].

The aim of the current study was to determine, whether by combining commonly available TAs and FeOs approved for clinical use, freshly extracted and primary cultured T cells can be efficiently and reliably labeled to an extent sufficient for the *in vivo* MRI detection. The efficiency of this labeling technique and the labeling yield was assessed using different readouts including the measurement of the transverse relaxation rate R_2 . Physico-chemical properties such as particle size and Zeta Potential, a critical determinant for membrane permeability [Kalish *et al.*, 2003], of each FeO/TA complex were determined. Cell physiological measurements were carried out to assess the potential of labeled T cells to exert their function, i.e. to become activated upon stimulation, and to evaluate eventual toxic effects of the label. Finally, labeling of T cells was confirmed under the microscope.

9.1.3 Material and Methods

Ferumoxides particles Labeling experiments were carried out with two kinds of negatively charged FeO particles: Endorem particles (Guerbet®, France) are approximately 140 nm in size according to the supplier, and Sinerem (Guerbet®, France) that have the same shape but smaller in size (40 nm in diameter). A stock solution of each compound was stored at 11.2 mg iron/ml. In order to determine the optimal FeO/TA ratio to form stable FeO/TA complexes, different concentrations of FeOs ($\mu\text{g/ml}$) were tested.

Transfection agents FuGene6® (Roche, Switzerland) is a lipidic multi-component transfection agent designed to shuttle DNA inside eukaryotic cells by forming vesicles. The concentration of the active transfecting substance in FuGene6 is not disclosed by the manufacturer. According to the transfection rate (1 $\mu\text{g}/\mu\text{l}$ of DNA to 2-3 μl of FuGene6) suggested in the user manual, we assumed that the stock solution contain at least 1 mg/ml of active reagent.

Poly-L-Lysin is a poly-amine TA (Sigma-Aldrich, Buchs, Switzerland). Different molecular weights ranging from 16 kD to 250 kD have been used to form FeO/PLL complexes. We tested four mixtures containing the following PLL molecules: 16 to 30 kD, 30 to 70 kD, 72 to 84 kD, and 125 to 250 kD. A stock solution of 1 mg/ml for each mixture was stored frozen at -20°C until requirement.

Lipofectamine™ 2000 (Invitrogen) is a lipid-based TA widely used to transfect eukaryotic cells. The stock solution is supplied at a concentration of 1 mg/ml.

Poly-Ethylene-Imine (PEI) (Sigma-Aldrich, Buchs, Switzerland) was supplied at 1 mg/mL. The polymer molecular weight was between 25 and 75 kD.

FeO/TA complexes preparation FeOs and TAs were always mixed apart from cell medium to allow complex formation. FeO/TA mixes were prepared in advance by mixing FeOs and TAs in RPMI medium without serum. For all labeling experiments, the volume of Endorem or Sinerem stock solution was calculated to have a final concentration of 22.5 μg iron/ml in FeO/TA mix.

Different concentrations for each TAs were tested. The final FeO/TA mixture volume was always 100 μ L. The FeO/TA mixture remained under gently agitation during 60 min before adding it into cell-culture complete medium.

Cell culture and labeling conditions T lymphocytes were extracted from young Lewis rat's spleen few days before labeling. Organs were destroyed using a Potter homogenizer and the solution was filtered several times through cell strainer with pores of 100, 70 and 40 μ m in diameter. After the last wash (centrifugation with phosphate-buffer), rat pan T cell was selected by the means of Miltenyi magnetic beads (Miltenyi Biotech) associated with antibodies against cells expressing α/β as well as γ/δ T cell receptor (TCR). An AutoMACS™ cell sorter was used to isolate the cells. In order to characterize MACS sorted cells, a FACS analysis of isolated cells has been performed on a LSR II flow cytometer (Bekton Dickinson, San Jose, CA, USA). using fluorescent monoclonal antibodies (BD Pharmingen, Franklin Lakes, NJ, USA).

The R2 relaxivity of Miltenyi beads associated to T cell membrane has been measured during the days following the MACS selection. By culturing and washing T cell in the conditions described thereafter, it appears that the iron labeling due to the magnetic selection totally disappeared after 4 days of culture (results not shown).

T cells were cultured in RPMI medium plus HEPES containing 1 mM Na-pyruvate, 1 \times MEM non-essential amino-acids, 50 μ M 2-mercaptoethanol, 50 μ M gentamicin antibiotic, 1 \times MEM vitamins, 2 mM L-glutamine and 10% Fetal Calf Serum. In order to avoid premature death and to stimulate T cells growth, rat T-STIM™ solution (Becton Dickinson) was added to the medium for a final concentration of 5%.

To label T cells, we added the 100 μ l FeO/TA mix to 10⁶ T cells to have a final labeling medium of 2 ml. We allow cells to rest in a humidified atmosphere at 37°C in 95% / 5% air/CO₂ during the labeling process.

Determination of physico-chemical properties of FeO/TA complexes The size and the Zeta potential (ZP) of pure FeO particle and pure TA as well as FE/TA complexes were measured with a Zetasizer® (Malvern, UK). Ferumoxide solutions at 22.5 μ g iron/mL and TA at 5 μ g/ml were diluted in filtered, distilled water. Size and ZP of FeO/TA complexes were also

measured in nanopure water at a final volume of 1 ml. While the FeOs concentration remain the same in all the measurements (22.5 µg/mL), different concentrations of TAs were tested i.e. 0.5, 1, 2.5 and 5 µg/ml. All measurements were at least repeated three times.

FE / TAs toxicity and T cell activation After a certain labeling period and before each other application, the number of living cells was estimated under the microscope by FDA (Fluorescein DiAcetate) exclusion. To have a quantitative confirmation of cell viability, the proliferate activity of FeO/TA labeled T cells was evaluated using the MTT (3-[4,5-2-yl]-2,5-diphenyl tetrazolium bromide) assay (Roche, Switzerland).

To determine the toxicity of FeOs or TAs separately, T cells were seeded into 96-well plates and then incubated at 37°C in 95% / 5% air/CO₂ with different doses of FeOs or TAs. MTT reagent was added 1h after mixing TAs and FEs and the whole mixture was incubated for 24h or 48h. Thereafter, the detergent reagent supplied within the MTT assay kit was added to each well and incubated in the dark at room temperature overnight. All measures were repeated three times and the mean value was used to make statistical studies.

T cell activation was evaluated based on their level of IL-2 secretion. The Elispot™ assay is designed for the detection of IL-2 secreting cells at the single cell level. We have used this method to monitor cellular responses in presence of either FeOs and TAs separately or FeO/TA complexes.

Estimation of the fraction of cells containing iron-oxide nanoparticles Cells labeled with superparamagnetic FeO were sorted exploiting their magnetic properties (magnetic selection). After labeling, T cells were centrifuged and washed three times to remove the excess of free FeO particles in solution. After the last centrifugation, the pellet was resuspended in 2 ml of phosphate buffer (PBS). Cells were counted and poured onto a magnetic column. Due to the magnetic field applied, FeO-labeled cells were retained in the column. The column was washed three times with PBS to remove unattached material. Thereafter, the magnetic field was switched off by removing the magnet surrounding the column and the remaining cells were eluted by adding 2 ml of PBS and counted by FDA staining.

Measurement of iron content X-ray fluorescence spectroscopy by wavelength dispersion was used to determine traces of heavy metals like iron within the cells. After labeling, washing and counting, cells were suspended in distilled water with Tris buffer 0.1%. Under osmotic pressure and detergent activity, cells were lysed and the iron released into the in solution. The mass absorption coefficient of the pellet was calculated or determined by measuring of the scattered X-ray radiation (Compton or Rayleigh scattering) experimentally. The trace content of the analyte is determined from the net impulse rate of its appropriate fluorescence line and from the intensity of the background line(s) using a matrix normalized curve.

MRI estimation of labeling efficiency After each labeling procedures, cells were washed three times with PBS and resuspended in 1 ml of PBS containing 3% gelatin at a concentration of 10^6 cells/ml. Superparamagnetic nanoparticles such as FeOs lead to a significant increase of the transverse relaxation rate R_2 . In fact, R_2 is proportional to the concentration of FeO particles c_{FeO} ,

$$R_2 = R_{20} + r_{2,FeO} \cdot c_{FeO} \quad (1)$$

with R_{20} being the relaxation rate in the absence of the contrast agent and $r_{2,FeO}$ to molar relaxivity (in $s^{-1}mM^{-1}$) of FeO. Alternatively, we can attribute the change in relaxivity the number of labeled cells in the medium N_{cell} according to

$$R_2 = R_{20} + r_{2,cell} \cdot N_{cell} \cdot V^{-1} \quad (1a)$$

with V being the sampling volume and $r_{2,cell}$ the average relaxivity of the labeled cell.

MRI experiments were carried out using a horizontal bore Pharmascan 70/16 spectrometer (Bruker Biospin GmbH, Germany) equipped with a self-shielded gradient insert of 90 mm inner diameter capable of switching 300 mT/m in 150 μ s. A 35 mm inner diameter bird-cage coil was used as transmitter/receiver device. The phantom consisted of a Plexiglas support containing Eppendorf vials filled with the corresponding cell suspensions. R_2 determinations were based on a multi-echo Carr-Purcell-Meiboom-Gill (CPMG) sequence with the measurement parameters : repetition delay TR = 2034 ms, echo spacing TE = 10.25 ms, number of echoes NE = 16 echoes, number of averages NEX = 1 and matrix dimension MD = 256 \times 192). In addition T_1 -weighted images were recorded using TR = 600 ms, TE = 8 ms, NEX = 4, and MD = 256 \times 128.

9.1.4 Results

Physico-chemical properties of FeO and FeO/TA complexes Two important characteristics for nanoparticulate materials are the average size and the average ZP. Almost all particles in contact with liquid acquire a surface charge. The ZP is an indicator of this charge predicting the stability of a colloidal suspension. The greater the ZP the more stable the suspension due to repelling forces in between particles overcoming their tendency to form aggregates. Average particle size and ZP for filtered FeO nanoparticles Endorem and Sinerem are given in the Table 1. We determined an average diameter of Endorem nanoparticles of 95nm rather than the 140nm as indicated by the manufacturer. Negative ZPs have been determined for iron-based CAs (e.g. -15 and -19 mV for Endorem and Sinerem, respectively) in agreement with results from Kalish et al. [Kalish et al., 2003], who found ZPs of -41.3 and -2.03 mV for Feridex and MION particles in water. Discrepancies between ZPs values are probably linked to differences in size, coating and concentrations of tested particles.

	Size (\varnothing nm)		Zeta Potential (mV)	
	Endorem	Sinerem	Endorem	Sinerem
Average value	119.49	31.58	-15.41	-19.06
Standard deviation	58.46	83.01	0.37	1.65

Table 1: Average and standard deviation values were calculated from a solution of iron particles (e.g. Endorem or Sinerem at 22.5 μ g iron/ml) diluted in filtered, de-ionized, distilled water at ph 7. Concerning the particle size, average and standard deviation calculations are weighted with particles occurrence in solution. In this case, the standard deviation represents the breadth of the particle-size distribution curve.

When Endorem iron beads are mixed with TAs (Fig.1A), the average size of resulting particles is around 114 nm. However, certain mixing conditions involving lipidic TAs (e.g. FuGene and Lipofectamine) at low concentration (0.5 mg/mL) induce the clustering of Endorem particles together resulting in the formation of larger agglomerated iron clusters. In a same manner, aggregation of Sinerem particles was observed at low concentration of TAs when using polymeric TAs such as PEI25-75 kD and PLL125-250 kD (Fig.1B). For all other conditions an average diameter of Sinerem/TAs complexes of 64 \pm 20 nm has been determined.

ZP of Endorem/TA complexes was found to be almost always positive except at low concentration of lipid TAs (e.g. FuGene6 and Lipofectamine). The average ZP obtained is 23.2 mV and PLL125-250 kD forms the highest positively-charged particles (Fig.1C). Concerning Sinerem/TA particles, the ZP is negative when using lipid TAs except for an excess concentration of Fugene (Fig1D). Using poly-amine TAs, ZP reach values around 17 mV. Again, PLL125-250 kD led to the formation of the highest positively-charged particles.

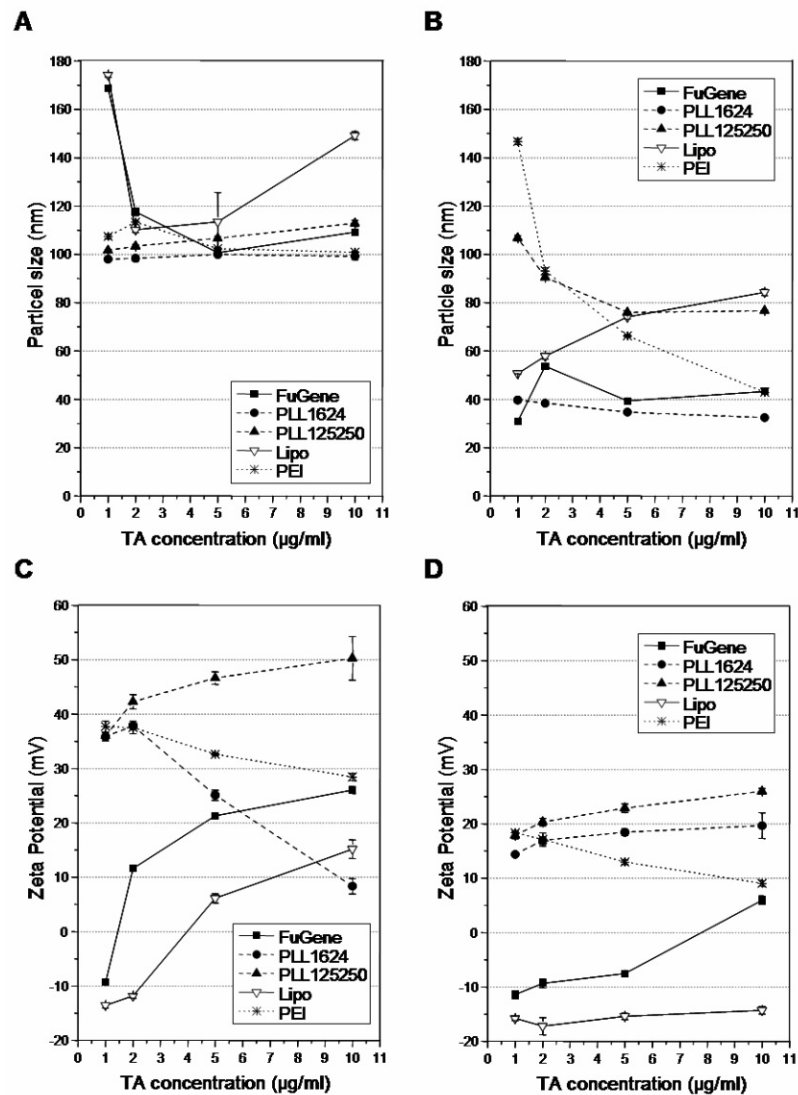


Figure 1: Average size of Endorem (SPIO, A) and Sinerem (USPIO, B) particles, respectively, when mixed with different TAs. Zeta potential for the various particle-TA clusters are shown in Figs C and D. The concentrations for TAs tested were 0.5, 1, 2.5 and 5 µg/ml.

FeO labeling studies of T cells without using TAs Previous studies have shown that larger iron particles (e.g. Endorem) led to a better labeling efficiency [Frank *et al.*, 2003]. To evaluate the effect of FeO nanoparticles on rat T cells, we carried out a series of experiments using Endorem as labeling substrate without adding TAs to enhance labeling efficiency.

Our results indicated that primary cultured T cell can be labeled by just adding of FeO nanoparticles to the culture medium. Based on previous studies which demonstrate that primary hematopoietic cells incorporate iron particles after 2 hours incubation without TA [Hinds *et al.*, 2003a], we decided to evaluate labeling efficiency for a time interval between 2 to 48 hours. Figure 2A shows that the R_2 relaxation rate of T cells started to increase after 2 hours exposure to FeO nanoparticles. The results indicate that iron contents within the cells remained constant between 2 and 8 hours of exposure to the label, but significantly increased between 8 and 48 hours of labeling. Obviously, longer incubation times led to a better labeling of T cells. These results are in line with observations from other groups [Arbab *et al.*, 2004a]. As anticipated, higher concentrations of Endorem in the culture medium increased the amount of label incorporated in the cells. This is reflected by larger values for the R_2 relaxation rates measured for higher Endorem concentrations (Fig.2B). However, too high concentrations of Endorem seem to compromise the viability of the T cells (see below).

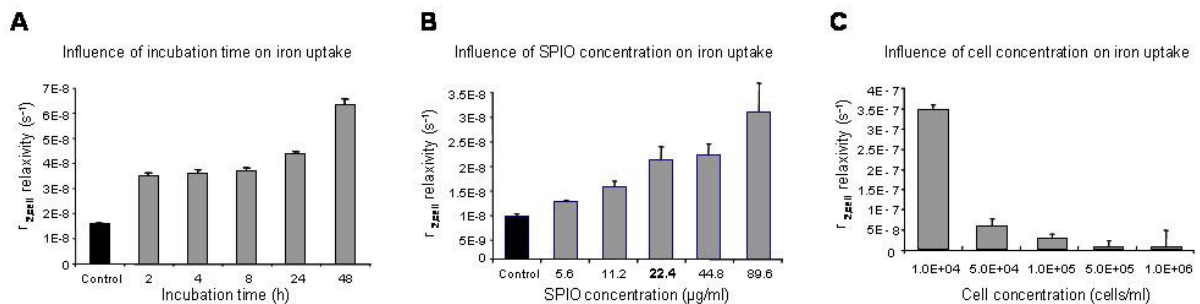


Figure 2: Optimization of T cell labeling with SPIO alone: Influence of incubation time (A), SPIO concentration (B) and cell concentration (C) on FeO uptake by primary cultured T cells as reflected by the transverse relaxation rate. The control value shown in A) and B) is the value for the T cells in the absence of any FeO nanoparticles (black bars). The Y axis shows the relaxivity per cell $r_{2,cell}$ (in s^{-1}) in the cell suspension. The number of cells were 10^6 cells/ml for the Figures A and B.

Also the cell concentration in the labeling medium had an influence on the labeling efficiency: the higher the cell concentration in the solution, the lesser the R_2 relaxation rate per cell (Fig.2C). In other words, cells are labeled more efficiently when they are not too concentrated in solution. This phenomenon might be due to effects of the micro-environment conditions and was already observed when labeling lymphocytes with monocrystalline iron oxide nanoparticles (MION) [Schoepf *et al.*, 1998b].

Toxicity and cell activation An important aspect in cell labeling studies is that the label or any of the co-added substances do not affect the normal cell physiology. Therefore potential toxic effects of the labeling procedures have to be carefully evaluated. A commonly used toxicological readout is the cell growth rate. First, we evaluated the influence of FeO concentration on T cell growth rate. An increase in the concentration of FeO particles decreased the number of cells in the culture dish indicating a cell-toxic effect at high FeO concentrations (Fig.3A). In comparison to smaller FeO particle (Sinerem), the negative effect of Endorem particles on T cell growth was more pronounced at concentrations exceeding 25 μg iron/ml. This concentration probably allows the most efficient labeling of T cells without significantly affecting the cell growth rate. Based on these results and in agreement with published data [Arbab *et al.*, 2003a], we decided to use nanoparticles at a iron concentration of 22.5 $\mu\text{g}/\text{ml}$ for further labeling experiments.

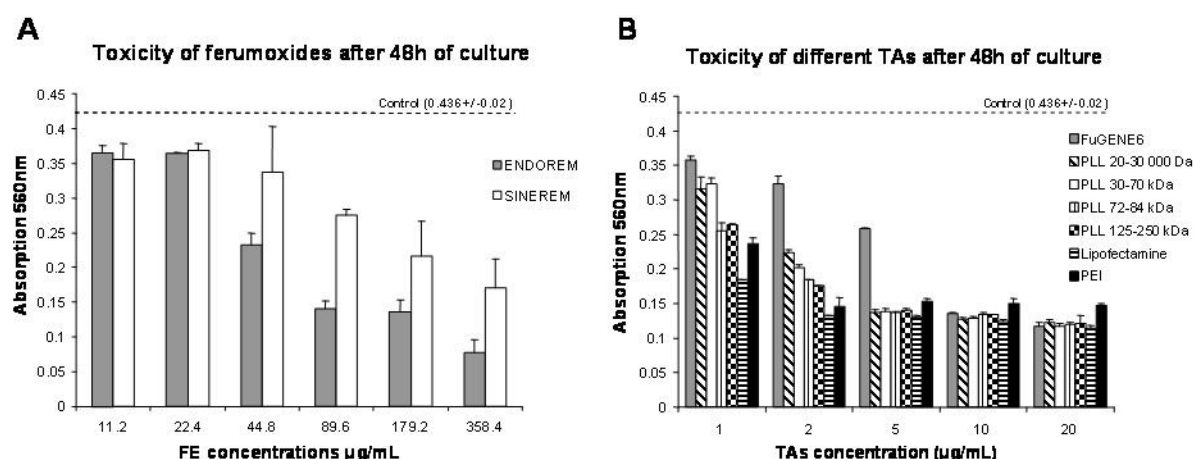


Figure 3: T cell toxicity of FeO nanoparticles and TAs: Assessment of cell toxic effects as a function of the FeO concentration (A) and the TA used (B). In the MTT assay, the absorption intensity at 560nm is proportional to the cell concentration in the suspension. All these experiments were carried out at the same time following incubation with FeO particles and TAs under the same conditions. The control value for cell cultures not exposed to TA nor FeO particles is indicated by the dashed line.

In a second study, potential toxic effects caused by TAs were investigated (Fig.3B). After 48h of culturing in presence of different TAs concentrations, the MTT test showed that all TAs seemed to impair T cell growth and cell survival *in vitro*. FuGene6 and different sized PLL appeared less toxic than Lipofectamine and PEI. With the exception of FuGene6, a TA dose greater than 2 $\mu\text{g/ml}$ dramatically impaired T cell survival for all TAs. For FuGene6 the corresponding ‘toxic’ level was reached at concentrations higher than 5 $\mu\text{g/ml}$. Toxicity tended to increase with higher molecular weight (MW) of PLL at concentrations between 1 and 2 $\mu\text{g/mL}$. Analogous results were observed when labeling dendritic cells (Antigen Presenting Cells: LADMAC cells) with PLL and FEs [Arbab *et al.*, 2004b]. Lipofectamine seemed to be the more toxic compared to the others TAs. In particular, PEI had less toxic effects than Lipofectamine at all concentrations tested.

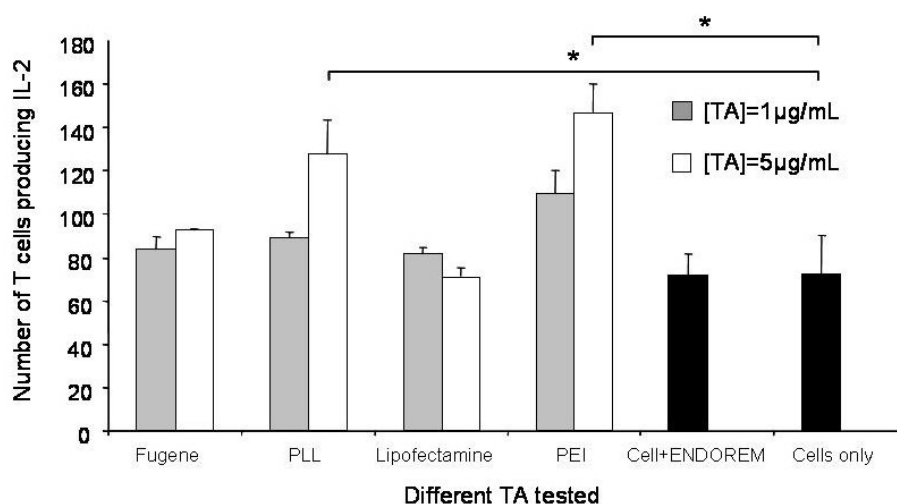


Figure 4: T cell activation by FeO nanoparticles and TAs: IL-2 production of rat T cells in the presence of different TAs at concentrations of 1 and 5 $\mu\text{g/ml}$. The IL-2 production is proportional to T cell immune activation state. Black bars are the control values for IL-2 synthesis by T cells with and without SPIO. IL-2 secretion of T cells increases significantly following administration of PLL ($p = 0.011$) and PEI ($p = 0.025$) at a concentration of 5 $\mu\text{g/ml}$.

Thirdly, as the purpose of current work was to evaluate the feasibility of labeling rat T cells for imaging studies *in vivo*, it was primordial to test whether T cell reactivity and activation were altered by presence of FeOs and/or TAs. Interleukin-2 (IL-2) is well known to play a critical role in T cell expansion [Nelson and Willerford, 1998] [Lin and Leonard, 1997] and to

participate in natural killer (NK) cell activation [Vitale *et al.*, 1998] [Itoh *et al.*, 1985] [Chun *et al.*, 1985]. Figure 4 shows the effects of FeOs and various TAs on the degree of IL-2 secretion by rat T lymphocytes. Compared to the native T cells, administration of Endorem alone to the medium did not affect IL-2 secretion. Similarly, Lipofectamine had no significant effect on activation on T cells as concluded from the measured IL-2 levels. Significantly increased IL-2 secretion was observed when T cells were exposed to poly-cationic agents such as PLL ($p = 0.011$) or PEI ($p = 0.025$), while FuGene6 had a minimal effect. Among the TAs tested, Lipofectamine had the weakest influence on rat T cell activation.

Efficiency estimation of cell labeling To estimate the efficiency of cell labeling, FeO labeled T cells were collected using a magnetic sorting device (MiniMACS™ Separator, Miltenyi Biotec) exploiting the superparamagnetic properties of FeO nanoparticles. Based on the assumption that FeO labeled cells should be retained in the column by the applied magnet field, this approach is commonly used to select immune cells presenting FeO beads at their surface [Suda *et al.*, 1998]. FACS analysis of MACS isolated cells demonstrated a clear predominance of T cells expressing only the CD3 receptor (CD3+) as well as cytotoxic T cells (CD3+/CD8+). As proven by the content of the negative MACS selection, the majority of monocytes, B cells and NK cells has been removed from our experimental sample.

	Spleen cells	MACS positive selection	MACS negative selection
T cells	27.0	48.7	17.0
Helper T cells	17.0	5.0	10.1
Cytotoxic T cells	10.0	43.7	6.9
Monocytes	18.4	0.7	13.2
B cells	23.4	1.7	27.9
NK cells	4.2	0.3	24.9

Table 2: FACS phenotyping of spleen and MACS isolated cells was performed by using fluorescent antibodies directed against receptors of CD3, CD4, CD8a, CD45RA and CD161a. Cell populations are given in percentages for 100% of living cells present in the sample before (first column) and after MACS selection (second and third column).

The fact that in our case the labeling FeO particles are supposed to be internalized by the lymphocytes should not affect the interaction between the magnetic field column and FeO tagged cells. As negative control, unlabeled cell have been run over the column: no retention of cells has been observed. Hence, retention of cells is indicative of the presence FeO label. Figure 5A shows the percentage of retained cells after 16h and 48h exposure to Endorem and different TAs. PEI yielded the highest labeling efficiency followed by PLL with up to 60% of the cells carrying FeO labels after 48h, and Lipofectamine. In contrast, FuGene6 did not increase uptake of FeO nanoparticles in comparison to FeO alone. Although other studies demonstrated no cell labeling in presence of FeOs without TAs after 24h incubation [Frank *et al.*, 2003], we found approximately 24% of rat T cells to be labeled with iron beads even in the absence of TAs. Optical microscopy observation of cells stained with Prussian blue confirmed that fraction of cells carried FeO particles (arrows, Fig. 5B).

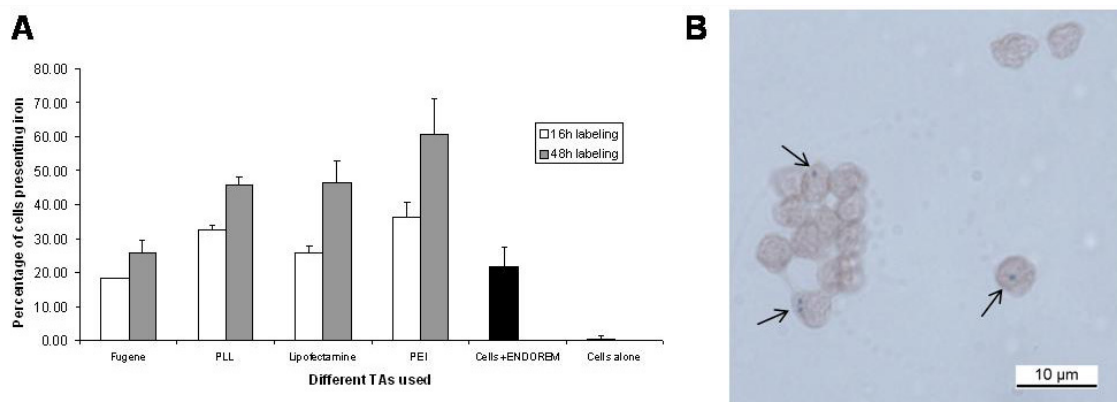


Figure 5: Efficiency of T cell labeling: A) Percentage of cell containing FeO nanoparticles after labeling for 16 and 48h, respectively, for the different TAs. A magnetic selection of labeled cell has been made in order to select only cells doped with FeO. Black bars show control values for T cells exposed to SPIOs only. Minimal retention was observed for cells not exposed to iron (cells only).

B) Microscopic image of T cells with 100x magnification after 16h labeling with SPIO in absence of TA. FeO nanoparticles (see arrows) appear as blue dots (Prussian blue staining) in neutral red-colored T cells.

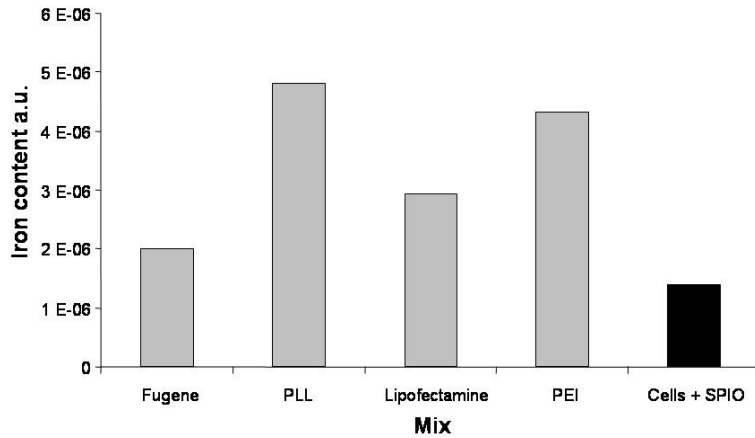


Figure 6: X-ray spectroscopic evaluation of the cellular iron content after 48h of labeling for the various TAs. The black bar indicates the amount of iron in T cells labeled without addition of TA.

Experiments using fluorescence spectroscopy of X-rays confirmed the efficiency of PLL and PEI for labeling rat primary cultured T cells (Fig.6). A quantification of iron trace in the pellet of lysed T cells revealed almost five times more iron when using PLL as TA as compared to the non-TA enhanced uptake. This experiment demonstrated that poly-amine TAs (PLL and PEI) led to significantly higher FeO loading to rat T cells than other TAs (lipofectamine and FuGene6).

MRI labeling The decrease of the echo amplitudes in the CPMG experiment followed single exponential characteristics described by the transverse relaxation rate; R_2 values were obtained from regression analysis and normalized to the concentration of the cells, in the solution, $N_{cell} \cdot V^{-1}$. From eq. (1a) we obtain

$$r_{2,cell} \cdot N_{cell} \cdot \frac{1}{V} = r_{2,FeO} \cdot c_{FeO} \quad (2)$$

Assuming that all FeO particles within the sampling volume are sequestered in the cell, the total amount of FeO per cell $m_{FeO,cell}$ can be estimated as

$$m_{FeO,cell} = \frac{c_{FeO} \cdot V}{N_{cell}} = \frac{r_{2,cell}}{r_{2,FeO}} \quad (3)$$

Figure 7 represents the average $r_{2,cell}$ values (eq. 1b) for the various FeO / TA combinations as derived from forty experiments carried out with different doses of TAs and different labeling time. The relaxivity of cells labeled with Endorem was found to be always higher than that measured for Sinerem labeling, supporting the notion that larger nanoparticles yield better labeling T cells labeled with PLL and Endorem resulted in the highest relaxivity values. Also for Sinerem nanoparticles, co-administration of PLL yielded the highest labeling efficiency. The relaxivity per cell $r_{2,cell}$ allows the estimation of the amount of FeO particles present in each cell (see eq.4): for $r_{2,cell}$ values in the range $2.5 \cdot 10^{-6} \text{ s}^{-1} \text{ cell}^{-1} < r_{2,cell} < 3 \cdot 10^{-5} \text{ s}^{-1} \text{ cell}^{-1}$ the amount of iron per cell is estimated to be $3.5 \text{ pg(Fe)/cell} < m_{FeO,cell} < 42 \text{ pg(Fe)/cell}$, or correspondingly in molar quantities $0.06 \text{ pmole (Fe)/cell} < m_{FeO,cell} < 0.75 \text{ pmole(Fe)/cell}$.

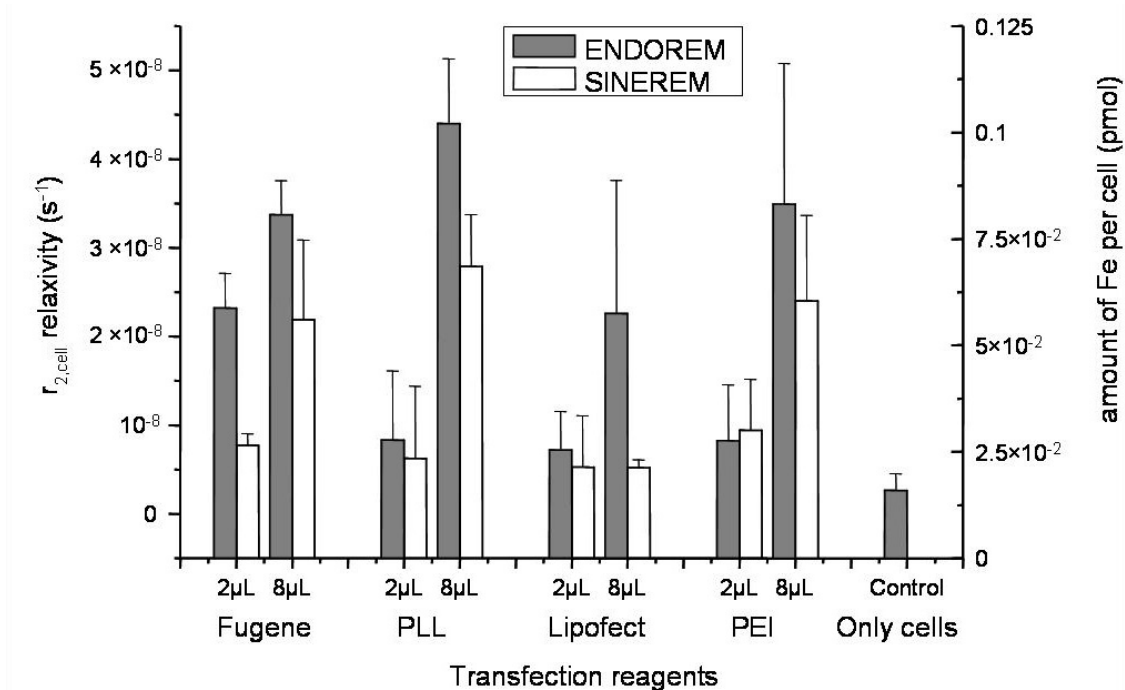


Figure 7: Efficiency of T cell labeling assessed via transverse relaxation rates: Measurement of the $r_{2,cell}$ relaxation rate in test vials containing a 1ml suspension of 10^6 cells labeled with $25\mu\text{g}$ FeO particles per ml and 2 and $8\mu\text{L}$ TAs. Values are given as relaxivity per cell and unit volume according to eq.(1b). The relaxation rates reflect the amount of iron in the sample and allows to estimate the labeling efficiency (eq.3). Results have been obtained as the average values of ten measurements per TA either with SPIO or with USPIO. The control value is for cell labeled with SPIO only without TA.

9.1.5 Discussion

The objective of this study was to compare the efficiency of the magnetic labeling of rat primary cultured T cell combining commonly available TAs and FeO nanoparticles. As magnetic tag we used superparamagnetic dextran-coated Endorem, which exert their effect on surrounding water molecules by increasing R_2 and R_2^* relaxation rates. It is known that FeOs in presence of TAs self-assemble into complexes that can be used to label cells [Arbab *et al.* 2003b]. Coating of FeO by TAs is shielding the water from the FeOs surface preventing any appreciable inner sphere relaxation of water molecules. As a consequence the effect of FeOs and FeO/TA complexes on water relaxivity is due to the local disturbance of the static magnetic field translating into increased of the relaxation rates R_2 and R_2^* . Since the change in the transverse relaxation rate is proportional to the amount of superparamagnetic particles per cell (eqs. 1 and 3) R_2 measurements can be used to estimate the efficiency of T cell labeling. From our measurements we estimated that cells were doped with 3.5 to 42 pg(Fe)/cell depending on the labeling conditions. These values are in good agreement with values obtained by Matuszewski *et al.* [Matuszewski *et al.*, 2005] for labeling of several human tumor cell lines. The structure and the self-assembling properties of the FeO/TA complexes depends on the surface charges on both the dextran and TA moieties [Arbab *et al.*, 2004a]. Complexation furthermore varies with the concentration of FeO nanoparticles and TA, the pH-value of the solution (all our experiments were carried out at pH=7), the incubation time, and the ionic strengths of environment. Correspondingly, these properties will also influence the ability of these complexes to label T cells.

Based on literature data [Arbab *et al.*, 2003b] [Frank *et al.*, 2003] and our own *in vitro* results, we choose a concentration around 25 μg iron/ml mixed with 1 to 2 $\mu\text{g}/\text{ml}$ of TA and an incubation time of 48h to achieve high labeling of primary cultured T cells. An Endorem concentration corresponding to about 25 μg iron/ml SPIO and 2 $\mu\text{g}/\text{ml}$ TA (ratio TA/SPIO = 2/25) were found to constitute thresholds for toxic effects, higher values leading to significant T cell toxicity as reflected by decreased growth rates and the occurrence of cell death. A cell loss of more than 35% has been observed when using TA doses exceeding 2 $\mu\text{g}/\text{ml}$, confirming results obtained by Arbab *et al.* on TAs toxicity [Arbab *et al.*, 2004a].

Large FeO particles (Endorem) turned out to be more toxic than smaller ones (Sinerem), however, also led to a better direct labeling of T cells in the absence of TA. As our culture conditions were the same in both cases, we can assume that the size of particles is the only factor affecting both the cell mortality and the enhanced labeling efficiency. Provided that particles are taken up into the cytoplasm, bigger particle sizes would imply more efficient endocytosis. The calculated size of the SPIO/TA particle at a ratio of 2/25 was of the order of 100 to 120 nm in diameter irrespective of the TA used (Fig.1A). However, the ZP of these particles clearly depended on the TA mixed with FeO. While PEI and different-sized PLL led to a positively-charged particle around with ZP $\approx +40\text{mV}$. The ZP of FeO-adducts with lipophilic TAs like FuGene6 and Lipofectamine was considerably smaller (ZP $\approx +10\text{mV}$) or as in the case of Lipofectamine at concentrations less than 2 $\mu\text{g/ml}$ even slightly negative (Fig.1C). Two features of the FeO particles seem to be relevant for high uptake of FeO/TA complexes: a particle size of the order of 100 nm (and potentially more) and reasonably high positive charge [Hinds *et al.*, 2003b] [Nicholas and Jones, 1986] [Schwendener *et al.*, 1984]. The latter is in line with the observation that membrane penetrating peptides comprise a large numbers of positively charged amino acids such as arginine [Goncalves *et al.*, 2005].

Although a previous study did not observe SPIO uptake in the absence of TA [Anderson *et al.*, 2004], we found that approximately 24% of the primary cultured rat T cell were loaded with FeO nanoparticles after 48h exposure to a culture medium containing only SPIO but no TA. This is probably due to the natural capacity of living cells to take up foreign complexes by endocytosis. Moreover, this capacity should be enhanced by the dextran-coating of iron particles. Indeed, DEAE-dextran (Diethylaminoethyl dextran) is widely used to transfect mammalian cells [Fregeau and Bleackley, 1991] leading to a remarkably reproducible inter-experimental and intra-experimental transfection efficiency [Gulick *et al.*, 2003]. The exact location of the FeO particles within the cells, however, remains unclear. Microscopic cell analyses revealed the occurrence of such particles both intracellular as well as extracellular, i.e. attached to the cell membrane (Fig. 8A). The same pattern was found for FeO/TA labeled cells. Although the presence of TA molecules at the surface of the FeO particles is supposed to enhance complex formation, thereby facilitating the penetration of cellular membranes, it appears that some particles remain sticking to the outer leaflet of plasma membrane. Concerning iron that has been internalized into cells, confocal microscopy experiments using

house-synthesized chimerical USPIO-Cy5.5 particles showed that iron within T cells is located in the cytoplasm (Fig. 8B).

X-ray spectroscopy experiments and NMR R_2 measurements demonstrated large PLL polymers to be the most efficient TA for labeling of primary cultured rat T cells. On the other hand, the presence of PLL caused a strong T cells activation pattern as reflected by the IL-2 secretion values. This increased activation state could explain the fact that T cells became adherent to culture plates and probably also to FeO/TA complexes, or from another perspective, the adherence of FeO/TA complexes to the T cell membrane. In presence of foreign antigens in the culture medium (such as the TA), primary cultured T cell become activated leading to the expression of adhesion proteins and cytokines synthesis [Peters and Ernst, 2003]. Hence, exposure of T cells to FeO/TA particles might result either in internalization of the particle or in the particle simply sticking to the T cell surface by interaction with adhesion molecules.

It has been established that intracellular tagging of T cells with 0.02 pg iron SPIO per cell can be achieved [Bulte *et al.*, 1996]. By using TAs, the ratio between FeO particles and TA should be defined in order to achieve a proper formation of complexes small enough for efficient endocytosis. In our studies the formation of aggregates between T cells and FeO/TA complexes has been observed over a considerable range of TAs concentrations (i.e. 0.5 and 1 $\mu\text{g/ml}$) due to the adherent behavior of activated T cells (e.g. with PEI in the Fig.8C). While PEI does not form iron clustering (Fig.1 A), it had the strongest effect on the IL-2 secretion of T cells (Fig.4). Not surprisingly, PEI displayed the most severe toxic effect on T cell viability of all the TAs evaluated (Fig.3B) at low concentrations. On the other hand, labeling efficiency of the SPIO-PEI combination was highest, resulting in approximately 60% of T cells containing/presenting FeO. This indicates that the increased immune activation state of T cell tends to increase the labeling efficiency. This higher number of selected lymphocytes includes T cells with internalized iron particles but also a large number of T cells with FeO/TA complexes sticking to their surface. Figure 8C shows clear aggregations of activated T cells after SPIO-PEI labeling process. Staining of these cells with annexin-V-based fluorescent dye (Vybrant™ Apoptosis Assay, Molecular Probes) revealed high fluorescence intensity in such clusters. As annexin-V targets externalized phosphatidylserine, which migrate to the outer leaflet of the plasma membrane during apoptosis, the high signal intensity is indicative of

programmed cell death. We speculate that the formation of aggregates of activated T cells with FeO/TA complexes might in fact lead to premature cell death.

Another undesired consequence of this kind of surface labeling is the ability of iron particles to interfere with basic function of cell surface signaling. FeO particles sticking to the outer membrane of the T lymphocytes could inhibit the normal immune response by steric hinderance of the antigen access to the cell surface receptors.

In summary, our results showed that labeling of primary cultured rat T cells after a fresh extraction from the spleen is feasible. Mixing of TA with dextrane-coated FeO nanoparticles led to the formation of complexes, which enhances the labeling efficiency compared to spontaneous uptake in the absence of TAs. Determination of physico-chemical properties of the FeO/TA particles demonstrated that large polymers of PLL led to the formation of the highest positively-charged particles suited for efficient uptake. Moreover, qualitative and quantitative assessment of iron content within cells showed that the number of labeled T cells was highest when using large PLLs as TAs. Hence, from a practical point of view and balancing toxicity versus labeling efficiency, the combination of SPIO (22.5 $\mu\text{g/ml}$) associated with PLL (1.5 $\mu\text{g/ml}$) yielded the best results for labeling primary cultured T cells. Although PLL showed no toxicity at concentrations used routinely (i.e. around 1 $\mu\text{g/ml}$), our findings revealed that the use of poly-amine TA provoked a significant T cell activation. As a consequence labeling occurs not only intracellularly but also on the surface of cells. This labeling is not negligible and may result in premature phagocytosis of labeled T cells by macrophages which could lead for instance to unspecific labeling of macrophages. By providing a detailed characterization of the bio-physical properties of FeO particles coupled with specific TAs and their capacity to label primary cultured T cells, the results from this study should aid in the determination of efficient procedures to tag T cells with FeO/TA complexes which would allow *in vivo* MR visualization after adoptive transfer of cells.

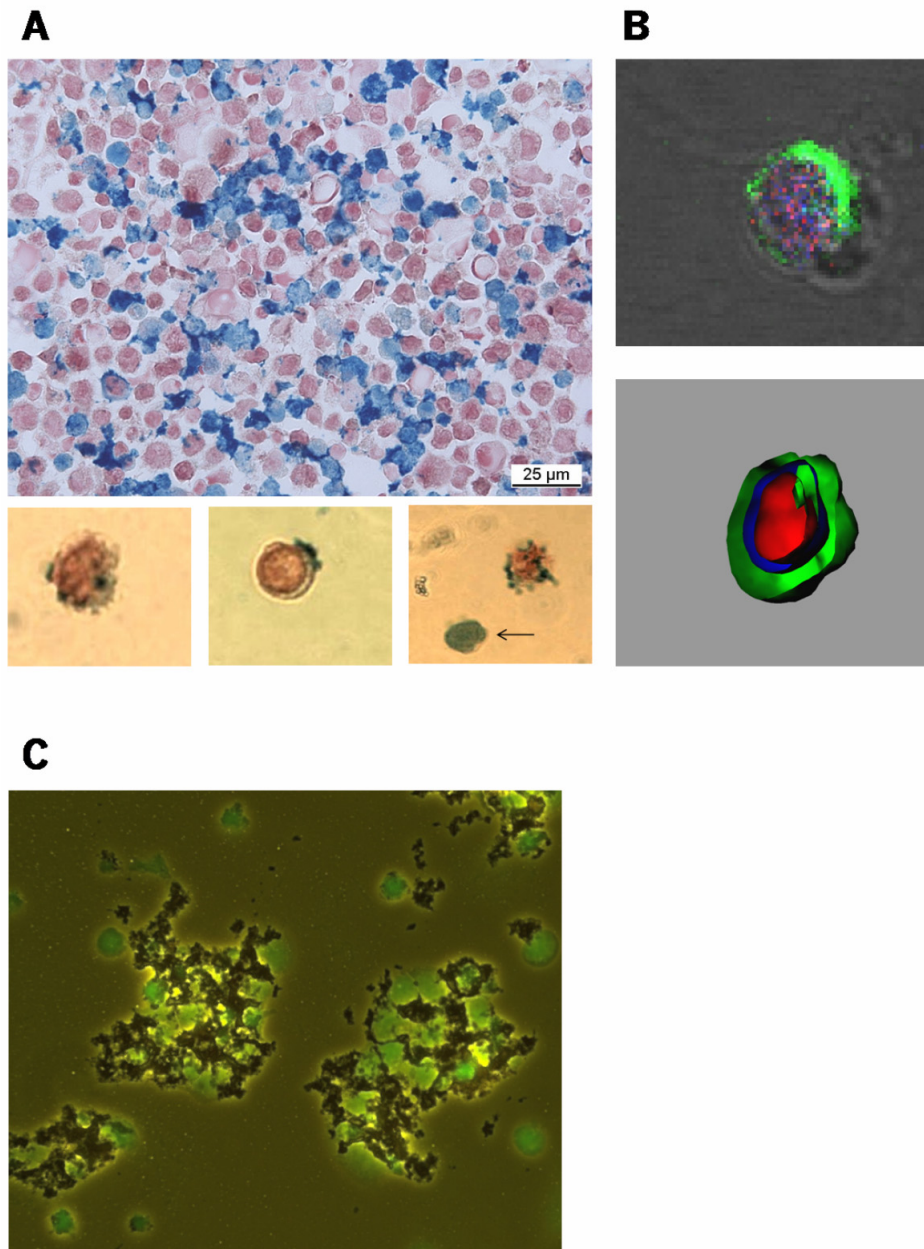


Figure 8: *Microscopy of labeled T cells:* A) Different examples of primary cultured T cells labeled with SPIO + PLL after cytopspin centrifugation. The overview image yields an estimate on the percentage of labeled cells. The three examples below show a cell containing FeO particles in the cytoplasm (left), a cell with FeO particles sticking to the cell membrane (middle) and a dead cell full of iron (at the bottom of the right image). Prussian blue staining was used to visualize the iron content.

B) Confocal image and 3D reconstruction (Imaris® Bitplane AG) of a T cell labeled with USPIO nanoparticles that were also labeled with the near-infrared fluorescent dye Cy5.5. FeO nanoparticles were unambiguously identified in the cytoplasm (blue areas). The cellular membrane and the nucleus were stained with Alexa488 (green) and Propidium Iodide (PI, red), respectively.

C) Clustering of T cells “glued together” by PEI vesicles containing iron. Green fluorescence signals indicate cells undergoing apoptosis (Molecular Probes® Apoptosis kit).

9.2 T Cells Labeling for NIRF Imaging

Tracking of Cy5.5-Tat Labeled Lymphocytes by Quantitative Near Infra-Red Imaging during Acute Brain Inflammation in a Rat Model of Experimental Autoimmune Encephalomyelitis

9.2.1 Abstract

Inflammation in multiple sclerosis (MS) and experimental autoimmune encephalomyelitis (EAE) is driven by T cells directed against myelin specific proteins. So far, *in vivo* imaging focused on downstream processes such as the infiltration of macrophages or structural alterations linked to inflammation and tissue damage. In this work, the infiltration of Cy5.5-labeled T lymphocytes into the brains of EAE rats was studied by near infrared fluorescence imaging. T cells, extracted from the spleens of naïve and immunized rats, were cultured in presence of Cy5.5-Tat (100 µg/ml) and administered intravenously to Lewis rats. Four groups of EAE animals have been studied: rats receiving activated labeled T cells at 5, 7, and 11 days post immunization (dpi) as well as EAE rats receiving naïve labeled T cells. The fourth group received naïve T cells at 7 dpi. Three control groups received either activated labeled T cells, naïve labeled T cells or the Cy5.5 dye only. Measurements were carried out from day 9 to 22 using a near-infrared fluorescence imaging system. The highest fluorescence signal was observed for EAE animals, which received myelin-activated T cells during the acute phase of EAE. The temporal profile of T cell accumulation in this group paralleled the pattern of neurological impairment during the acute phase, the remittance and first relapse. No disease specific fluorescence pattern was observed for EAE animals, which received naïve T cells. Inoculation of myelin-activated T cells in naïve animals led to a peak of fluorescence signal on day 13, which was less pronounced than in the EAE group. These results demonstrate that Cy5.5-Tat labeling of T cells is suitable for *in vivo* fluorescence imaging. This approach may particularly be useful for evaluation of novel anti-inflammatory therapies. Nevertheless, intrinsic problems for longitudinal studies is that, due to short life time of labeled T cells, unspecific labeling of scavenger cells (e.g. macrophages) will always occur.

9.2.2 Introduction

Multiple Sclerosis (MS) is characterized by neurological deficits that are attributed to the demyelination of nerve fibers in the central nervous system (CNS) [Julien and Ferrer, 1989]. Inflammation processes can occur anywhere in the central nervous system (brain, spinal cord or optic nerve) causing symptoms such as weakness, sensory deficits and optic neuritis [Miller, 1998]. MS is believed to be an auto-immune disease mediated by lymphocytes [Calopa *et al.*, 1995; Goust *et al.*, 1978] while hematogenous macrophages and microglial cells act as effectors degrading the myelin sheets [Benveniste, 1997]. Evidences of T lymphocyte initiative role in MS are for instance the presence of many active T cells subsets in early CNS lesions [Babbe *et al.*, 2000], and the fact that one of the existing method to induce MS animal model is to inject myelin activated T cells [Kojima *et al.*, 1997] [Ben Nun *et al.*, 1981]. Chronic-relapsing MS involves alternating phases relapsing episodes, with significant, frequently aggravating manifestations of neurological symptoms, and remitting episodes, during which patients recover partially or fully [Barnett and Prineas, 2004]. There is concluding evidences that even during remission the underlying disease processes leading to axonal injury is still ongoing. Today there is compelling evidences that T lymphocytes as initiates [Hickey, 1991], orchestrate [Traugott *et al.*, 1983a], and also effects the immune response in MS [Huseby *et al.*, 2001] [Steinman, 2001]. Hence, assessment of the T cell immune activity, in particular during phases devoid of clinical symptoms, would be of high diagnostic and prognostic value and would allow the guidance of therapeutic interventions.

Chronic experimental autoimmune encephalomyelitis (EAE) is a rodent model that mimics multiple aspects clinical MS [Feurer *et al.*, 1985]. EAE is an immune-mediated disease, in which immune cells become reactive against myelin components leading to the destruction of myelin sheets. As in MS, T lymphocytes are believed to be responsible for initiating the immune reaction against myelin, because inflammatory CNS infiltrates were shown to contain predominantly T lymphocytes [Hauser *et al.*, 1986]. Moreover, EAE can be adoptively transferred to animals by intravenous injection of myelin-activated T cells [Reynolds *et al.*, 1996]. Both, brain resident microglia cells and blood-derived macrophages are supposed to be rapidly activated and recruited to sites of inflammation by the lymphocytes [Raivich and Banati, 2004]. These two cell types seem to be responsible for the immune-mediated myelin

injury, which lead to an impairment of the nerve signal transmission and as a consequence to the neurological deficits.

Today, a number of non-invasive imaging approaches have been developed that allow *in vivo* monitoring of the migration of labeled cells. Magnetic resonance imaging (MRI) using e.g. superparamagnetic iron oxide nanoparticles as contrast agents provides excellent spatial resolution [Bulte *et al.*, 1999]. This approach is limited by the inherent low sensitivity and by background signal of MRI. In contrast, positron emission tomography (PET) involving radiolabelling of cells is characterized by excellent sensitivity [Adonai *et al.*, 2002]. PET is limited by low spatial resolution, the relatively short lifetime of the radiolabel preventing long term studies (days, weeks), as well as the study costs. Similar to PET, optical imaging using bioluminescent or fluorescent labels provides high sensitivity, sufficient to detect low numbers of cells [Doyle *et al.*, 2004] [Edinger *et al.*, 2003] [Lin *et al.*, 2003]. Fluorescent labels are relatively stable allowing longitudinal studies. The principal limitation is spatial resolution due to diffuse photon propagation in tissues caused by light scattering. Fluorescence imaging has e.g. been applied for the detection of endocrine tumor cells by using a fluorescent ligand targeting somatostatin cell surface receptors [Becker *et al.*, 2000] [Becker *et al.*, 2001] or to monitor apoptotic tumor cells using fluorescently labeled annexin-V targeting externalized phosphatidylserines [Kietselaer *et al.*, 2003] [Petrovsky *et al.*, 2003]. The purpose of this study was to monitor the infiltration of T lymphocytes into the CNS of rats in a model of chronic relapsing EAE using fluorescence reflectance imaging (FRI) in the near-infrared spectral domain. T cells were labeled *ex vivo* using chimerical Cy5.5-Tat peptide developed in house. Labeled cells were administered to EAE rats to test the feasibility of RFI to visualize and quantify T lymphocytes activity during the early inflammation stages of EAE.

9.2.3 Experimental Protocol

Animal model The EAE model in the Lewis rat is characterized by a first acute monophasic attack around eleven days post immunizing (dpi). The disease course can be prolonged by increasing the concentration of foreign antigens (guinea-pig spinal cord fragments) and/or *Mycobacterium tuberculosis* in the inoculum resulting in a remitting-relapsing pattern [Feurer *et al.*, 1985]. In our study rats typically went through an acute inflammation period (9-15 dpi) followed by a remitting phase (15-20 dpi), during which the animals recovered, and a first relapse (20-26 dpi), during which inflammation symptoms reappeared. Brain inflammation was monitored only between days 9 to 22, i.e. during the acute phase up to the first relapse. Inbred (RT1^l) female Lewis rats (N=42) from Charles River (Sulzfeld, Germany) were kept in a temperature and humidity-controlled room in line with sawdust with access to standard rodent chow and water *ad libitum*. The rats, weighing 140-160 g, were lightly anesthetized with isoflurane (Abbott, Baar/Zug, Switzerland) and immunized intradermally (i.d.) at the dorsal tail root by injecting 100 µl of a suspension consisting of 1 part (volume:volume) guinea pig spinal cord emulsified in 0.9% NaCl to 1 part complete Freund's adjuvant (CFA, Difco, Detroit, MI, US) supplemented with *M. tuberculosis* strain H37RA (Difco). The final inoculum per rat comprised about 66 mg Gp-sc and 2 mg mycobacterium.

Neurological score: The diseased status was assessed using a scoring scale for the neurological state of the animals. A careful examination of animal symptoms was carried out on a daily basis [Rausch *et al.*, 2003]. Considering the state of paralysis of each animals, individual scores were estimated as following: 0 = normal healthy animal; 0.5 = loss of tail tonus; 1 = complete tail paralysis; 2 = hind limb weakness; 3 = complete hind limb paralysis, incontinence; 4 = complete paralysis.

Cy5.5-Tat synthesis The Tat (Twin Arginine Translocation) peptide is a fragment of protein from the HIV virus containing multiple arginine groups. This peptide is ferrying foreign proteins through the plasma membrane of a cell by an energy dependent process involving endocytosis [Vives *et al.* 2003]. In our study, the indocyanine dye Cy5.5-Mal (Amersham Biosciences GmbH, Otelfingen, Switzerland) was covalently coupled to the Tat peptide in order to be shuttled across the plasma membrane of primary cultured T lymphocytes.

Coupling was achieved by adding Tat-peptide-Cys (Biosynton GmbH, Berlin, Germany) in DMSO to 1 equivalent Cy5.5-Mal dissolved in DMSO and stirring the mixture for 2h at room temperature. The product was purified by chromatography (Biogel P-2; MWCO: 1800, bidest. water) and the first fraction was isolated and lyophilized. All operations were done under protection from excess light. For labeling of fresh T cells, a stock solution of Cy5.5-Tat was prepared by diluting Cy5.5-Tat powder in phosphate buffer (D-PBS, Gibco, Basel, Switzerland) to a concentration of 2 mg/ml. This solution was stored at 4°C until use.

Spectral analysis in the UV/VIS domain was performed using a Lambda 19 spectrophotometer (Perkin-Elmer AG, Schwerzenbach, Switzerland). The absorption spectrum was measured in the wavelength range 850-200 nm with a slit width of 2 nm, a scan rate of 120 nm/min and phosphate-buffered saline solution (PBS) in the reference channel.

Fluorescence measurements were carried out using a Spex Fluorolog II (HORIBA Jobin Yvon Inc, Edison, USA), equipped with a 450W Xe-lamp and a cooled detector R928P (Solvias AG, Basel, Switzerland). Fluorescence spectra were measured with slit widths for excitation and emission mono-chromators set to 1.0 mm (= half width 1.8 nm). Emission spectra were measured for excitation at two wavelengths, 678 nm and 630 nm, respectively, 678 nm corresponding to the absorption maxima. Excitation spectra were measured by setting the detector to 697 nm (fluorescence maximum). Quantum yields were determined in reference to cresylvioletperchlorate in methanol, for which a quantum yield of 0.54 was assumed, and which has been excited at 594 nm.

T cell preparation Splenocytes were extracted from Lewis rat's spleens. Organs were destroyed in Hanks' balanced salt solution (Gibco AG, Basel, Switzerland) using a Potter homogenizer. The mixture obtained was filtered several times through cell strainers with pores sizes of 100 µm, 70 µm and 40 µm in diameter. After the last centrifugation, erythrocytes were lysed by resuspending the cell pellet in 0.13 M ammonium chloride. Remaining white blood cells were incubated in a 25 cm² cell culture flask (Falcon®, Becton Dickinson Discovery Labware, Basel, Switzerland) in complete medium (CM) composed of RPMI medium plus HEPES buffer, 1 mM Na-pyruvate, 1× MEM non-essential amino-acids (Gibco AG, Basel, Switzerland), 50 µM 2-mercaptoethanol, 50 µM gentamicin antibiotic, 1× MEM vitamins (Gibco AG, Basel, Switzerland), 2 mM L-glutamine, 10% fetal calf serum and interleukin-2 (IL-2) stimulating factor (5% rat T-STIM™ solution, Becton Dickinson

Biosciences, CA, USA). To remove the majority of monocytes/macrophage population, the non-adherent cell population was transferred into a new flask. This method yielded a cell population containing about 95% lymphocytes, as determined by morphology analysis [Schoepf *et al.*, 1998a]. Rat pan T cells were isolated by immunomagnetic bead selection (Miltenyi Biotec Inc, Auburn, CA) according to the manufacturer instruction. A FACS analysis of MACS isolated cells was performed to confirm the only presence of T cells in the isolated population (results not shown).

Cell labeling Rat pan T cells was resuspended in 1 ml CM at a final concentration of 10^6 cells/ml and incubated with Cy5.5-Tat for 1, 2, 4h or overnight at 37°C in 95% / 5% air / CO₂. Different concentrations of Cy5.5-Tat ranging from 5 µg/ml to 200 µg/ml have been tested. To remove free fluorescent probes in solution, cells were washed three times after labeling with Hanks' balanced salt solution (HBSS), counted with Fluorescein Di-Acetate (FDA) exclusion method and used for *in vivo* adoptive transfer, FACS experiments or confocal microscopy.

Confocal and FACS analysis Confocal microscopy was performed using a Leica TCS SP II (Leica Microsystems AG, Glatbrugg, Switzerland). Cy5.5-Tat labeled cells were dumped on glass slices, allowed to dry and incubated with a immunostaining mixture composed of PBS, 0.1% Triton X-100 (Sigma, Buchs, Switzerland), an anti-CD3 monoclonal antibody coupled to the Alexa488 dye (Molecular Probes, Invitrogen AG, Basel, Switzerland), and propidium iodide (PI) for nucleus staining.

Fluorescence automated cell sorting (FACS) experiments were carried out using a LSR II flow cytometer (Becton Dickinson, San Jose, CA, USA). The FACS buffer used was composed of PBS with 3% fetal bovine serum (FBS) and 0.02% sodium azide.

For FACS analyses and confocal microscopy studies the Cy5.5-Tat peptide was excited at 678 nm and the emitted fluorescence was detected at 698 nm.

Immunolabeling To phenotype splenocytes by FACS, labeled monoclonal antibodies have been used. Helper T cells were targeted using an anti-rat CD4 antibody coupled with phycoerythrin (PE) (Pharmingen, San Diego, CA, USA), cytotoxic T cells using an anti-rat CD8-peridinin chlorophyll protein (perCP), and pan T cells using an anti-rat CD3-

allophycocyanin (APC) antibody. Cells were incubated for 20 min at 4°C with the antibody at the appropriate concentration according to the instructions of the manufacturer. Four-channel FACS analysis was performed using the LSR II cytometer.

Cell uptake measurement After washing centrifugations, cell suspensions (10^6 rat pan T cells) were transferred into plastic tubes containing 1 ml PBS. To determine the retention of Cy5.5-Tat peptide in cells as a function of time; the fluorescence signal of cell suspensions was measured using bonSAI FRI prototype device (Siemens AG, Medical Solutions, Erlangen, Germany). The fluorescence intensity of reference concentrations of the pure Cy5.5-Tat dye were measured in parallel enabling an estimate of the Cy5.5-Tat concentration per T cell.

T cells adoptive transfer and in vivo protocol Prior to FRI measurements, animals were anesthetized using isoflurane (2% volume) in nitrous oxide / oxygen. A cannula was placed in the tail vein using a catheter (0.5×25 mm, Becton-Dickinson Discovery Labware, Basel, Switzerland) for infusion of Cy5.5 labeled T cells. Ten millions (10^7) cells suspended in PBS were injected intravenously. Animals were placed on a heated support, allowing maintaining body temperature at 37°C using warm air. FRI measurements were carried out once per day for two weeks, starting at 1 day after T cell injection. Whole body scans were carried out for all animals at the first and second day after T cell injection to monitor the unspecific signal contribution due to free label or labeled cells in blood circulation (and peripheral organs).

EAE rats were divided into four groups of 6 animals: E-AT-5, E-NT-7, E-AT-7, and E-AT-11. Three groups of six naïve rats each have been used as controls: N-AT-7, N-NT-7, and N-Cy5.5. The nomenclature is such that the first letter correspond to the type of animal used (E = EAE, N = naïve rat), the second term describes the type of cells the animal received (AT = Cy5.5-Tat tagged activated T cells and NT = Cy5.5-Tat tagged naïve T cells), while the number correspond to the day of T cell injection. All T cells injected have been labeled with Cy5.5-Tat, the activated T cells originated from EAE animals, whereas of naïve cell were derived from healthy animals. The experiment setup is summarized in Table 1.

Group name	Animal	Injected cells	Day of injection
E-AT-5	EAE	Cy5.5 Activated T cells	5 dpi
E-NT-7	EAE	Cy5.5 Naïve T cell	7 dpi
E-AT-7	EAE	Cy5.5 Activated T cells	7 dpi
E-AT-11	EAE	Cy5.5 Activated T cells	11 dpi
N-AT-7	naïve	Cy5.5 Activated T cells	7 dpi
N-NT-7	naïve	Cy5.5 Naïve T cell	7 dpi
N-Cy5.5	naïve	Cy5.5-Tat peptide	7 dpi

Table 1: Experimental setup of the *in vivo* experiment. Cy5.5 labeled activated T cells and Cy5.5 labeled naïve T cell were extracted respectively from the spleen of EAE animals and naïve animals, respectively. Cells were injected i.v. in the tail vein. The injection days are either 5, 7 or 11 days post EAE immunization (dpi).

In vivo NIRF imaging For FRI experiments, rats were anaesthetized using 1.5% isoflurane (Abott) in nitrous oxide (2:1) administered with a facemask. Total FRI scanning time was 5 min per rat. To avoid problems caused by light scattering due to the fur, we shaved animals for the FRI experiments.

For time-resolved *in vivo* brain imaging, a eXplore Optics™ (GE Healthcare) small animal imager was used. A laser at 670 nm powered at 4.4 mW and pulsed at repetition rate of 80 MHz with pulse durations of 60 psec was used for fluorescence excitation. The fluorescent light emitted from the sample (rat) was detected by a photo-multiplier tube (PMT-detector) at 700 nm. FRI images have been analyzed quantitatively on a ROI basis using the same software tool provided by the manufacturer.

Whole body and *ex vivo* organ imaging were performed with the bonSAI FRI system. For fluorescence excitation, three laser diodes at 660 nm with a total power of 10 mW/cm² have been used yielding a uniform illumination of the whole animal. The fluorescent light emitted from the sample (rat) was detected by a charged-coupled device (CCD) camera (Hamamatsu ORCA, Solothurn, Switzerland) equipped with a focusing lens system (macro lens 60 mm, 1:2.8, Nikon, Egg/ZH, Switzerland). The image matrix comprised 532 × 256 pixels. A bandpass filter was used for the selection of the detection wavelength (698 nm). Experiments were controlled by a PC using the Siemens SYNGO software. Autofluorescence measured

immediately before cell adoptive transfer turned out to be negligible. All experiments were in strict concordance to the Swiss Federal law for animal protection.

Ex vivo analysis and histopathology One animal of each group has been sacrificed at 12 and 22 dpi. For group N-Cy5.5 three more rats have been sacrificed at one, two and four hours after Cy5.5-Tat injection in order to visualize the bio-distribution of the probe in healthy animals (results not shown). Rats were killed by an overdose of isoflurane immediately after FRI studies. Animals were perfused intracardially 5 minutes with a D-PBS to clear organs from blood. Thereafter a solution of 4% formalin (4 mg in 100 ml) was infused during 10 minutes to fix organs. *Ex vivo* imaging of the brain and the spleen of each animal was performed before embedding them in paraffin. Semi-serial slices of 5 μ m thickness were cut in brain areas displaying Cy5.5 signals *in vivo*. Slices were first treated with a classical hematoxylline-eosin (H&E) stain to localize inflamed areas. Morphometric analyses were performed on sections stained immunohistochemically (IHC) for ED-1 (macrophages) and CD3 (T cells) using the Histolab™ software (Microvision Instruments, Evry, France). Stained slides were examined with a light microscope (Eclipse E600, Nikon, Egg/ZH, Switzerland) connected to a 3CDD color video camera (DXC-970MD, Sony, Tokyo, Japan). After capturing of the total surface of the brain slice, at x20 magnification, the color corresponding to each IHC staining (ED1 and CD3 respectively) was extracted by threshold settings and the occupied area automatically calculated. The results were expressed as percentage values, describing the fraction of the total surface area displaying IHC labeling. Another set of histological sections has been stained with monoclonal antibodies directed against CD3 (coupled to Alexa488) and against ED-1 receptors (coupled to Alexa496), respectively, for confocal microscopic analysis.

9.2.4 Results and Discussion

Dye description The UVVIS-spectrum of the Cy5.5-Tat complex is shown in Fig.1. The corresponding absorbance values for wavelengths $\lambda = 278$ nm, 630 nm and 678 nm are listed in Table 2 together with the fluorescence quantum yields determined for excitation wavelengths 678 nm and at 630 nm.

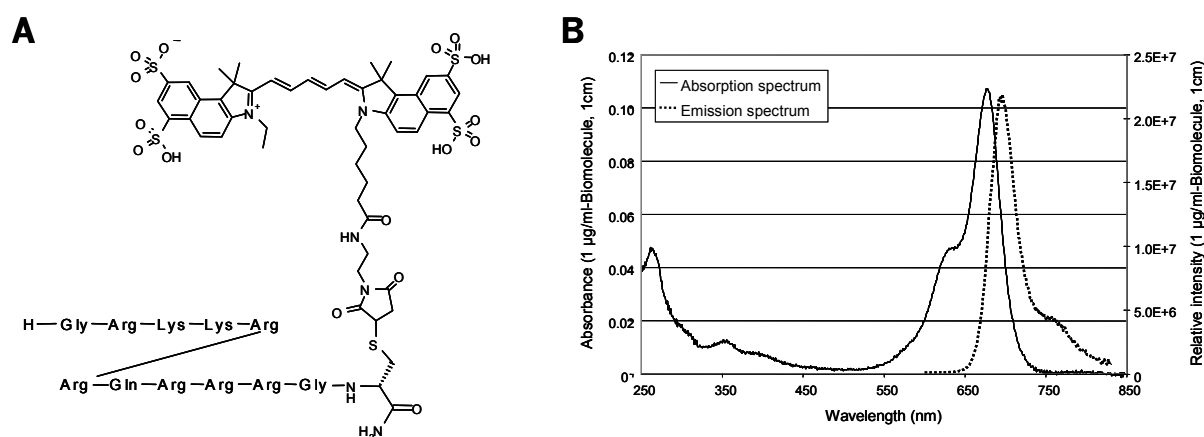


Figure 1: (A) Molecular structure of Cy5.5-Tat (B) Absorption and emission spectra. Spectrum for a Cy5.5-Tat at a concentration of $1 \mu\text{g/ml}$ and pathlength $d = 1\text{cm}$. Fluorescence excited at 678nm.

wavelength	Absorbance [$\text{g}\cdot\text{ml}^{-1}\cdot\text{cm}^{-1}$]			Quantum Yield	
	278nm	630nm	678nm	Excitation at 630nm	Excitation at 678nm
Cy5.5-Tat	1.775	2.875	6.576	0.17	0.22

Table 2: Absorbance and quantum yield value of the Cy5.5-Tat biomolecules when excited at 278, 630 and 678nm

Estimation of cellular uptake The *in vitro* fluorescence intensity was found to be proportional to the incubation concentration of the Cy5.5-Tat probe (Fig.2). In addition, Fig.2b shows the relationship between the number of living T cells following the labeling procedure as counted by FDA exclusion. When using low concentrations of Cy5.5-Tat concentrations in the range 1 to 50 $\mu\text{g/ml}$ cell viability was not affected. However, concentrations of Cy5.5-Tat exceeding 100 $\mu\text{g/ml}$ displayed dose-dependent toxicity resulting in a diminution of surviving cells by 10 to 30% respectively.

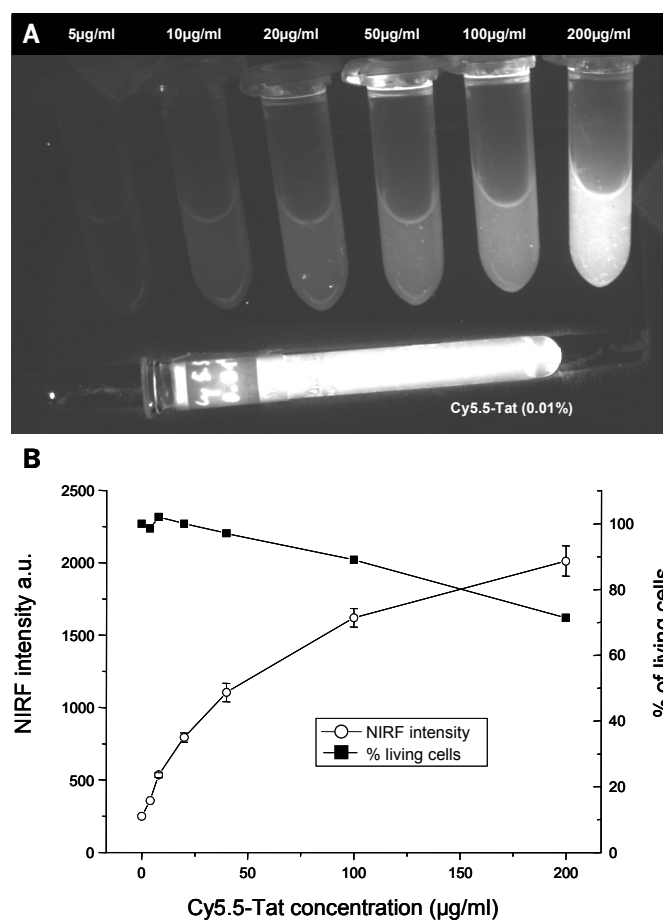


Figure 2: *In vitro* cell fluorescence. T cells near infrared fluorescence (A) after overnight incubation with 5, 10, 20, 50, 100 and 200 µg/ml of Cy5.5-Tat peptide. The fluorescence was quantified by comparing to a standard concentration of 0.01% of pure Cy5.5-Tat (0.01g in 100ml distilled water). (B) NIRF intensity as a function of Cy5.5-Tat concentration (circles) compared with the number of living T cells remaining in solution after the overnight incubation (black squares).

Although the total number of viable cells decreased significantly for $[Cy5.5-Tat] = 200 \mu\text{g/ml}$ the total fluorescence signal of the T cell suspension still increased as compared to $100 \mu\text{g/ml}$ indicating that the amount of dye complexes per cell increases when incubating with high concentration of Cy5.5-Tat. The dose dependence of the fluorescence intensity deviates from linearity (Fig.2b), which may reflect saturation of the labeling process or non-linear optical effects such a fluorescence quenching at high concentration or a combination of both. In reference to the standard fluorescence (0.01% = 10 mg in 100 ml; long tube in Figure 2a), the amount of Cy5.5-Tat peptide present in one T cells is estimated to be in the range 5pg to 50pg for an overnight incubation complex concentrations between 5 and 200 µg/ml respectively.

In order to further investigate both labeling efficiency as well as the toxic effect of the dye, a kinetic study of Cy5.5-Tat uptake was performed and analyzed using FACS. Isolated T cells were incubated during 1h, 2h, 4h and 12h with a solution of Cy5.5-Tat complexes at a concentration of 200 $\mu\text{g}/\text{ml}$. Fig. 3 shows FACS data of the T cell population that was incubated for 12h. Pie charts show the fractions of helper and cytotoxic T lymphocytes that were tagged with Cy5.5-Tat, as well as of dead and unlabeled T cells. After incubating for 1h, 19.5% of the living population of lymphocytes was already labeled. This fraction increases up to 36.4% for overnight incubation (12h). In parallel, the population of dead lymphocytes, identified on the basis of propidium iodide incorporation, increases from 12.3% to 34.2% of the total population. The value is in agreement with data displayed in Fig.2b showing a decrease of the number of living cells to 70% after incubating overnight.

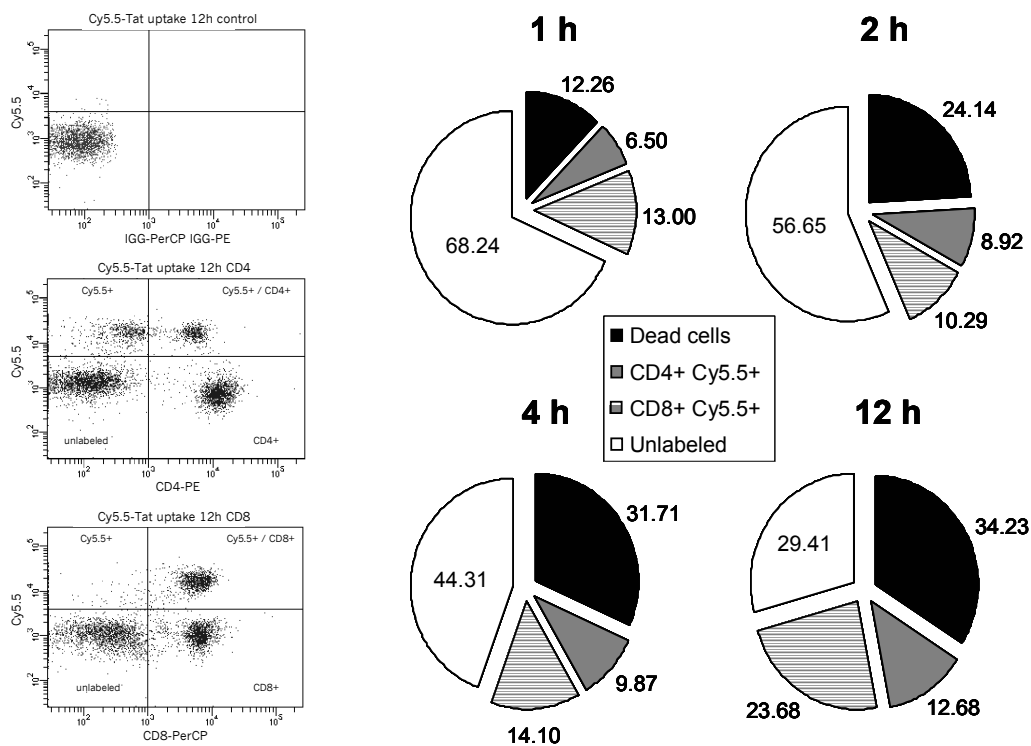


Figure 3: Kinetic of Cy5.5-Tat uptake by FACS analysis. FACS data (on the left) represent dual color flow-cytometry analysis of Cy5.5-Tat labeled T cells after 12h incubation. The y-axis represents the mean intensity of Cy5.5 fluorescence, whereas the x-axis refers to conjugated immunoglobulins controls for non-specific labeling of T cells (top), CD4-PE for specific labeling of T-helper (middle) and CD8-PerCP for cytotoxic T cells (bottom).

Pie charts represent the sub-populations in 100% of T lymphocytes after 1h, 2h, 4h and 12h incubation with Cy5.5-Tat dye (at 200 $\mu\text{g}/\text{ml}$). Dead cells (identified by PI staining) are represented in black. Populations of living helper (CD4+) and cytotoxic (CD8+) lymphocytes are represented by grey and dashed sectors respectively. White sectors represent the population of unlabeled lymphocytes.

Even after an exposure of 12h, one third of the total T cell population did not show a fluorescent signal, i.e. these cells have not been labeled. We speculate that either these cells represent sub-population of T cells that are not sensible to Tat sequence penetration or that the label has been degraded in these cell, e.g. due to the cleavage of the sulfide Mal-Tat bond leading to the release/destruction of the cyanine dye. Alternatively, the Cy5.5-Tat probe might be released into the cell culture medium, as described by Ensoli *et al.* [Ensoli *et al.*, 1993]. Confocal microscopy analysis confirmed the main intracellular localization of the dye within the T cells is the cytoplasmic compartment (Fig.4). Nevertheless, in some cells a significant nuclear staining has been observed consistent with previous reports using different Tat peptide-derived sequences in Hela cells and mouse splenocytes [Schimmelpfennig *et al.*, 2005] [Lewin *et al.*, 2000]. Cytoplasmic staining was visible after 1h as described by Fawell *et al.* [Fawell *et al.*, 1994]. Referring to these previous studies, we presume that Tat-mediated uptake by T cells occurs via adsorptive endocytosis [Fawell *et al.*, 1994] [Mann and Frankel, 1991].

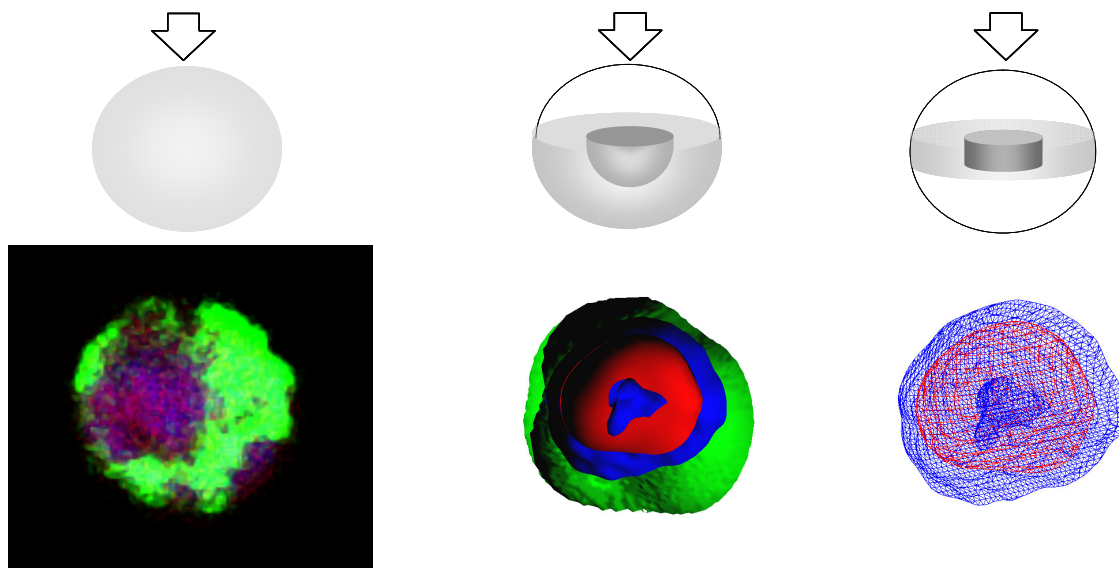


Figure 4: *Confocal microscopy of labeled T lymphocytes.* Confocal raw image (left) of labeled lymphocyte and 3D reconstruction (middle and right) with the Imaris® software (Bitplane AG, Switzerland). A schematic view of the cell is represented on the top of confocal images. Lymphocytes have been incubated with Cy5.5-Tat (200µg/ml) for 1h. The cytoplasmic membrane and the nucleus were stained with CD3-Alexa488 (green) and Propidium Iodide (red) respectively. The Cy5.5 dye (blue) was mainly localized in the cytoplasm but also within the nucleus.

T cells adoptive transfer in immunized animals Fig. 5a displays the average neurological score of EAE rats as function of time following immunization. Animals showed neurological impairment up to a score of 3 in the interval 10 to 12 dpi. The acute phase was followed by a remitting phase (15 to 20 dpi), during which the neurological status returned almost completely to normal. During the first relapse (21 to 26 dpi), neurological impairment resulted in a average score of 0.85, i.e. the symptoms were significantly weaker as during the acute stage.

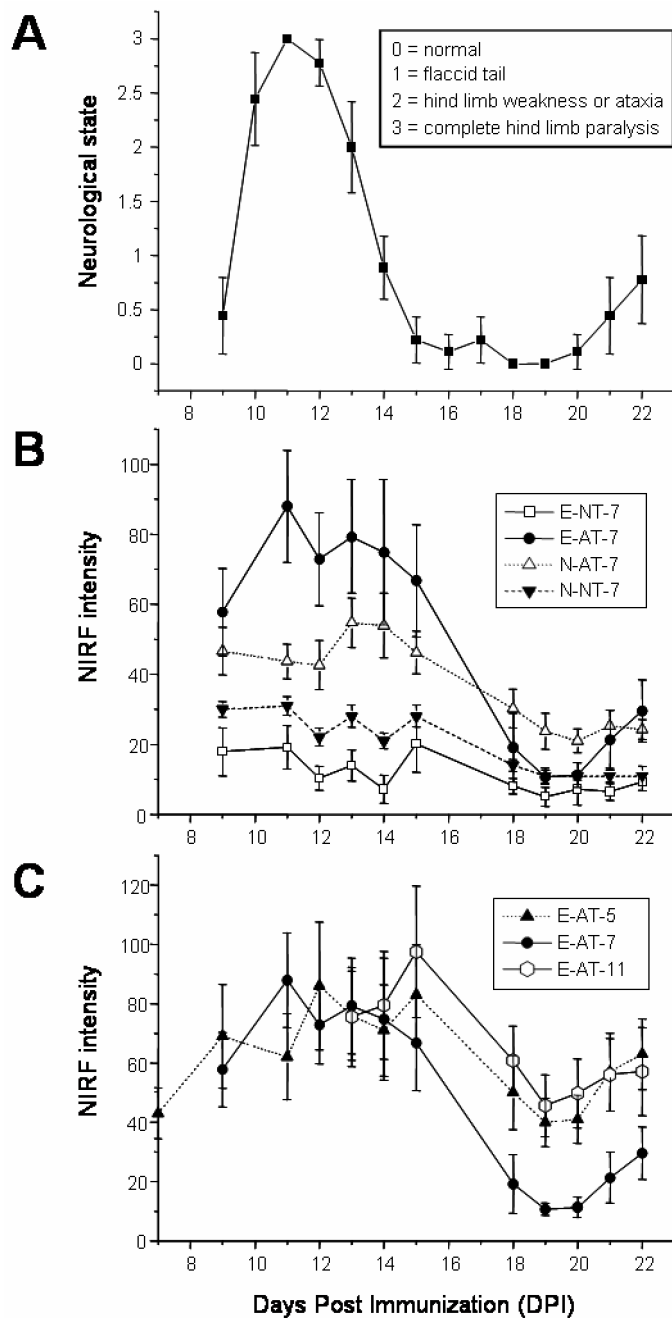


Figure 5: (A) Neurological score of animals during the different phases of EAE. Animals display neurological impairment during the acute phase and the first relapse, while they show almost complete remission between the two periods. The acute inflammatory phase ranges from 9 to 15 dpi, the remitting phase from 15 and 20 dpi, and the first relapse from 21 to 26 dpi.

(B) NIR fluorescence signal evolution in rat brain based on T cell activation state. In this experiment, Cy5.5-Tat labeled T cells were transferred adoptively at 7 dpi. Animals from groups E-AT-7 and N-AT-7 received myelin-activated T cell while rats from groups E-NT-7 and N-NT-7 received naïve T cells. The NIR fluorescence intensity is given in percentage of the initial value at 8 dpi, i.e. one day after cell transfer (not shown).

(C) NIR fluorescence signal evolution in rat brain based on the time of adoptive transfer. Similarly to the previous diagram, NIR fluorescence intensity is given in percentage of the initial value. This value is 5 dpi for the group E-AT-5, 7 dpi for E-AT-7 and 11 dpi for E-AT-11. All animals received myelin-activated T cells preliminary labeled with Cy5.5-Tat.

Rats received intravenously 10^7 T lymphocytes at 5, 7 and 11 dpi. For all groups, an intense fluorescence signal could be detected in the brain immediately following the injection. This signal decreased to a lower signal for control groups (N-AT-7, N-NT-7 and N-CY5.5) one day after injection. For these animals, no fluorescence signal was detectable in brain and peripheral organs one day after T cell transfer with the exception for spleen and liver (result not shown). The fluorescence signals of organs harvested from the group N-CY5.5 suggest that i.v. injected dye redistributes to spleen and liver during the next hours in agreement with published data [Schimmelpfennig *et al.*, 2005] [Basse, 1995].

In vivo FRI imaging FRI measurements were carried on from day 1 following T cells injection until the middle of the first relapsing phase (22 dpi). Semi quantitative information of the fluorescence signal evolution was derived from FRI images by normalizing in a region of interest comprising the brain actual fluorescence intensity to that of the first measurement (=100%) recorded 1 day after T cell injection [Hintersteiner *et al.*, 2005]. A significant difference in the NIRF signal has been found between EAE groups (E-AT-5, E-NT-7, E-AT-7 and E-AT-11) and control groups (N-AT-7, N-NT-7 and N-CY5.5) throughout the duration of the experiment. While EAE groups revealed large differences in fluorescence intensity as a function of time, the signal in control animals remained essentially constant at lower intensity. The brain fluorescence measured in animals of the group N-CY5.5 (results not shown) was equal to the background signal within error limits.

The role of lymphocyte activation state on their migratory properties towards sites of inflammation has been analyzed by comparing groups which received either activated or naïve T cells (E-NT-7 versus E-AT-7, N-AT-7 versus N-NT-7). Fig. 5b shows the progression of the fluorescence intensity in both EAE and naïve animals following the injection of either myelin-activated or naïve T lymphocytes. Animals in the group E-AT-7 show the strongest signal during the acute phase up to 90% of the initial value. Transferred lymphocytes must find their way towards their target (i.e. myelin) by the means of a chemotactic gradient [Hickey, 1991], taking part in the already-activated endogenous immune response [Carrithers *et al.*, 2000]. Although animals from group N-AT-7 were healthy, adoptive transfer of myelin-activated T cell led to a 50% NIR signal in the time period 12 to 15dpi, which decreased subsequently. It is known that transfer of myelin activated T lymphocytes may prompt an

immune response in immuno-deficient mice and induce EAE [Lafaille *et al.*, 1997]. Since Lewis rats we used for this experiment were not immuno-deficient, this response is considerably weaker than in the EAE model (i.e. the fluorescence signal in N-AT-7 rats was significantly weaker than the group E-AT-7). Control groups E-NT-7 and N-NT-7 showed no significant changes in fluorescence signal following lymphocyte transfer.

Another aspect that might influence the migration of labeled T cells to the brain parenchyma is the time point of injection. Fig. 5c shows the fluorescence signal in rat brain following adoptive transfer of T cell at different time points (i.e. 5, 7 and 11 dpi). For the groups E-AT-5, E-AT-7 and E-AT-11, the highest fluorescent intensity was reached at the end of the acute phase (15 dpi) followed by a decrease of fluorescence intensity during the remitting period. During the acute phase, a significant increase of the fluorescence intensity to an average value of 80% of the initial signal irrespective of the time point of T cell injection. During the remitting and relapsing phase, the brain fluorescence signals followed course of the neurological state decreasing to 32% at 19 dpi. During the first relapse, when increasing migration of labeled T cells to the CNS occurs (at 20 dpi) the average fluorescence intensity increased concomitantly to reach 50% of the initial value. Data in the Figure 6 illustrate that the fluorescence signals, reflecting the amount of labeled T cells in the brain, correlate with the neurological state of animals, which is linked to the cellular and molecular activity of the immune system within the parenchymal brain tissues [Tabira, 1989].

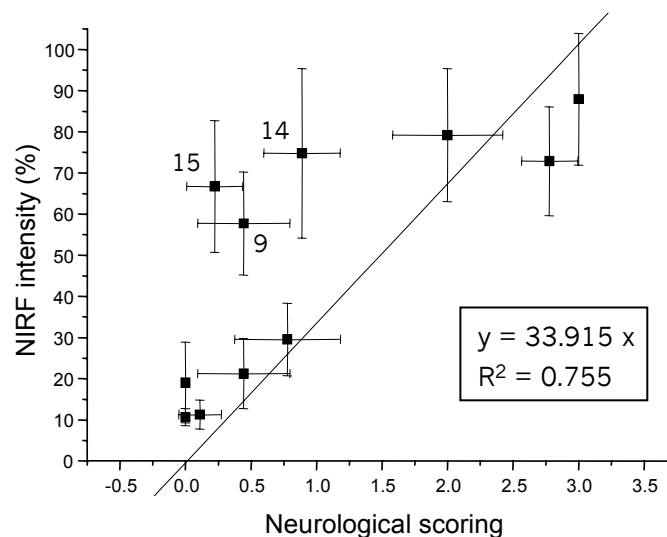


Figure 6: Correlation diagram. The NIRF intensity is represented as a function of the neurological scoring of animals. Numbers beside points correspond to dpi.

In the EAE groups, the fluorescence signal paralleled course of the EAE disease. Correlation of the E-AT-7 fluorescence data with the neurological (Fig. 6) score yielded a correlation coefficient of $R^2=0.75$, indicating that the fluorescence intensity is linked to the immune activity in the brain. We presume that this increase of fluorescence prior to the onset of symptoms (at 9 dpi) reflects the accumulation of myelin-activated T cells in inflammation sites, which trigger the infiltration of activated monocytes causing tissue damage and thereby neurological deficits. Fluorescence peaks at 11 dpi indicating increasing recruitment of activated T cells involved in the immune reaction against myelin [Babbe *et al.*, 2000]. These data obtained from non-invasive imaging are in line with previous EAE studies demonstrating the initiative role of T lymphocytes, which recognize the major histocompatibility complex (MHC) complex expressed by affected brain cells [Neumann *et al.*, 2002] and myelin antigens [Hartung and Rieckmann, 1997]. A small increase in the fluorescence signal intensity is observed at the beginning of the first relapse phase (20 dpi), the origin of which is not unambiguously revealed. It rather difficult to attribute this signal to T lymphocytes because T cells that are present in acute brain lesions seem to undergo apoptosis when EAE animals recover (i.e. remitting phase) [Schmied *et al.*, 1993] [Gold *et al.*, 1997]. Although, T cell apoptosis appear to be restricted to cells located in the neuroectodermal parenchyma [Bauer *et al.*, 1998], we speculate that this signal increase arises either from unharmed labeled T cells present in the brain's connecting tissue compartments or from macrophages entering brain parenchyma that have been labeled by phagocytosing apoptotic T cells and accordingly the Cy5.5-Tat probes. It has been shown that both microglial cells and hematogenous macrophages that interact closely with T cells influence their susceptibility to apoptosis [Pender and Rist, 2001] and also participate in the phagocytosis of apoptotic lymphocytes in the CNS [Nguyen and Pender, 1998].

Ex vivo imaging and correlative histology *In vivo* results were confirmed by *ex vivo* fluorescence measurements on brains excised at 12 and 22 dpi. *Ex vivo* imaging and fluorescence microscopy demonstrated the presence of Cy5.5 fluorescence signal in the brains of animals from groups E-AT-5, E-AT-7 and E-AT-11 and N-AT-7 whereas signals from groups E-NT-7 and N-NT-7 were significantly weaker or not observed at all. Fig. 7 illustrates the *ex vivo* analysis procedure. After *in vivo* localization of the region of interest, the corresponding histological brain section was selected, immunohistochemically stained in

order to identify T lymphocytes and macrophages. Histo-morphometrical analyses showed the exact co-localization of CD3 and ED1 tracers in the periphery of the medulla (Fig.7b) confirming the predominant infiltration of these cells into EAE lesions [Hauser *et al.*, 1986]. Confocal images (Fig.7c) revealed more detailed information on inflamed areas demonstrating labeling of both rat T lymphocytes and macrophages with Cy5.5-Tat. Clearly, labeled T cells had been taken up by activated monocytes.

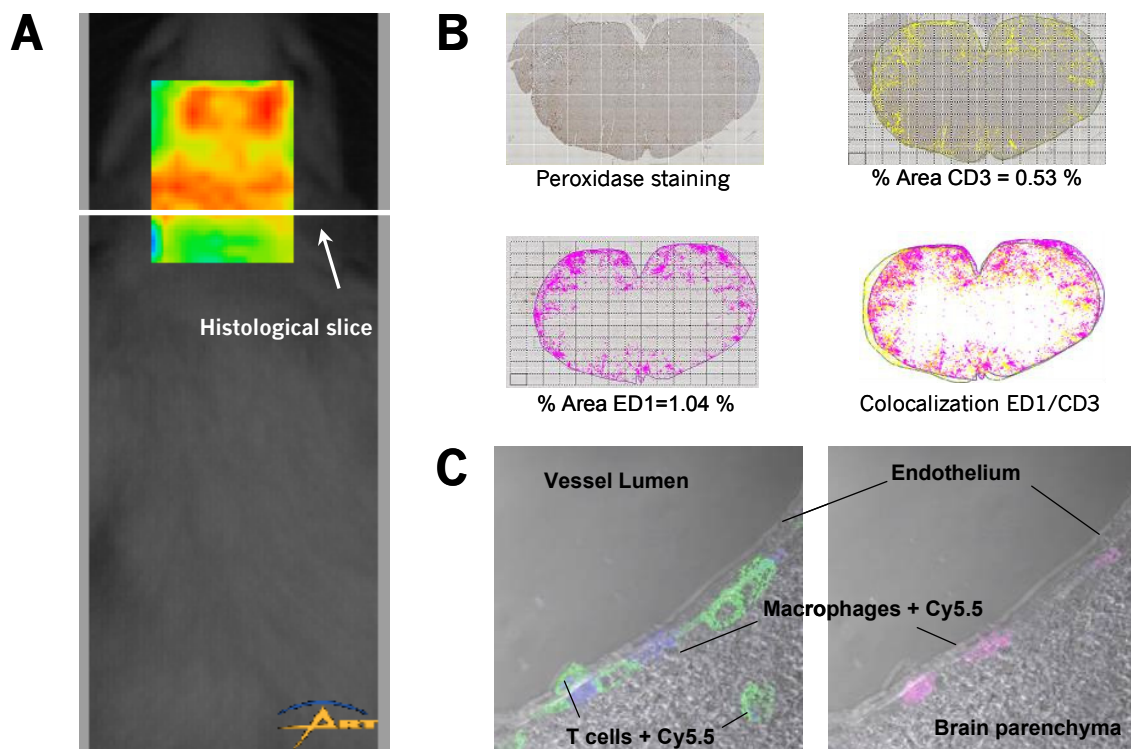


Figure 7: (A) *In vivo* raw image of the Cy5.5-Tat fluorescence signal in the brain. The exact localization of *ex vivo* and histological investigation has been define in the medulla where the signal was the strongest (white line). In this case, the animal belong to the group E-AT-11 and histological investigations were performed on day 12 dpi.

(B) *Histological correlation.* Peroxidase staining of T lymphocytes (CD3+) and macrophages (ED1) present in the brain has been performed. T cells and macrophages colocalize unambiguously in inflammation areas (i.e. periphery of the medulla). For all measurements, the area occupied by T cells was approximately half of the area occupied by macrophage

(C) *Confocal microscopy.* Cy5.5-Tat fluorescence, CD3+ and ED1 labeling appear in blue, green and red respectively. Lymphocytes but also macrophages are labeled with Cy5.5.

In summary, our study demonstrated that the indocyanine dye Cy5.5 can be shuttle into primary cultured T lymphocytes using the Tat peptide as vector. The Cy5.5-Tat complex exhibits low toxicity and a sufficiently high fluorescence quantum yield for *in vivo* detection of labeled cells after intravenous injection. Microscopic analyses of labeled cells revealed probe presence in the cytoplasm after 1h incubation, and to a lesser extent in the nucleus. Adoptive transfer of labeled T cells permitted visualization of T cell infiltration into the brain parenchyma during the acute inflammation episode of EAE. This approach allows studying mechanistic aspects of the immune response, in particular the early lymphocyte infiltration leading to the recruitment of effector cells. In later phases, phagocytosis of dead T cells by macrophages will lead to unspecific labeling of the latter. However, removal of dead cells reflects a normal activity of the immune system, and irrespective of the cell type and label used, unspecific labeling of macrophages might occurs in every longitudinal studies.

10 Overall conclusion

Important developments in computer sciences in the past decade have provided powerful tools to improve imaging technologies. Advances in the imaging sciences could change the face of medicine, making possible to non-invasively detect, diagnose and guide therapy for a large variety of diseases. Positron emission tomography (PET), magnetic resonance imaging (MRI), fluorescence optical tomography or nuclear medicine techniques are examples of the detection methodologies used with molecular probes and contrast agents that typify the powerful new field of molecular imaging. Although the science of molecular imaging needs further development to be used as a routine clinical tool, imaging technologies such as MRI and computed tomography (CT) scanning have become standard tests in disease detection and patient management. As a consequence, new clinical modalities with improved sensitivity such as brain imaging for the characterization of neurological diseases are on the horizon. In order to enhance the ability to detect disease at its early stages, scientists must determine how to define disease better in terms of the specific biological (i.e. molecular and genetic) abnormalities underlying symptoms.

In the EAE rat model of neuroinflammation, blood derived macrophages and microglia activity in brain lesions is directly linked to the destruction of myelin sheets [Bauer *et al.* 1994]. Longitudinal imaging of macrophages by MRI can thus allow a non-invasive localization of active myelin degradation spots in the brain. The protocol to tag macrophages with iron consist on injecting ultra small particles of iron oxide (USPIOs) intravenously 24h hours before MR measurements [Rausch *et al.* 2001]. As we discussed it in our first report [Berger *et al.* 2006], we attribute the decrease in the T2 to the recruitment of iron-labeled blood-born macrophages because passive diffusion of USPIOs (around 30 nm) across inflamed BBB fenestration (20 nm) [Rapoport 2000] can not be expected. However, it is still not clear whether the internalization of iron particles occurs exclusively in the blood by hematogenous macrophages or on inflamed lesions by microglial cells and brain-resident macrophages [Modo *et al.* 2005]. The main problem arises from the broad size-distribution of iron particles which can influence their physicochemical and pharmacokinetic properties [Wang *et al.* 2001]. For instance, although manufacturers indicate a size of 20-40 nm for SINEREM particles, we measured an average size of 31 nm with values ranging from less than 10 nm up to 75 nm. As the rate of internalization by macrophages is determined by

particle size [Rogers and Basu 2005], size discrepancies of USPIOs may not only lead to labeling of macrophages but also to penetrate brain parenchyma (i.e. particle smaller than 20 nm passing through the impaired BBB). In this context, further kinetic uptake measurements of iron particles by phagocytic leukocytes and an estimation of free iron particles entering brain parenchyma should be analyzed.

A new kind of contrast agents for MR investigation are dendrimers [Kobayashi and Brechbiel 2004]. As these macromolecules complexes are polymeric compounds synthesized through a sequence of iterative reactions, it is possible to control their size, shape and surface chemistry at the molecular level [Tomalia *et al.* 1990]. By coupling dendrimers with the adequate size to Gd ions, it should be possible to label macrophages for T1 imaging.

Strategies to improve the specificity of cell labeling for MR imaging have been investigated. An other way to target contrast agent to inflammation zones is to couple them with molecules specific for immune activity. The expression of adhesion proteins such as selectin [Bernardes-Silva *et al.* 2001] or apoptosis marker like annexin-V [Kietselaer *et al.* 2003] are characteristic for ongoing inflammation processes. Experiments, carried out recently, relate the possibility to synthesize and characterize new generation of Gd-chelates contrast agents coupled to the sialyl Lewis X molecule, which bind to E-selectin [Laurent *et al.* 2004]. Dendrimers which present multiple terminal reactive groups on the exterior of the molecule [Venditto *et al.* 2005] are also potential macromolecular contrast agents that can be associated to inflammation markers.

An other challenge in the molecular imaging field is to label non-phagocytotic cells. Due to their high therapeutic implications, stem cells have been studied extensively for *in vivo* tracking [Hoehn *et al.* 2002] by labeling them using magnetodendrimers [Bulte *et al.* 2001] or iron oxide particles combined with commonly available transfection agents [Frank *et al.* 2003]. The results we have obtained in this thesis show that it is possible to translate this technique to T cells labeling for T2 MR imaging. Recent *in vivo* results have shown the possibility to monitor such cells in the spleen [Dodd *et al.* 2001], in tumors [Kircher *et al.* 2003], but also in the spinal cord [Anderson *et al.* 2004] and in the brain [Pirko *et al.* 2003] of neurodegenerative animal models. However, the MRI technique lacks sensitivity and i.v. injected labeled cells diluted in the blood circulation and redistribute mainly to the liver and the spleen [Schimmelpfennig *et al.* 2005] [Basse 1995]. To overcome these problems, contrast agents exhibiting a higher tissue discrimination potential (e.g. T1 paramagnetic CAs) [Rudelius *et al.* 2003] or bimodal imaging properties can be used to corroborate *in vivo*

visualization of cells by correlative histology [Huber *et al.* 1998] should be used to label T cells. The use of bimodal agents (MRI / fluorescence) has the further advantage of complementing the high spatial resolution of structural information given by MRI by a more sensitive detection using optical imaging technology [Modo, Hoehn, and Bulte, 2005]. A new promising technique in this regard is near infrared fluorescence imaging that exploits the narrow window in the 700-900 nm range which allows a very sensitive display of changes at the cellular level to depths of several millimeters [Wolbarst and Hendee 2006]. Results presented in the thesis confirmed the ability to monitor immune cells movement within the rat brain during acute inflammation.

However, despite the versatility of contrast agents, a large number of CA molecule are needed in each cell to allow a clear *in vivo* visualization. Heavily labeling cells can lead to CA induced cell toxicity and thus to the premature death of such labeled cells. Consequently, unspecific labeling of phagocytic cells such as macrophages may be inevitable as they will internalize fragments from dead CA labeled cells.

References

- Abbott NJ. Astrocyte-endothelial interactions and blood-brain barrier permeability. *J.Anat.* 2002; 200: 629-638.
- Abbott NJ, Chugani DC, Zaharchuk G, Rosen BR, Lo EH. Delivery of imaging agents into brain. *Adv.Drug Deliv.Rev.* 1999; 37: 253-277.
- Aboul-Enein F, Rauschka H, Kornek B *et al.* Preferential loss of myelin-associated glycoprotein reflects hypoxia-like white matter damage in stroke and inflammatory brain diseases. *J.Neuropathol.Exp.Neurol.* 2003; 62: 25-33.
- Adonai N, Nguyen KN, Walsh J *et al.* Ex vivo cell labeling with ⁶⁴Cu-pyruvaldehyde-bis(N4-methylthiosemicarbazone) for imaging cell trafficking in mice with positron-emission tomography. *Proc.Natl.Acad.Sci.U.S.A.* 2002; 99: 3030-3035.
- Allen IV, Glover G, Anderson R. Abnormalities in the macroscopically normal white matter in cases of mild or spinal multiple sclerosis (MS). *Acta Neuropathol.Suppl (Berl)* 1981; 7:176-8.: 176-178.
- Allport JR, Weissleder R. In vivo imaging of gene and cell therapies. *Exp.Hematol.* 2001; 29: 1237-1246.
- Anderson SA, Shukaliak-Quandt J, Jordan EK *et al.* Magnetic resonance imaging of labeled T-cells in a mouse model of multiple sclerosis. *Ann.Neurol.* 2004; 55: 654-659.
- Arbab AS, Bashaw LA, Miller BR, Jordan EK, Bulte JW, Frank JA. Intracytoplasmic tagging of cells with ferumoxides and transfection agent for cellular magnetic resonance imaging after cell transplantation: methods and techniques. *Transplantation* 2003a; 76: 1123-1130.
- Arbab AS, Bashaw LA, Miller BR *et al.* Characterization of biophysical and metabolic properties of cells labeled with superparamagnetic iron oxide nanoparticles and transfection agent for cellular MR imaging. *Radiology* 2003b; 229: 838-846.
- Arbab AS, Yocum GT, Wilson LB *et al.* Comparison of transfection agents in forming complexes with ferumoxides, cell labeling efficiency, and cellular viability. *Mol.Imaging* 2004a; 3: 24-32.
- Arbab AS, Yocum GT, Wilson LB *et al.* Comparison of transfection agents in forming complexes with ferumoxides, cell labeling efficiency, and cellular viability. *Mol.Imaging* 2004b; 3: 24-32.
- Babbe H, Roers A, Waisman A *et al.* Clonal expansions of CD8(+) T cells dominate the T cell infiltrate in active multiple sclerosis lesions as shown by micromanipulation and single cell polymerase chain reaction. *J.Exp.Med.* 2000; 192: 393-404.
- Bach-Gansmo T. Ferrimagnetic susceptibility contrast agents. *Acta Radiol.Suppl* 1993; 387:1-30.: 1-30.
- Baggiolini M, Dahinden CA. CC chemokines in allergic inflammation. *Immunol.Today* 1994; 15: 127-133.
- Balaban RS, Ceckler TL. Magnetization transfer contrast in magnetic resonance imaging. *Magn Reson.Q.* 1992; 8: 116-137.
- Ballabh P, Braun A, Nedergaard M. The blood-brain barrier: an overview: structure, regulation, and clinical implications. *Neurobiol.Dis.* 2004; 16: 1-13.
- Barkhof F, van Walderveen M. Characterization of tissue damage in multiple sclerosis by nuclear magnetic resonance. *Philos.Trans.R.Soc.Lond B Biol.Sci.* 1999; 354: 1675-1686.
- Barnett MH, Prineas JW. Relapsing and remitting multiple sclerosis: pathology of the newly forming lesion. *Ann.Neurol.* 2004; 55: 458-468.

- Basse PH. Tissue distribution and tumor localization of effector cells in adoptive immunotherapy of cancer. *APMIS Suppl.* 1995; 55:1-28.: 1-28.
- Bauer J, Bradl M, Hickley WF *et al.* T-cell apoptosis in inflammatory brain lesions: destruction of T cells does not depend on antigen recognition. *Am.J.Pathol.* 1998; 153: 715-724.
- Bauer J, Sminia T, Wouterlood FG, Dijkstra CD. Phagocytic activity of macrophages and microglial cells during the course of acute and chronic relapsing experimental autoimmune encephalomyelitis. *J.Neurosci.Res.* 1994; 38: 365-375.
- Bauer J, Wekerle H, Lassmann H. Apoptosis in brain-specific autoimmune disease. *Curr.Opin.Immunol.* 1995; 7: 839-843.
- Becker A, Hassenius C, Bhargava S *et al.* Cyanine dye labeled vasoactive intestinal peptide and somatostatin analog for optical detection of gastroenteropancreatic tumors. *Ann.N.Y.Acad.Sci.* 2000; 921:275-8.: 275-278.
- Becker A, Hassenius C, Licha K *et al.* Receptor-targeted optical imaging of tumors with near-infrared fluorescent ligands. *Nat.Biotechnol.* 2001; 19: 327-331.
- Ben Nun A, Wekerle H, Cohen IR. Vaccination against autoimmune encephalomyelitis with T-lymphocyte line cells reactive against myelin basic protein. *Nature.* 1981; 292: 60-61.
- Benveniste EN. Role of macrophages/microglia in multiple sclerosis and experimental allergic encephalomyelitis. *J.Mol.Med.* 1997; 75: 165-173.
- Berg D, Supprian T, Thomae J *et al.* Lesion pattern in patients with multiple sclerosis and depression. *Mult.Scler.* 2000; 6: 156-162.
- Berger C, Hiestand P, Kindler-Baumann D, Rudin M, Rausch M. Analysis of lesion development during acute inflammation and remission in a rat model of experimental autoimmune encephalomyelitis by visualization of macrophage infiltration, demyelination and blood-brain barrier damage. *NMR Biomed.* 2006.
- Bernardes-Silva M, Anthony DC, Issekutz AC, Perry VH. Recruitment of neutrophils across the blood-brain barrier: the role of E- and P-selectins. *J.Cereb.Blood Flow Metab* 2001; 21: 1115-1124.
- Bevilacqua MP. Endothelial-leukocyte adhesion molecules. *Annu.Rev.Immunol.* 1993; 11:767-804.: 767-804.
- Bignami A, Eng LF, Dahl D, Uyeda CT. Localization of the glial fibrillary acidic protein in astrocytes by immunofluorescence. *Brain Res.* 1972; 43: 429-435.
- Billinghurst LL, Taylor RM, Snyder EY. Remyelination: cellular and gene therapy. *Semin.Pediatr.Neurol.* 1998; 5: 211-228.
- Bitsch A, Schuchardt J, Bunkowski S, Kuhlmann T, Bruck W. Acute axonal injury in multiple sclerosis. Correlation with demyelination and inflammation. *Brain* 2000; 123: 1174-1183.
- Bloembergen N, Purcell EM, and Pound RV. Relaxation effects in nuclear magnetic resonance absorption. *Physical Review* 73, 679-710. 1948.
Ref Type: Magazine Article
- Brinkmann V, Davis MD, Heise CE *et al.* The immune modulator FTY720 targets sphingosine 1-phosphate receptors. *J.Biol.Chem.* 2002; 277: 21453-21457.
- Brinkmann V, Pinschewer DD, Feng L, Chen S. FTY720: altered lymphocyte traffic results in allograft protection. *Transplantation.* 2001; 72: 764-769.
- Bruck W, Bitsch A, Kolenda H, Bruck Y, Stiefel M, Lassmann H. Inflammatory central nervous system demyelination: correlation of magnetic resonance imaging findings with lesion pathology. *Ann.Neurol.* 1997; 42: 783-793.

- Bruck W, Stadelmann C. Inflammation and degeneration in multiple sclerosis. *Neurol.Sci.* 2003; 24 Suppl 5:S265-7.: S265-S267.
- Bulte JW, Douglas T, Witwer B *et al.* Magnetodendrimers allow endosomal magnetic labeling and in vivo tracking of stem cells. *Nat.Biotechnol.* 2001; 19: 1141-1147.
- Bulte JW, Douglas T, Witwer B *et al.* Monitoring stem cell therapy in vivo using magnetodendrimers as a new class of cellular MR contrast agents. *Acad.Radiol.* 2002; 9 Suppl 2:S332-5.: S332-S335.
- Bulte JW, Kraitchman DL. Iron oxide MR contrast agents for molecular and cellular imaging. *NMR Biomed.* 2004; 17: 484-499.
- Bulte JW, Laughlin PG, Jordan EK, Tran VA, Vymazal J, Frank JA. Tagging of T cells with superparamagnetic iron oxide: uptake kinetics and relaxometry. *Acad.Radiol.* 1996; 3 Suppl 2:S301-3.: S301-S303.
- Bulte JW, Vymazal J, Brooks RA, Pierpaoli C, Frank JA. Frequency dependence of MR relaxation times. II. Iron oxides. *J.Magn Reson.Imaging* 1993; 3: 641-648.
- Bulte JW, Zhang S, van Gelderen P *et al.* Neurotransplantation of magnetically labeled oligodendrocyte progenitors: magnetic resonance tracking of cell migration and myelination. *Proc.Natl.Acad.Sci.U.S.A* 1999; 96: 15256-15261.
- Calopa M, Bas J, Mestre M, Arbizu T, Peres J, Buendia E. T cell subsets in multiple sclerosis: a serial study. *Acta Neurol.Scand.* 1995; 92: 361-368.
- Caravan P, Ellison JJ, McMurry TJ, Lauffer RB. Gadolinium(III) Chelates as MRI Contrast Agents: Structure, Dynamics, and Applications. *Chem.Rev.* 1999; 99: 2293-2352.
- Carrithers MD, Visintin I, Kang SJ, Janeway CA, Jr. Differential adhesion molecule requirements for immune surveillance and inflammatory recruitment. *Brain.* 2000; 123: 1092-1101.
- Chun M, Krim M, Granelli-Piperno A, Hirst JA, Hoffmann MK. Enhancement of cytotoxic activity of natural killer cells by interleukin 2, and antagonism between interleukin 2 and adenosine cyclic monophosphate. *Scand.J.Immunol.* 1985; 22: 375-381.
- Clark JF, Harris GI, Dillon PF. Multisite saturation transfer using DANTE and continuous wave. *Magn Reson.Med.* 1991; 17: 274-278.
- De Simone R, Ajmone-Cat MA, Tirassa P, Minghetti L. Apoptotic PC12 cells exposing phosphatidylserine promote the production of anti-inflammatory and neuroprotective molecules by microglial cells. *J.Neuropathol.Exp.Neurol.* 2003; 62: 208-216.
- Dodd CH, Hsu HC, Chu WJ *et al.* Normal T-cell response and in vivo magnetic resonance imaging of T cells loaded with HIV transactivator-peptide-derived superparamagnetic nanoparticles. *J.Immunol.Methods* 2001; 256: 89-105.
- Dodd SJ, Williams M, Suhan JP, Williams DS, Koretsky AP, Ho C. Detection of single mammalian cells by high-resolution magnetic resonance imaging. *Biophys.J.* 1999; 76: 103-109.
- Dousset V, Ballarino L, Delalande C *et al.* Comparison of ultrasmall particles of iron oxide (USPIO)-enhanced T2-weighted, conventional T2-weighted, and gadolinium-enhanced T1-weighted MR images in rats with experimental autoimmune encephalomyelitis. *AJNR Am.J.Neuroradiol.* 1999a; 20: 223-227.
- Dousset V, Delalande C, Ballarino L *et al.* In vivo macrophage activity imaging in the central nervous system detected by magnetic resonance. *Magn Reson.Med.* 1999b; 41: 329-333.
- Dousset V, Gomez C, Petry KG, Delalande C, Caille JM. Dose and scanning delay using USPIO for central nervous system macrophage imaging. *MAGMA.* 1999c; 8: 185-189.

- Dousset V, Grossman RI, Ramer KN *et al.* Experimental allergic encephalomyelitis and multiple sclerosis: lesion characterization with magnetization transfer imaging. *Radiology*. 1992; 182: 483-491.
- Doyle TC, Burns SM, Contag CH. In vivo bioluminescence imaging for integrated studies of infection. *Cell Microbiol*. 2004; 6: 303-317.
- Edinger M, Hoffmann P, Contag CH, Negrin RS. Evaluation of effector cell fate and function by in vivo bioluminescence imaging. *Methods*. 2003; 31: 172-179.
- Emerit J, Beaumont C, Trivin F. Iron metabolism, free radicals, and oxidative injury. *Biomed.Pharmacother*. 2001; 55: 333-339.
- Ensoli B, Buonaguro L, Barillari G *et al.* Release, uptake, and effects of extracellular human immunodeficiency virus type 1 Tat protein on cell growth and viral transactivation. *J.Virol*. 1993; 67: 277-287.
- Esiri MM. Immunoglobulin-containing cells in multiple-sclerosis plaques. *Lancet* 1977; 2: 478.
- Esiri MM. Multiple sclerosis: a quantitative and qualitative study of immunoglobulin-containing cells in the central nervous system. *Neuropathol.Appl.Neurobiol*. 1980; 6: 9-21.
- Fadok VA, Bratton DL, Konowal A, Freed PW, Westcott JY, Henson PM. Macrophages that have ingested apoptotic cells in vitro inhibit proinflammatory cytokine production through autocrine/paracrine mechanisms involving TGF-beta, PGE2, and PAF. *J.Clin.Invest* 1998; 101: 890-898.
- Fawell S, Seery J, Daikh Y *et al.* Tat-mediated delivery of heterologous proteins into cells. *Proc.Natl.Acad.Sci.U.S.A* 1994; 91: 664-668.
- Ferrucci JT, Stark DD. Iron oxide-enhanced MR imaging of the liver and spleen: review of the first 5 years. *AJR Am.J.Roentgenol*. 1990; 155: 943-950.
- Feurer C, Prentice DE, Cammisuli S. Chronic relapsing experimental allergic encephalomyelitis in the Lewis rat. *J.Neuroimmunol*. 1985; 10: 159-166.
- Floris S, Blezer EL, Schreiber G *et al.* Blood-brain barrier permeability and monocyte infiltration in experimental allergic encephalomyelitis: a quantitative MRI study. *Brain* 2004; 127: 616-627.
- Frangioni JV. In vivo near-infrared fluorescence imaging. *Curr.Opin.Chem.Biol*. 2003; 7: 626-634.
- Frank JA, Miller BR, Arbab AS *et al.* Clinically applicable labeling of mammalian and stem cells by combining superparamagnetic iron oxides and transfection agents. *Radiology* 2003; 228: 480-487.
- Frank JA, Zywicke H, Jordan EK *et al.* Magnetic intracellular labeling of mammalian cells by combining (FDA-approved) superparamagnetic iron oxide MR contrast agents and commonly used transfection agents. *Acad.Radiol*. 2002; 9 Suppl 2:S484-7.: S484-S487.
- Fregeau CJ, Bleackley RC. Factors influencing transient expression in cytotoxic T cells following DEAE dextran-mediated gene transfer. *Somat.Cell Mol.Genet*. 1991; 17: 239-257.
- Fujino M, Funeshima N, Kitazawa Y *et al.* Amelioration of experimental autoimmune encephalomyelitis in Lewis rats by FTY720 treatment. *J.Pharmacol.Exp.Ther*. 2003; 305: 70-77.
- Gay D, Esiri M. Blood-brain barrier damage in acute multiple sclerosis plaques. An immunocytological study. *Brain* 1991; 114: 557-572.
- Gay FW, Drye TJ, Dick GW, Esiri MM. The application of multifactorial cluster analysis in the staging of plaques in early multiple sclerosis. Identification and characterization of the primary demyelinating lesion. *Brain* 1997; 120: 1461-1483.

- Gehrmann J, Gold R, Lington C, Lannes-Vieira J, Wekerle H, Kreutzberg GW. Microglial involvement in experimental autoimmune inflammation of the central and peripheral nervous system. *Glia* 1993; 7: 50-59.
- Gehrmann J, Matsumoto Y, Kreutzberg GW. Microglia: intrinsic immune effector cell of the brain. *Brain Res. Brain Res. Rev.* 1995; 20: 269-287.
- Gibby WA. MR contrast agents: an overview. *Radiol. Clin. North Am.* 1988; 26: 1047-1058.
- Gloor SM, Wachtel M, Bolliger MF, Ishihara H, Landmann R, Frei K. Molecular and cellular permeability control at the blood-brain barrier. *Brain Res. Brain Res. Rev.* 2001; 36: 258-264.
- Gold R., Hartung H-P, and Toyka K.V. Animal models for autoimmune demyelinating disorders of the nervous system. *Molecular medicine today* 6(2), 88-91. 2000.
Ref Type: Magazine Article
- Gold R, Hartung HP, Lassmann H. T-cell apoptosis in autoimmune diseases: termination of inflammation in the nervous system and other sites with specialized immune-defense mechanisms. *Trends Neurosci.* 1997; 20: 399-404.
- Goncalves E, Kitas E, Seelig J. Binding of oligoarginine to membrane lipids and heparan sulfate: structural and thermodynamic characterization of a cell-penetrating peptide. *Biochemistry* 2005; 44: 2692-2702.
- Goust JM, Chenais F, Carnes JE, Hames CG, Fudenberg HH, Hogan EL. Abnormal T cell subpopulations and circulating immune complexes in the Guillain-Barre syndrome and multiple sclerosis. *Neurology* 1978; 28: 421-425.
- Graham SJ, Henkelman RM. Understanding pulsed magnetization transfer. *J. Magn Reson. Imaging* 1997; 7: 903-912.
- Griot C, Vandeveld M, Richard A, Peterhans E, Stocker R. Selective degeneration of oligodendrocytes mediated by reactive oxygen species. *Free Radic. Res. Commun.* 1990; 11: 181-193.
- Groman et al. Biologically degradable superparamagnetic materials for use in clinical applications. (4,827,945). 1989.
Ref Type: Patent
- Gulick T. Transfection Using DEAE-Dextran. *Current Protocols in Cell Biology* 2003; 20.
- Gutteridge JM, Rowley DA, Halliwell B. Superoxide-dependent formation of hydroxyl radicals and lipid peroxidation in the presence of iron salts. Detection of 'catalytic' iron and anti-oxidant activity in extracellular fluids. *Biochem. J.* 1982; 206: 605-609.
- Haase A, Matthaei D. Biophysical and medical aspects of fast NMR-imaging. *Med. Prog. Technol.* 1987; 13: 57-67.
- Hartung HP, Rieckmann P. Pathogenesis of immune-mediated demyelination in the CNS. *J. Neural Transm. Suppl.* 1997; 50:173-81.: 173-181.
- Hauser SL, Bhan AK, Gilles F, Kemp M, Kerr C, Weiner HL. Immunohistochemical analysis of the cellular infiltrate in multiple sclerosis lesions. *Ann. Neurol.* 1986; 19: 578-587.
- Hauser SL, Bhan AK, Gilles FH *et al.* Immunohistochemical staining of human brain with monoclonal antibodies that identify lymphocytes, monocytes, and the Ia antigen. *J. Neuroimmunol.* 1983a; 5: 197-205.
- Hauser SL, Fosburg M, Kevy S, Weiner HL. Plasmapheresis, lymphocytapheresis, and immunosuppressive drug therapy in multiple sclerosis. *Prog. Clin. Biol. Res.* 1982; 106:239-54.: 239-254.

- Hauser SL, Reinherz EL, Hoban CJ, Schlossman SF, Weiner HL. Immunoregulatory T-cells and lymphocytotoxic antibodies in active multiple sclerosis: weekly analysis over a six-month period. *Ann.Neurol.* 1983b; 13: 418-425.
- Hellings N, Gelin G, Medaer R *et al.* Longitudinal study of antimyelin T-cell reactivity in relapsing-remitting multiple sclerosis: association with clinical and MRI activity. *J.Neuroimmunol.* 2002; 126: 143-160.
- Helmberger T, Semelka RC. New contrast agents for imaging the liver. *Magn Reson.Imaging Clin.N.Am.* 2001; 9: 745-66, vi.
- Hendrick RE, Haacke EM. Basic physics of MR contrast agents and maximization of image contrast. *J.Magn Reson.Imaging* 1993; 3: 137-148.
- Henkelman RM, Stanisz GJ, Graham SJ. Magnetization transfer in MRI: a review. *NMR Biomed.* 2001; 14: 57-64.
- Henson PM, Bratton DL, Fadok VA. The phosphatidylserine receptor: a crucial molecular switch? *Nat.Rev.Mol.Cell Biol.* 2001; 2: 627-633.
- Hickey WF. Migration of hematogenous cells through the blood-brain barrier and the initiation of CNS inflammation. *Brain Pathol.* 1991; 1: 97-105.
- Hickey WF, Hsu BL, Kimura H. T-lymphocyte entry into the central nervous system. *J.Neurosci.Res.* 1991; 28: 254-260.
- Hielscher AH, Bluestone AY, Abdoulaev GS *et al.* Near-infrared diffuse optical tomography. *Dis.Markers* 2002; 18: 313-337.
- Hinds KA, Hill JM, Shapiro EM *et al.* Highly efficient endosomal labeling of progenitor and stem cells with large magnetic particles allows magnetic resonance imaging of single cells. *Blood* 2003a; 102: 867-872.
- Hinds KA, Hill JM, Shapiro EM *et al.* Highly efficient endosomal labeling of progenitor and stem cells with large magnetic particles allows magnetic resonance imaging of single cells. *Blood* 2003b; 102: 867-872.
- Hintersteiner M, Enz A, Frey P *et al.* In vivo detection of amyloid-beta deposits by near-infrared imaging using an oxazine-derivative probe. *Nat.Biotechnol.* 2005; 23: 577-583.
- Hoehn M, Kustermann E, Blunk J *et al.* Monitoring of implanted stem cell migration in vivo: a highly resolved in vivo magnetic resonance imaging investigation of experimental stroke in rat. *Proc.Natl.Acad.Sci.U.S.A* 2002; 99: 16267-16272.
- Huber JD, Egleton RD, Davis TP. Molecular physiology and pathophysiology of tight junctions in the blood-brain barrier. *Trends Neurosci.* 2001; 24: 719-725.
- Huber MM, Staubli AB, Kustedjo K *et al.* Fluorescently detectable magnetic resonance imaging agents. *Bioconjug.Chem.* 1998; 9: 242-249.
- Huseby ES, Liggitt D, Brabb T, Schnabel B, Ohlen C, Goverman J. A pathogenic role for myelin-specific CD8(+) T cells in a model for multiple sclerosis. *J.Exp.Med.* 2001; 194: 669-676.
- Ishikawa M, Anzai Y. MR imaging of lymph nodes in the head and neck. *Magn Reson.Imaging Clin.N.Am.* 2002; 10: 527-542.
- Itoh K, Shiiba K, Shimizu Y, Suzuki R, Kumagai K. Generation of activated killer (AK) cells by recombinant interleukin 2 (rIL 2) in collaboration with interferon-gamma (IFN-gamma). *J.Immunol.* 1985; 134: 3124-3129.
- Izikson L, Klein RS, Charo IF, Weiner HL, Luster AD. Resistance to experimental autoimmune encephalomyelitis in mice lacking the CC chemokine receptor (CCR)2. *J.Exp.Med.* 2000; 192: 1075-1080.

- Josephson L, Tung CH, Moore A, Weissleder R. High-efficiency intracellular magnetic labeling with novel superparamagnetic-Tat peptide conjugates. *Bioconjug.Chem.* 1999; 10: 186-191.
- Julien J, Ferrer X. Multiple sclerosis: an overview. *Biomed.Pharmacother.* 1989; 43: 335-346.
- Kahan BD. FTY720: a new immunosuppressive agent with novel mechanism(s) of action. *Transplant.Proc.* 1998; 30: 2210-2213.
- Kalish H, Arbab AS, Miller BR *et al.* Combination of transfection agents and magnetic resonance contrast agents for cellular imaging: relationship between relaxivities, electrostatic forces, and chemical composition. *Magn Reson.Med.* 2003; 50: 275-282.
- Kam-Hansen S. Distribution and function of lymphocytes from the cerebrospinal fluid and blood in patients with multiple sclerosis. *Acta Neurol.Scand.Suppl* 1980; 75:1-81.: 1-81.
- Kanwar JR. Anti-inflammatory immunotherapy for multiple sclerosis/experimental autoimmune encephalomyelitis (EAE) disease. *Curr.Med.Chem.* 2005; 12: 2947-2962.
- Kappos L, Moeri D, Radue EW *et al.* Predictive value of gadolinium-enhanced magnetic resonance imaging for relapse rate and changes in disability or impairment in multiple sclerosis: a meta-analysis. *Gadolinium MRI Meta-analysis Group. Lancet* 1999; 353: 964-969.
- Katz D, Taubenberger JK, Cannella B, McFarlin DE, Raine CS, McFarland HF. Correlation between magnetic resonance imaging findings and lesion development in chronic, active multiple sclerosis. *Ann.Neurol.* 1993; 34: 661-669.
- Kerschensteiner M, Bareyre FM, Buddeberg BS *et al.* Remodeling of axonal connections contributes to recovery in an animal model of multiple sclerosis. *J.Exp.Med.* 2004a; 200: 1027-1038.
- Kerschensteiner M, Stadelmann C, Buddeberg BS *et al.* Targeting experimental autoimmune encephalomyelitis lesions to a predetermined axonal tract system allows for refined behavioral testing in an animal model of multiple sclerosis. *Am.J.Pathol.* 2004b; 164: 1455-1469.
- Kettman H., Ransom B. *Neuroglia.* New York: Oxford University Press, 1995.
- Kiefer R, Streit WJ, Toyka KV, Kreutzberg GW, Hartung HP. Transforming growth factor-beta 1: a lesion-associated cytokine of the nervous system. *Int.J.Dev.Neurosci.* 1995; 13: 331-339.
- Kietselaer BL, Hofstra L, Dumont EA, Reutelingsperger CP, Heidendal GA. The role of labeled Annexin A5 in imaging of programmed cell death. From animal to clinical imaging. *Q.J.Nucl.Med.* 2003; 47: 349-361.
- Kircher MF, Allport JR, Graves EE *et al.* In vivo high resolution three-dimensional imaging of antigen-specific cytotoxic T-lymphocyte trafficking to tumors. *Cancer Res.* 2003; 63: 6838-6846.
- Kirsch JE. Basic principles of magnetic resonance contrast agents. *Top.Magn Reson.Imaging* 1991; 3: 1-18.
- Kobayashi H, Brechbiel MW. Dendrimer-based nanosized MRI contrast agents. *Curr.Pharm.Biotechnol.* 2004; 5: 539-549.
- Kojima K, Wekerle H, Lassmann H, Berger T, Linington C. Induction of experimental autoimmune encephalomyelitis by CD4+ T cells specific for an astrocyte protein, S100 beta. *J.Neurol Transm.Suppl.* 1997; 49:43-51.: 43-51.
- Kucharczyk J, Asgari H, Mintorovitch J *et al.* Magnetic resonance imaging of brain perfusion using the nonionic contrast agents Dy-DTPA-BMA and Gd-DTPA-BMA. *Invest Radiol.* 1991; 26 Suppl 1:S250-2; discussion S253-4.: S250-S252.

- Lafaille JJ, Keere FV, Hsu AL *et al.* Myelin basic protein-specific T helper 2 (Th2) cells cause experimental autoimmune encephalomyelitis in immunodeficient hosts rather than protect them from the disease. *J.Exp.Med.* 1997; 186: 307-312.
- Laurent S, Vander EL, Fu Y, Muller RN. Synthesis and physicochemical characterization of Gd-DTPA-B(sLex)A, a new MRI contrast agent targeted to inflammation. *Bioconjug.Chem.* 2004; 15: 99-103.
- Lassmann H. Basic mechanisms of brain inflammation. *J.Neural Transm.Suppl* 1997; 50:183-90.: 183-190.
- Lassmann H, Bruck W, Lucchinetti C, Rodriguez M. Remyelination in multiple sclerosis. *Mult.Scler.* 1997; 3: 133-136.
- Lassmann H, Rossler K, Zimprich F, Vass K. Expression of adhesion molecules and histocompatibility antigens at the blood-brain barrier. *Brain Pathol.* 1991; 1: 115-123.
- Lassmann H, Vass K, Brunner C, Wisniewski HM. Peripheral nervous system lesions in experimental allergic encephalomyelitis. Ultrastructural distribution of T cells and Ia-antigen. *Acta Neuropathol.(Berl)* 1986; 69: 193-204.
- Laufer RB. Magnetic resonance contrast media: principles and progress. *Magn Reson.Q.* 1990; 6: 65-84.
- Laurent S, Vander EL, Fu Y, Muller RN. Synthesis and physicochemical characterization of Gd-DTPA-B(sLex)A, a new MRI contrast agent targeted to inflammation. *Bioconjug.Chem.* 2004; 15: 99-103.
- Lewin M, Carlesso N, Tung CH *et al.* Tat peptide-derivatized magnetic nanoparticles allow in vivo tracking and recovery of progenitor cells. *Nat.Biotechnol.* 2000; 18: 410-414.
- Lin JX, Leonard WJ. Signaling from the IL-2 receptor to the nucleus. *Cytokine Growth Factor Rev.* 1997; 8: 313-332.
- Lin Y, Weissleder R, Tung CH. Synthesis and properties of sulfhydryl-reactive near-infrared cyanine fluorochromes for fluorescence imaging. *Mol.Imaging.* 2003; 2: 87-92.
- Linington C, Berger T, Perry L *et al.* T cells specific for the myelin oligodendrocyte glycoprotein mediate an unusual autoimmune inflammatory response in the central nervous system. *Eur.J.Immunol.* 1993; 23: 1364-1372.
- Luckey T.D., Venugopal B. Metal toxicity in mammals: chemical toxicity of metals and metalloids. New York: Plenum Press, 1977.
- MacKay A, Whittall K, Adler J, Li D, Paty D, Graeb D. In vivo visualization of myelin water in brain by magnetic resonance. *Magn Reson.Med.* 1994; 31: 673-677.
- Mahmood U, Tung CH, Bogdanov A, Jr., Weissleder R. Near-infrared optical imaging of protease activity for tumor detection. *Radiology.* 1999; 213: 866-870.
- Mahmood U, Tung CH, Tang Y, Weissleder R. Feasibility of in vivo multichannel optical imaging of gene expression: experimental study in mice. *Radiology.* 2002; 224: 446-451.
- Mandler RN. Dysfunction of the blood brain barrier in the pathogenesis of multiple sclerosis. Proceeding of a 2001 Chicago international Conference 2002; Sero Symposia International.
- Mann DA, Frankel AD. Endocytosis and targeting of exogenous HIV-1 Tat protein. *EMBO J.* 1991; 10: 1733-1739.
- Matuszewski L, Persigehl T, Wall A *et al.* Cell tagging with clinically approved iron oxides: feasibility and effect of lipofection, particle size, and surface coating on labeling efficiency. *Radiology* 2005; 235: 155-161.
- Mayhan WG. Regulation of blood-brain barrier permeability. *Microcirculation.* 2001; 8: 89-104.

- Mayhan WG, Heistad DD. Permeability of blood-brain barrier to various sized molecules. *Am.J.Physiol* 1985; 248: H712-H718.
- McCord JM. Iron, free radicals, and oxidative injury. *Semin.Hematol.* 1998; 35: 5-12.
- Meeson AP, Piddlesden S, Morgan BP, Reynolds R. The distribution of inflammatory demyelinated lesions in the central nervous system of rats with antibody-augmented demyelinating experimental allergic encephalomyelitis. *Exp.Neurol.* 1994; 129: 299-310.
- Mempel TR, Scimone ML, Mora JR, von Andrian UH. In vivo imaging of leukocyte trafficking in blood vessels and tissues. *Curr.Opin.Immunol.* 2004; 16: 406-417.
- Mendonca-Dias MH, Gaggelli E, Lauterbur PC. Paramagnetic contrast agents in nuclear magnetic resonance medical imaging. *Semin.Nucl.Med.* 1983; 13: 364-376.
- Miller A. Diagnosis of multiple sclerosis. *Semin.Neurol.* 1998; 18: 309-316.
- Miller DH, Grossman RI, Reingold SC, McFarland HF. The role of magnetic resonance techniques in understanding and managing multiple sclerosis. *Brain.* 1998; 121: 3-24.
- Minagar A, Shapshak P, Fujimura R, Ownby R, Heyes M, Eisdorfer C. The role of macrophage/microglia and astrocytes in the pathogenesis of three neurologic disorders: HIV-associated dementia, Alzheimer disease, and multiple sclerosis. *J.Neurol.Sci.* 2002; 202: 13-23.
- Modo M, Hoehn M, Bulte JW. Cellular MR imaging. *Mol.Imaging.* 2005; 4: 143-164.
- Morrissey SP, Stodal H, Zettl U *et al.* In vivo MRI and its histological correlates in acute adoptive transfer experimental allergic encephalomyelitis. Quantification of inflammation and oedema. *Brain* 1996; 119: 239-248.
- Nelson BH, Willerford DM. Biology of the interleukin-2 receptor. *Adv.Immunol.* 1998; 70:1-81.: 1-81.
- Neumann H, Medana IM, Bauer J, Lassmann H. Cytotoxic T lymphocytes in autoimmune and degenerative CNS diseases. *Trends Neurosci.* 2002; 25: 313-319.
- Nguyen KB, Pender MP. Phagocytosis of apoptotic lymphocytes by oligodendrocytes in experimental autoimmune encephalomyelitis. *Acta Neuropathol.(Berl).* 1998; 95: 40-46.
- Nicholas AR, Jones MN. The absorption of phospholipid vesicles by perfused rat liver depends on vesicle surface charge. *Biochim.Biophys.Acta* 1986; 860: 600-607.
- Nicolle GM, Toth E, Schmitt-Willich H, Raduchel B, Merbach AE. The impact of rigidity and water exchange on the relaxivity of a dendritic MRI contrast agent. *Chemistry.* 2002; 8: 1040-1048.
- Ntziachristos V, Bremer C, Weissleder R. Fluorescence imaging with near-infrared light: new technological advances that enable in vivo molecular imaging. *Eur.Radiol.* 2003; 13: 195-208.
- Nyland H, Mork S, Matre R. In-situ characterization of mononuclear cell infiltrates in lesions of multiple sclerosis. *Neuropathol.Appl.Neurobiol.* 1982; 8: 403-411.
- Oksendal AN, Hals PA. Biodistribution and toxicity of MR imaging contrast media. *J.Magn Reson.Imaging* 1993; 3: 157-165.
- Okuhata Y. Delivery of diagnostic agents for magnetic resonance imaging. *Adv.Drug Deliv.Rev.* 1999; 37: 121-137.
- Ordidge RJ, Helpern JA, Knight RA, Qing ZX, Welch KM. Investigation of cerebral ischemia using magnetization transfer contrast (MTC) MR imaging. *Magn Reson.Imaging* 1991; 9: 895-902.
- Ostergaard L. Cerebral perfusion imaging by bolus tracking. *Top.Magn Reson.Imaging* 2004; 15: 3-9.

- Pender MP, Rist MJ. Apoptosis of inflammatory cells in immune control of the nervous system: role of glia. *Glia* 2001; 36: 137-144.
- Perry VH, Anthony DC, Bolton SJ, Brown HC. The blood-brain barrier and the inflammatory response. *Mol.Med.Today* 1997; 3: 335-341.
- Peters W, Ernst JD. Mechanisms of cell recruitment in the immune response to *Mycobacterium tuberculosis*. *Microbes.Infect.* 2003; 5: 151-158.
- Petrovsky A, Schellenberger E, Josephson L, Weissleder R, Bogdanov A, Jr. Near-infrared fluorescent imaging of tumor apoptosis. *Cancer Res.* 2003; 63: 1936-1942.
- Pirko I, Ciric B, Johnson AJ, Gamez J, Rodriguez M, Macura S. Magnetic resonance imaging of immune cells in inflammation of central nervous system. *Croat.Med.J.* 2003; 44: 463-468.
- Pochon S, Hyacinthe R, Terrettaz J, Robert F, Schneider M, Tourmier H. Long circulating superparamagnetic particles with high T2 relaxivity. *Acta Radiol.Suppl* 1997; 412:69-72.: 69-72.
- Prineas J. Pathology of the early lesion in multiple sclerosis. *Hum.Pathol.* 1975; 6: 531-554.
- Prineas JW, Connell F. The fine structure of chronically active multiple sclerosis plaques. *Neurology* 1978; 28: 68-75.
- Prineas JW, Wright RG. Macrophages, lymphocytes, and plasma cells in the perivascular compartment in chronic multiple sclerosis. *Lab Invest* 1978; 38: 409-421.
- Raine CS, Cannella B, Duijvestijn AM, Cross AH. Homing to central nervous system vasculature by antigen-specific lymphocytes. II. Lymphocyte/endothelial cell adhesion during the initial stages of autoimmune demyelination. *Lab Invest.* 1990; 63: 476-489.
- Raine CS, Traugott U. Experimental autoimmune demyelination. Chronic relapsing models and their therapeutic implications for multiple sclerosis. *Ann.N.Y.Acad.Sci.* 1984; 436:33-51.: 33-51.
- Raine CS, Wu E. Multiple sclerosis: remyelination in acute lesions. *J.Neuropathol.Exp.Neurol.* 1993; 52: 199-204.
- Raivich G, Banati R. Brain microglia and blood-derived macrophages: molecular profiles and functional roles in multiple sclerosis and animal models of autoimmune demyelinating disease. *Brain Res.Brain Res.Rev.* 2004; 46: 261-281.
- Ramón y Cajal S. *Histology of the Nervous System*. New York: Oxford University Press, 1995.
- Randall B.Lauffer. Paramagnetic metal complexes as water proton relaxation agents for NMR imaging: theory and design. *Chem.rev.* 901-927. 1987.
Ref Type: Report
- Ransom BR. Vertebrate glial classification, lineage, and heterogeneity. *Ann.N.Y.Acad.Sci.* 1991; 633:19-26.: 19-26.
- Rapoport SI. Osmotic opening of the blood-brain barrier: principles, mechanism, and therapeutic applications. *Cell Mol.Neurobiol.* 2000; 20: 217-230.
- Rausch M, Baumann D, Neubacher U, Rudin M. In-vivo visualization of phagocytotic cells in rat brains after transient ischemia by USPIO. *NMR Biomed.* 2002a; 15: 278-283.
- Rausch M, Baumann D, Wiessner C, Rudin M. Measurement of USPIO Accumulation, Vascular Permeability and Cerebral Blood Volume after Unilateral Permanent Middle Cerebral Artery Occlusion (pMCAO) in rats. *Molecular Imaging* 2002b; 97-103.

- Rausch M, Hiestand P, Baumann D, Cannet C, Rudin M. MRI-based monitoring of inflammation and tissue damage in acute and chronic relapsing EAE. *Magn Reson.Med.* 2003; 50: 309-314.
- Rausch M, Hiestand P, Foster CA, Baumann DR, Cannet C, Rudin M. Predictability of FTY720 efficacy in experimental autoimmune encephalomyelitis by in vivo macrophage tracking: clinical implications for ultrasmall superparamagnetic iron oxide-enhanced magnetic resonance imaging. *J.Magn Reson.Imaging* 2004; 20: 16-24.
- Rausch M, Sauter A, Frohlich J, Neubacher U, Radu EW, Rudin M. Dynamic patterns of USPIO enhancement can be observed in macrophages after ischemic brain damage. *Magn Reson.Med.* 2001; 46: 1018-1022.
- Reynolds R., Cenci, di Bello, I, Meeson I., and Piddlesden S. Comparison of a chemically mediated and an immunologically mediated demyelinating lesion model. 1996.
Ref Type: Patent
- Robinson PJ. Facilitation of drug entry into brain by osmotic opening of the blood-brain barrier. *Clin.Exp.Pharmacol.Physiol* 1987; 14: 887-901.
- Roitt I., Brostoff J., Male D. *Immunology.* Mosby, 2005.
- Rogers WJ, Basu P. Factors regulating macrophage endocytosis of nanoparticles: implications for targeted magnetic resonance plaque imaging. *Atherosclerosis.* 2005; 178: 67-73.
- Rovaris M, Filippi M, Falautano M *et al.* Relation between MR abnormalities and patterns of cognitive impairment in multiple sclerosis. *Neurology* 1998; 50: 1601-1608.
- Rudelius M, Daldrup-Link HE, Heinzmann U *et al.* Highly efficient paramagnetic labelling of embryonic and neuronal stem cells. *Eur.J.Nucl.Med.Mol.Imaging.* 2003; 30: 1038-1044.
- Rudin M, Sauter A. Measurement of reaction rates in vivo using magnetization transfer techniques. In: Springer, editor. *In vivo magnetic resonance spectroscopy II: Localization and spectral editing.* Heidelberg: 1992: 239-48.
- Rusinek H, Kaur M, Lee VS. Renal magnetic resonance imaging. *Curr.Opin.Nephrol.Hypertens.* 2004; 13: 667-673.
- Schimmelpfennig CH, Schulz S, Arber C *et al.* Ex vivo expanded dendritic cells home to T-cell zones of lymphoid organs and survive in vivo after allogeneic bone marrow transplantation. *Am.J.Pathol.* 2005; 167: 1321-1331.
- Schluesener HJ, Meyermann R. Intercines in brain pathology. Expression of intercrines in a multiple sclerosis and Morbus Creutzfeldt-Jakob lesion. *Acta Neuropathol.(Berl)* 1993; 86: 393-396.
- Schmied M, Breitschopf H, Gold R *et al.* Apoptosis of T lymphocytes in experimental autoimmune encephalomyelitis. Evidence for programmed cell death as a mechanism to control inflammation in the brain. *Am.J.Pathol.* 1993; 143: 446-452.
- Schoepf U, Marecos EM, Melder RJ, Jain RK, Weissleder R. Intracellular magnetic labeling of lymphocytes for in vivo trafficking studies. *Biotechniques* 1998b; 24: 642-651.
- Schoepf U, Marecos EM, Melder RJ, Jain RK, Weissleder R. Intracellular magnetic labeling of lymphocytes for in vivo trafficking studies. *Biotechniques* 1998a; 24: 642-651.
- Schwendener RA, Lagocki PA, Rahman YE. The effects of charge and size on the interaction of unilamellar liposomes with macrophages. *Biochim.Biophys.Acta* 1984; 772: 93-101.
- Scolding NJ, Morgan BP, Campbell AK, Compston DA. Complement mediated serum cytotoxicity against oligodendrocytes: a comparison with other cells of the oligodendrocyte-type 2 astrocyte lineage. *J.Neurol.Sci.* 1990; 97: 155-162.

- Selmaj KW, Raine CS. Tumor necrosis factor mediates myelin and oligodendrocyte damage in vitro. *Ann.Neurol.* 1988; 23: 339-346.
- Sevick-Muraca EM, Houston JP, Gurfinkel M. Fluorescence-enhanced, near infrared diagnostic imaging with contrast agents. *Curr.Opin.Chem.Biol.* 2002; 6: 642-650.
- Shah GV, Fischbein NJ, Patel R, Mukherji SK. Newer MR imaging techniques for head and neck. *Magn Reson.Imaging Clin.N.Am.* 2003; 11: 449-69, vi.
- Shahbazi-Gahrouei D, Williams M, Rizvi S, Allen BJ. In vivo studies of Gd-DTPA-monoclonal antibody and gd-porphyrins: potential magnetic resonance imaging contrast agents for melanoma. *J.Magn Reson.Imaging* 2001; 14: 169-174.
- Sobel RA, Mitchell ME, Fondren G. Intercellular adhesion molecule-1 (ICAM-1) in cellular immune reactions in the human central nervous system. *Am.J.Pathol.* 1990; 136: 1309-1316.
- Sobol WT. Magnetic resonance contrast agents. Physical basis of relaxation. *Neuroimaging Clin.N.Am.* 1994; 4: 27-42.
- Solomon I. Relaxation processes in a system of two spins. *Physical Review* 99, 559-568. 1955.
Ref Type: Magazine Article
- Springer TA. Traffic signals for lymphocyte recirculation and leukocyte emigration: the multistep paradigm. *Cell* 1994; 76: 301-314.
- Steinman L. Multiple sclerosis: a coordinated immunological attack against myelin in the central nervous system. *Cell* 1996; 85: 299-302.
- Steinman L. Assessment of animal models for MS and demyelinating disease in the design of rational therapy. *Neuron* 1999; 24: 511-514.
- Steinman L. Myelin-specific CD8 T cells in the pathogenesis of experimental allergic encephalitis and multiple sclerosis. *J.Exp.Med.* 2001; 194: F27-F30.
- Stewart WA, MacKay AL, Whittall KP, Moore GR, Paty DW. Spin-spin relaxation in experimental allergic encephalomyelitis. Analysis of CPMG data using a non-linear least squares method and linear inverse theory. *Magn Reson.Med.* 1993; 29: 767-775.
- Stinissen P, Raus J. Autoreactive T lymphocytes in multiple sclerosis: pathogenic role and therapeutic targeting. *Acta Neurol.Belg.* 1999; 99: 65-69.
- Suda T, McCarthy K, Vu Q, McCormack J, Schneeberger EE. Dendritic cell precursors are enriched in the vascular compartment of the lung. *Am.J.Respir.Cell Mol.Biol.* 1998; 19: 728-737.
- Swanborg RH. Experimental autoimmune encephalomyelitis in rodents as a model for human demyelinating disease. *Clin.Immunol.Immunopathol.* 1995; 77: 4-13.
- Tabi Z, McCombe PA, Pender MP. Apoptotic elimination of V beta 8.2+ cells from the central nervous system during recovery from experimental autoimmune encephalomyelitis induced by the passive transfer of V beta 8.2+ encephalitogenic T cells. *Eur.J.Immunol.* 1994; 24: 2609-2617.
- Tabira T. Cellular and molecular aspects of the pathomechanism and therapy of murine experimental allergic encephalomyelitis. *Crit Rev.Neurobiol.* 1989; 5: 113-142.
- Tachovsky TG, Lisak RP, Koprowski H, Theofilopoulos AN, Dixon FJ. Circulating immune complexes in multiple sclerosis and other neurological diseases. *Lancet* 1976; 2: 997-999.
- Tani M, Ransohoff RM. Do chemokines mediate inflammatory cell invasion of the central nervous system parenchyma? *Brain Pathol.* 1994; 4: 135-143.

- Thompson AJ, Miller D, Youl B *et al.* Serial gadolinium-enhanced MRI in relapsing/remitting multiple sclerosis of varying disease duration. *Neurology* 1992; 42: 60-63.
- Tomalia D, Naylor AM, Goddard WA. III Starburst dendrimers: molecular-level control of size, shape, surface chemistry, topology and flexibility from atoms to microscopic mytter. *Angew.Chem.Int.Ed.Engl* 1990; 29: 138-175.
- Trapp B., Ransohoff R., and Rudick, R. Axonal pathology in multiple sclerosis: relationship to neurologic disability. *Axonal pathology in multiple sclerosis: relationship to neurologic disability* 12, 295-302. 1999. Ref Type: Magazine Article
- Traugott U, Reinherz EL, Raine CS. Multiple sclerosis. Distribution of T cells, T cell subsets and Ia-positive macrophages in lesions of different ages. *J.Neuroimmunol.* 1983a; 4: 201-221.
- Traugott U, Reinherz EL, Raine CS. Multiple sclerosis: distribution of T cell subsets within active chronic lesions. *Science.* 1983b; 219: 308-310.
- Traugott U, Scheinberg LC, Raine CS. Multiple sclerosis: circulating antigen-reactive lymphocytes. *Ann.Neurol.* 1979; 6: 425-429.
- Truyen L, van Waesberghe JH, van Walderveen MA *et al.* Accumulation of hypointense lesions ("black holes") on T1 spin-echo MRI correlates with disease progression in multiple sclerosis. *Neurology* 1996; 47: 1469-1476.
- Turner A, Cuzner ML, Davison AN, Rudge P. On the role of sensitised T-lymphocytes in the pathogenesis of multiple sclerosis. *J.Neurol.Neurosurg.Psychiatry* 1980; 43: 305-309.
- Uhlenbroock K. [On the question of the toxicity of cyanine dyes]. *Arzneimittelforschung.* 1965; 15: 1349-1352.
- van Walderveen MA, Kamphorst W, Scheltens P *et al.* Histopathologic correlate of hypointense lesions on T1-weighted spin-echo MRI in multiple sclerosis. *Neurology* 1998; 50: 1282-1288.
- Vass K, Lassmann H, Wekerle H, Wisniewski HM. The distribution of Ia antigen in the lesions of rat acute experimental allergic encephalomyelitis. *Acta Neuropathol.(Berl)* 1986; 70: 149-160.
- Venditto VJ, Regino CA, Brechbiel MW. PAMAM dendrimer based macromolecules as improved contrast agents. *Mol.Pharm.* 2005; 2: 302-311.
- Virchow R. *Cellularpathology.* Berlin: Hirschwald, 2005.
- Vitale M, Bottino C, Sivori S *et al.* NKp44, a novel triggering surface molecule specifically expressed by activated natural killer cells, is involved in non-major histocompatibility complex-restricted tumor cell lysis. *J.Exp.Med.* 1998; 187: 2065-2072.
- Vives E, Richard JP, Rispal C, Lebleu B. TAT peptide internalization: seeking the mechanism of entry. *Curr.Protein Pept.Sci.* 2003; 4: 125-132.
- Wang YX, Hussain SM, Krestin GP. Superparamagnetic iron oxide contrast agents: physicochemical characteristics and applications in MR imaging. *Eur.Radiol.* 2001; 11: 2319-2331.
- Wehrli FW, MacFall JR, Shutts D, Breger R, Herfkens RJ. Mechanisms of contrast in NMR imaging. *J.Comput.Assist.Tomogr.* 1984; 8: 369-380.
- Weissleder R, Elizondo G, Wittenberg J, Rabito CA, Bengele HH, Josephson L. Ultrasmall superparamagnetic iron oxide: characterization of a new class of contrast agents for MR imaging. *Radiology* 1990; 175: 489-493.
- Wekerle H, Engelhardt B, Risau W, Meyermann R. Interaction of T lymphocytes with cerebral endothelial cells in vitro. *Brain Pathol.* 1991; 1: 107-114.

Wiessner C, Bareyre FM, Allegrini PR *et al.* Anti-Nogo-A antibody infusion 24 hours after experimental stroke improved behavioral outcome and corticospinal plasticity in normotensive and spontaneously hypertensive rats. *J.Cereb.Blood Flow Metab* 2003; 23: 154-165.

William G.Bradley. MR contrast in the brain. 2004.
Ref Type: Generic

Wolbarst AB, Hendee WR. Evolving and experimental technologies in medical imaging. *Radiology*. 2006; 238: 16-39.

Wolburg H, Lippoldt A. Tight junctions of the blood-brain barrier: development, composition and regulation. *Vascul.Pharmacol.* 2002; 38: 323-337.

Wolburg H, Wolburg-Buchholz K, Engelhardt B. Involvement of tight junctions during transendothelial migration of mononuclear cells in experimental autoimmune encephalomyelitis. *Ernst.Schering.Res.Found.Workshop* 2004; 17-38.

Wolburg H, Wolburg-Buchholz K, Engelhardt B. Diapedesis of mononuclear cells across cerebral venules during experimental autoimmune encephalomyelitis leaves tight junctions intact. *Acta Neuropathol.(Berl)* 2005; 109: 181-190.

Wood ML, Hardy PA. Proton relaxation enhancement. *J.Magn Reson.Imaging* 1993; 3: 149-156.

Xu Y, Szoka FC, Jr. Mechanism of DNA release from cationic liposome/DNA complexes used in cell transfection. *Biochemistry* 1996; 35: 5616-5623.

Yamamura T, Namikawa T, Endoh M, Kunishita T, Tabira T. Passive transfer of experimental allergic encephalomyelitis induced by proteolipid apoprotein. *J.Neurol.Sci.* 1986; 76: 269-275.

Yeh TC, Zhang W, Ildstad ST, Ho C. In vivo dynamic MRI tracking of rat T-cells labeled with superparamagnetic iron-oxide particles. *Magn Reson.Med.* 1995; 33: 200-208.

Zamvil S, Nelson P, Trotter J *et al.* T-cell clones specific for myelin basic protein induce chronic relapsing paralysis and demyelination. *Nature* 1985; 317: 355-358.

Curriculum vitae

Personal details:

Name Cedric Berger

Current address Mülhauserstrasse 88
CH-4056 BASEL
Switzerland

Nationality French

Date of birth Erlangen (Germany), the 4th of March 1977

Education:

2003-2006 **PhD in Biophysics**, Universität Basel, Switzerland

2001-2002 **M.Sc. in biomedical imaging & engineering** , Université Louis Pasteur, Strasbourg, France

1999-2000 **B. Sc. in cell and molecular biology**, Université Louis Pasteur, Strasbourg, France